Title
Lactate Metabolism and the Response to Nanoparticle Exposure in Normal and Cancerous Breast Cells

Author
HUSSIEN, RAJAA Mohamad

Publication Date
2014

Peer reviewed|Thesis/dissertation

Lactate Metabolism and the Response to Nanoparticle Exposure in Normal and Cancerous Breast Cells

By

Rajaa Mohamad Hussien

A dissertation submitted in partial satisfaction of the

requirements for the degree of

Doctor of Philosophy

in

Integrative Biology

in the

Graduate Division

of the

University of California, Berkeley

Committee in charge:

Professor George A. Brooks, Chair
Professor Daniela Kaufer
Professor Gary Firestone

Spring 2014

Lactate Metabolism and the Response to Nanoparticle Exposure in Normal and Cancerous Breast Cells

by Rajaa Mohamad Hussien

Abstract

Lactate Metabolism and the Response to Nanoparticle Exposure in Normal and Cancerous Breast Cells

by

Rajaa Mohamad Hussien

Doctor of Philosophy in Integrative Biology

University of California, Berkeley

Professor George A. Brooks, Chair

To understand lactate metabolism and the response of normal and cancerous breast cells to nanoparticle exposure, we performed two studies using breast cancer cell lines MCF-7 and MDA-MB-231, and a normal breast cell line HMEC 184.

In my first study I examined the expression and the localization of the lactate shuttle proteins monocarboxylate transporter (MCT) and lactate dehydrogenase (LDH) isoforms in two breast cancer cell lines MCF-7, MDA-MB-231, compared to the normal breast cell line HMEC 184. I hypothesized that there are changes in the localization and expression of MCTs and LDH isoforms in cancerous breast cells when compared to normal breast cells, and that these changes are associated with the Warburg Effect and correspond to the oxidative capacity of the cancerous cells. My data show that MCT (1, 2, and 4), and LDH isoforms (A and B) are expressed in both normal and cancerous breast cell lines, except that MDA-MB-231 did not express MCT1. MCT1 was highly expressed in normal cells when compared to cancer cell lines. MCT4 was highly expressed in MDA-MB-231, and MCT2 was highly expressed in MCF-7. LDH was highly expressed in both cancerous cell lines compared to the normal cell line, and MCF-7 expressed mainly LDH5 (LDHB), while MDA-MB-231 and HMEC 184 expressed mainly LDH1 (LDHA). Using confocal laser scanning microscopy, I found that MCT2, MCT4, and LDH are localized in mitochondria in addition to their localization in the plasma membrane and cytosol, whereas MCT1 is mainly localized in the plasma membrane. This localization was the same in cancerous and normal cell lines. The changes in the expression of MCT and LDH isoforms corresponded to the metabolic status of each cell line. Both cell lines MCF-7 and MDA-MB-231 produced higher amounts of lactate than the HMEC 184 cell line, but have less endogenous and maximum respiration than the HMEC 184 cell line. In conclusion, I reported changes in the expression of MCT and LDH in breast cancer cells with no change in their localization. These changes corresponded to the breast cancer cells' oxidative capacity. My data support the existence of the previously reported lactate shuttle in cancer, and add a new explanation of its function.

My next project examined the effect of co-polymer nanoparticles, Eudragit® RS 100 (ENPs), increasingly being used to coat and deliver drugs including chemotherapy

agents, on the metabolic activity and proliferation of the human epithelial breast cells (HMEC 184, MCF-7, MDA-MB-231). I reported novel responses of human epithelial breast cells when exposed to Eudragit nanoparticles. I showed that cells displayed dose-dependent increases in metabolic activity and growth, but lower proliferation rates, than control cells, as evidenced in tetrazolium salt (WST-1) and 5-bromo-2'-deoxyuridine (BrdU) assays. Using mass spectrometry and micrroarry analyses I found that the mechanism for this behaviour stems from the ability of Eudragit nanoparticles to bind to certain proteins in culture media and to bring them closer to the surface of cells. Those proteins are involved in cell adhesion, growth, differentiation, and migration. The effect of nanoparticle treatment in increasing cancer and normal human epithelial breast cell metabolic activity and growth has not been reported previously, and this project highlighted the need for further research to address the potentially counter-productive effects of using nanoparticles in cancer chemotherapy.

TABLE OF CONTENTS

ACKNOWLEDGEMENTS

I want to take this opportunity to thank the individuals who have inspired and helped me during graduate school, and in my dissertation research. Professor George A. Brooks has been my greatest mentor in learning to be a successful scientist. His support during my graduate studies has been tremendously important to my development. His vision, guidance, and wisdom will stay with me and will always influence my scientific career. I am thankful to have had the chance to study in Dr. Brooks' laboratory.

I want to thank my qualifying examination committee members (Chair Steve L. Lehman, Daniela Kaufer, Thomas J. Carlson, and outside member Gregory W. Aponte) for taking the time to meet with me and guide me in preparing for the exam. Their questions and suggestions expanded my perspectives on my research. I want to thank my dissertation committee members (Chair George A. Brooks, Daniela Kaufer, and Gary Firestone) for their advice and encouragement during graduate school and in preparing my dissertation. Without their help my research would not have been possible.

Finally, I am thankful to my husband, Jeff Piatt. His care, support, and love have always helped me to get where I want to be.

CHAPTER 1

Introduction to the Warburg Effect

Increased Glycolysis

The Warburg Effect, which was first recognized by the Nobel laureate Otto Warburg in 1920, is the observation that most cancer cells prefer to produce energy by glycolysis rather than by oxidative phosphorylation, even in the presence of oxygen (59, 60). The Warburg Effect got the attention of many cancer researchers, because while cancer cells demand energy for their biosynthesis and proliferation, glycolysis less efficiently produces ATP than does oxidative phosphorylation. However, the Warburg Effect may be advantageous in sudden hypoxic conditions in the cancer microenvironment. Despite the promise of Warburg Effect study, it was not a prominent object of investigation in the cancer research of the last 60 years for two reasons. First, Otto Warburg believed that cellular metabolic abnormality and the Warburg Effect were the main causes of cancer, but this hypothesis was not supported by evidence. Second, the oncogenic revolution began around the same time, and took center stage in cancer research for more than 60 years (7, 13). There is no doubt that mutations in oncogenes and tumor suppressor genes are the main causes of cancer, but they are heterogeneous and numerous, and many of those mutations change cancer metabolism as well (7, 13, 25, 32). Currently, the focus of cancer research is shifting towards other aspects of tumors, such as their microenvironment and metabolism (7, 22). While it is recognized that the Warburg Effect is not a cause of cancer, it remains an important factor in the thriving of cancer cells.

The Warburg Effect is widely viewed as a result of oncogenic pathway activity generating changes in cell metabolism and activation of cell proliferation, and is thus regarded as a consequence of cancer progression, not a cause. The oncogenic activity of several genes, such as hypoxia-inducible factor 1-alpha (HIF-1α), c-Myc, Phosphoinositide 3-kinase (PI3K), and the mammalian target of rapamycin (mTOR), along with the loss of function of both AMP-activated protein kinase (AMPK) and the tumor suppressor p53, can lead to increased glucose uptake, increased expression of crucial glycolytic enzymes, suppression of oxidative phosphorylation, and increased lactate production (Figure 1) (The suggested role of these genes in the Warburg Effect is covered in detail in reviews (7, 8, 15, 28, 49)). HIF-1α is considered the most important genetic regulator that controls the metabolism in cells and links it to their surrounding environment and oxygen availability (46). HIF-1α regulates a large number of genes involved in angiogenesis, glycolysis, and cell survival (48). HIF-1α protein expression levels are tightly controlled through the oxygen level in cells (45, 47). In normal oxygenated healthy cells, prolyl hydroxylase enzymes (PHD2) use oxygen to hydroxylate HIF-1α, which then becomes recognizable by the tumor suppresser gene von Hippel-Lindau (VHL) that causes its degradation (7, 45, 47). HIF-1α can be stabilized in cancer cells through hypoxia when oxygen supply becomes limited by tumor-mass growth (7). HIF-1α gets activated even in normoxic conditions in cancer cells through inactivation mutations in PHD2, VHL, fumarate hydratase (FH), or succinate dehydrogenase (SDH), or activation of PI3K. Mutations in FH and SDH cause the accumulation of fumarate and succinate, two metabolites that inhibit HIF-1α hydroxylation (7, 8, 49). The activated HIF-1α increases glucose uptake through activating glucose transporters (GLUT 1, 2, and 3), speeding up glycolysis through increased glycolytic enzyme expression (hexokinase (HK), phosphorfructo-kinase (PFK), glyceraldehyde 3-phosphate dehydrogenase (GAPDH), and Lactate dehydrogenase (LDH)), and suppressing oxidative

phosphorylation through increased expression of pyruvate dehydrogenase kinases (PDKs) (7, 28, 49). PDK inactivates pyruvate dehydrogenase, thus blocking the movement of pyruvate to TCA cycles (28). Similarly, c-Myc, a transcription factor constitutively activated in most cancer cells, has been shown to support HIF-1α in increasing glycolysis under normoxic condition through increasing the expression of glucose transporters, glycolytic enzymes, and PDKs (11, 28). c-Myc has also been shown to increase glutaminolysis and fatty acid synthesis in cancer cells (7, 49, 65).

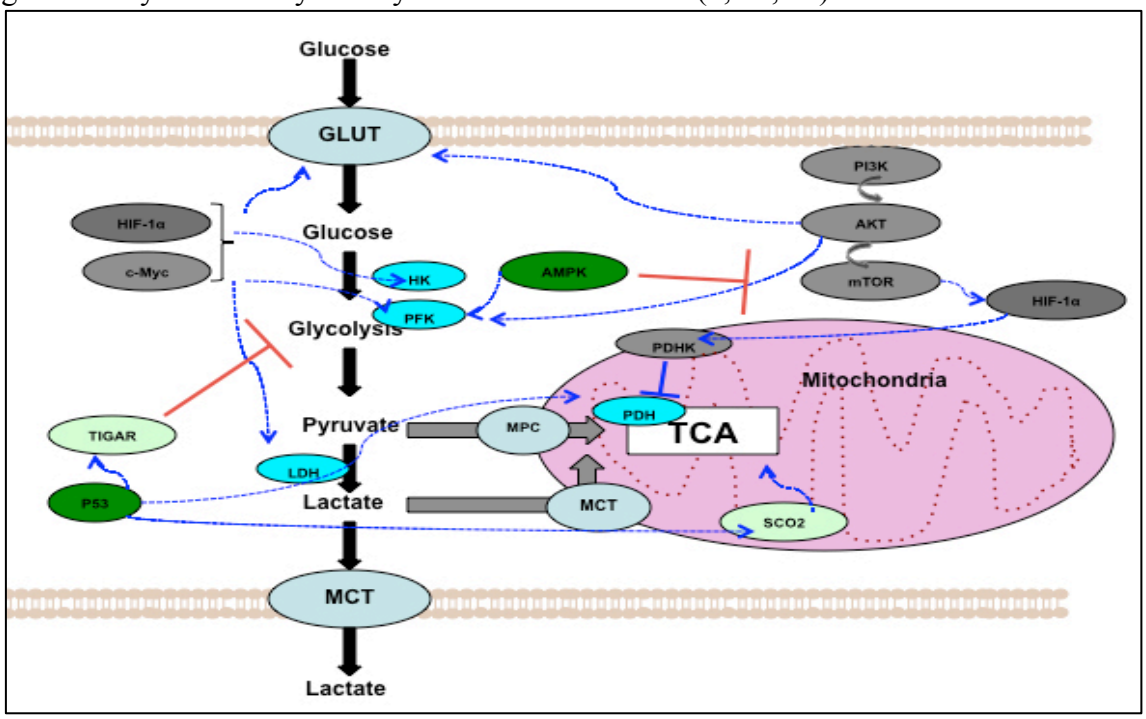

Figure. 1. Adapted from Cairns et al. (7) and Jang et al.(28). Illustration showing how increased glycolysis in cancer cells is a result of oncogenic pathway activity generating changes in cell metabolism. The oncogenic activity of several genes, can lead to increased glucose transporter expression, increased expression of crucial glycolytic enzymes, and suppression of oxidative phosphorylation. These genes include hypoxia-inducible factor 1-alpha (HIF-1α), the transcription factor c-Myc, Phosphoinositide 3-kinase (PI3K), the mammalian target of rapamycin (mTOR), AMP-activated protein kinase (AMPK), and tumor suppressor p53.
(AKT: protein kinase B, HK: Hexokinase, GLUT:glucose transporters, LDH: lactate dehydrogenase, MCT: Monocarboxylate Transporters, MPC: pyruvate transporters. PDH: Pyruvate dehydrogenase, PDHK: Pyruvate dehydrogenase kinase, PFK: Phosphorfructo-kinase, SCO2: Cytochrome oxidase 2, TIGAR: TP53-induced glycolysis and apoptosis regulator.

PI3K is highly activated and altered in a wide range of human cancers, and has an important role in regulating cell metabolism in response to growth signals and energy status. P13K also showed a role in cell metabolism and the Warburg Effect (8, 61). PI3K and its downstream targets AKT and mTOR activate glucose transport, glycolytic enzymes, and HIF-1α (8, 28).

On the other hand, P53 and AMPK indirectly contribute to increased glycolysis when their function is lost in cancer cells. AMPK, which is considered the master regulator of cell metabolism, couples energy availability to growth signals (7). During low energy availability, AMPK gets activated and blocks mTOR and cell proliferation while at the same time activating glycolysis and lipid oxidation. It seems that the role of AMPK is affected in cancer cells (7). The tumor suppressor P53 has an important role in

DNA repair, apoptosis, and cell cycle arrest as well a role in controlling cell metabolism. The tumor suppressor P53 suppresses glycolysis and stimulates oxidative phosphorylation, glutaminolysis, and fatty acid oxidation (29, 33, 34, 56). P53 suppresses glycolysis through decreasing the expression of GLUT1/4 and NFKB (which activates GLUT3 expression); up-regulating TP53-induced glycolysis and apoptosis regulator gene (TIGAR) (which decreases F-2-6-P_2 level by dephosphorylation); and down regulating PI3K/mTOR/AKT pathway (28). P53 stimulates oxidative phosphorylation through increasing the expression of cytochrome oxidase 2 (SCO2), pyruvate dehydrogenase, and reducing pyruvate dehydrogenase kinases. P53 also stimulates glutaminolysis, and fatty acid oxidation through increasing the expression of glutaminase 1 (GLS1), Guanidinoacetate methyltransferase (GAMT), and Lipin1 (29, 33, 34, 56). Mutated P53 is found in many cancer types, thus its function suppressing glycolysis is lost (7, 8, 28, 49).

Genetic sequencing and research into pyruvate kinase and isocitrate dehydrogenase enzymes in cancer cells have offered new insights about the role of the Warburg Effect in cancer. Research suggests that the goal of increased glycolysis in cancer cells is not to provide more ATP, but to provide precursors for other metabolic pathways (Figure 2). It seems that glycolysis and glutaminolysis, both increased in cancer cells, work together to produce metabolic intermediates used in fatty acid, nucleic acid, and amino acid synthesis. Also produced are macromolecules for histone modification, enzymatic reaction, and antioxidant defense (7, 8, 28). Studies of pyruvate kinase enzyme (PK), an enzyme that converts phosphoenolpyruvate (PEP) to pyruvate, found that most cancer cells contain an inactive, slow dimeric form of this enzyme (PKM2). In contrast, most normal cells contain an active tetrameric form of this enzyme (38). The sluggish action of inactive PKM2 slows glycolysis and allows its upstream intermediates to accumulate and shuttle to other synthesis pathways such as the hexosamine pathway, the pentose phosphate pathway, and the glycerol synthesis pathway. Inactive PKM2's sluggish action also provides reducing equivalents such as NADPH for enzymatic reaction and antioxidant defense (1, 63) (Figure 2). Studies of isocitrate dehydrosenase enzyme (IDH1, IDH2) showed that the novel gains in function mutation of these enzymes, found in many cancers, make them produce 2-hydroxyglutarate (2HG) from α-ketoglutarate (α-KG). 2-hydroxyglutarate (2HG) inhibits many enzymes that act on histone and DNA methylation, thus contributing to histone modification in cancer (35, 65). IDH1 and IDH2 are also found in the cytoplasm, and negative mutations in these enzymes can lead to a reduction of cytoplasmic α-KG level. α-KG inhibits PHD enzymes and stabilizes HIF-1α, thus increasing glycolysis (28). Others have found that lactate and pyruvate generated from increased glycolysis in cancer cells were exported from mitochondria as citrate to support fatty acid synthesis, and that glutamine was used to replenish the TCA cycle as compensation for citrate export (14). All those data suggest that the significance of the Warburg Effect is much greater than what we thought 30 years ago.

A new study from the Bissell laboratory using the 3D model of Human Mammary Epithelial Cells (HMECs) shows that increased glucose uptake in normal HMEC cells disrupts their polarized structure and activates known oncogenic signaling pathways (such as epidermal growth factor receptor (EGFR), β1 integrin, mitogen-activated protein kinase kinase (MEK), and protein kinase B (Akt) pathways). On the other hand, reduction

of glucose uptake in malignant HMEC cells was shown to lead to suppression of oncogenic pathways, and to the subsequent formation of organized, growth-arrested, polarized structures (40). Surprisingly, the mammalian target of rapamycin (mTOR) and hypoxia-inducible factor 1-alpha (HIF-1α) pathways were not involved in the changes seen in these cells. The activation of oncogenic pathways following increased glycolysis was found to be linked to cyclic adenosine monophosphate (cAMP), spindle assembly checkpoint protein (sAC), exchange proteins activated by cAMP (EPAC), Ras-related protein 1 (Rap1), and the hexosamine biosynthetic pathway (HBP) (Figure. 3). These results potentially alter our view of the Warburg Effect from a consequence of cancer progression to a possible trigger or participant, highlighting its importance in tumor development. At the same time, the results point to the need for further research to understand the complex role played by the Warburg Effect.

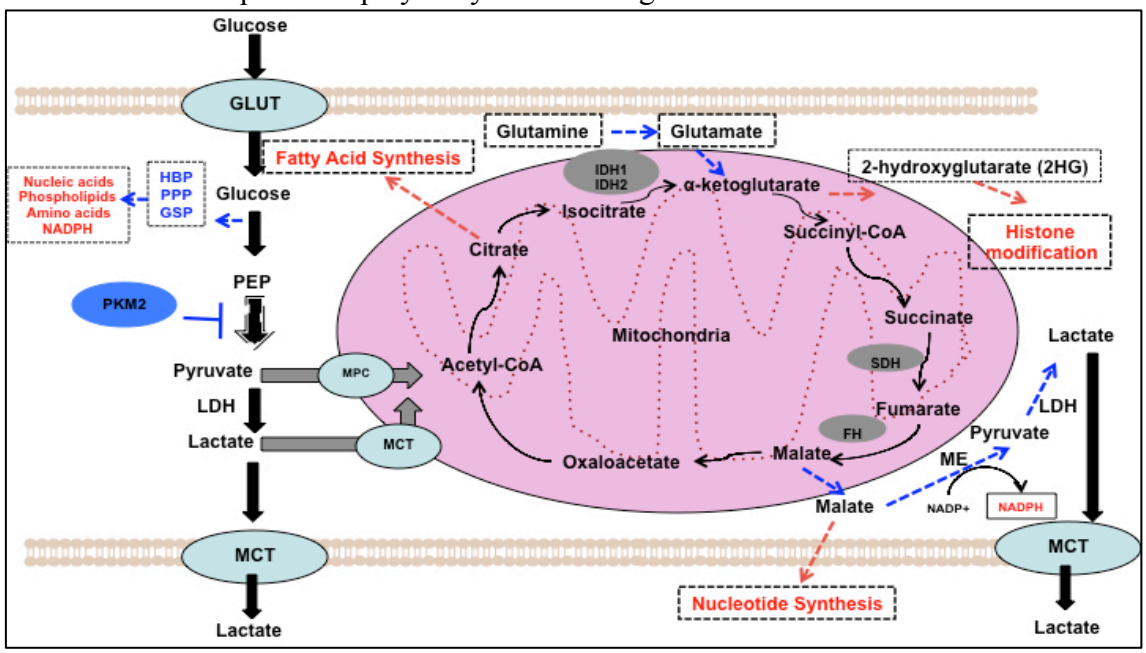

Figure 2. Adapted from DeBerardinis et al. (14) and Jang et al. (28). Illustration showing how glycolysis and glutaminolysis, both increased in cancer cells, work together to produce metabolic intermediates used in fatty acid, nucleic acid, and amino acid synthesis. Also produced are macromolecules for histone modification, enzymatic reaction, and antioxidant defense. Lactate is produce either from glycolysis or glutaminolysis.
(GLUT: glucose transporters, GSP: glycerol synthesis pathway, FH: fumarate hydratase, HB: hexosamine biosynthetic pathway, LDH: lactate dehydrogenase, MCT: Monocarboxylate Transporters, ME: malic enzyme, MPC: pyruvate transporters, PEP: phosphoenolpyruvate, PKM2: pyruvate kinase enzyme type M2, PPP: pentose phosphate pathway, SDH: succinate dehydrogenase)

Increased Lactate Production

As a result of the Warburg Effect, lactate is produced in cancer cells in large quantities, which has been shown to lead to negative outcomes (25). High lactate concentration is correlated with low patient survival in cervical cancer (58), and in head and neck squamous cell carcinoma (66). Lactate is also positively correlated with incidence of metastases in all types of cancer (25, 57), and with increased radioresistance (20, 25, 44). While lactate is correlated with bad outcomes, its exact role in cancer is still under investigation. Studies of lactate metabolism in healthy cells in humans and rodents have shown that lactate is an important energy fuel, gluconeogenic precursor, and a

paracrine signal molecule (4-6) that can stimulates mitochondrial biogenesis (24) and angiogenesis (30). Recent data suggest that lactate may play roles in cancer similar to those it plays in normal cells through the reverse, or direct Warburg effect. Le Floch et al (31) showed evidence for the reverse Warburg effect in the breast cancer micro-environment. In their study, they showed that fibroblast cells, surrounding epithelial breast cancer cells, release lactate to the nearby cancer cells, which oxidize it due to its higher mitochondrial activity. Vegran et al (55) showed that lactate released from cancer cells stimulates angiogenesis in human umbilical vein endothelial cells. Despite the fact that Pinheiro et al (43) disagreed with Vegran et al's hypothesis and showed on the contrary that endothelial cells surrounding cervical, colorectal, and breast epithelial cancer cells do not express MCT1, these studies still point out the possibility of the existence of lactate shuttles in cancer microenvironments, and that lactate may be a paracrine signal used in them (16).

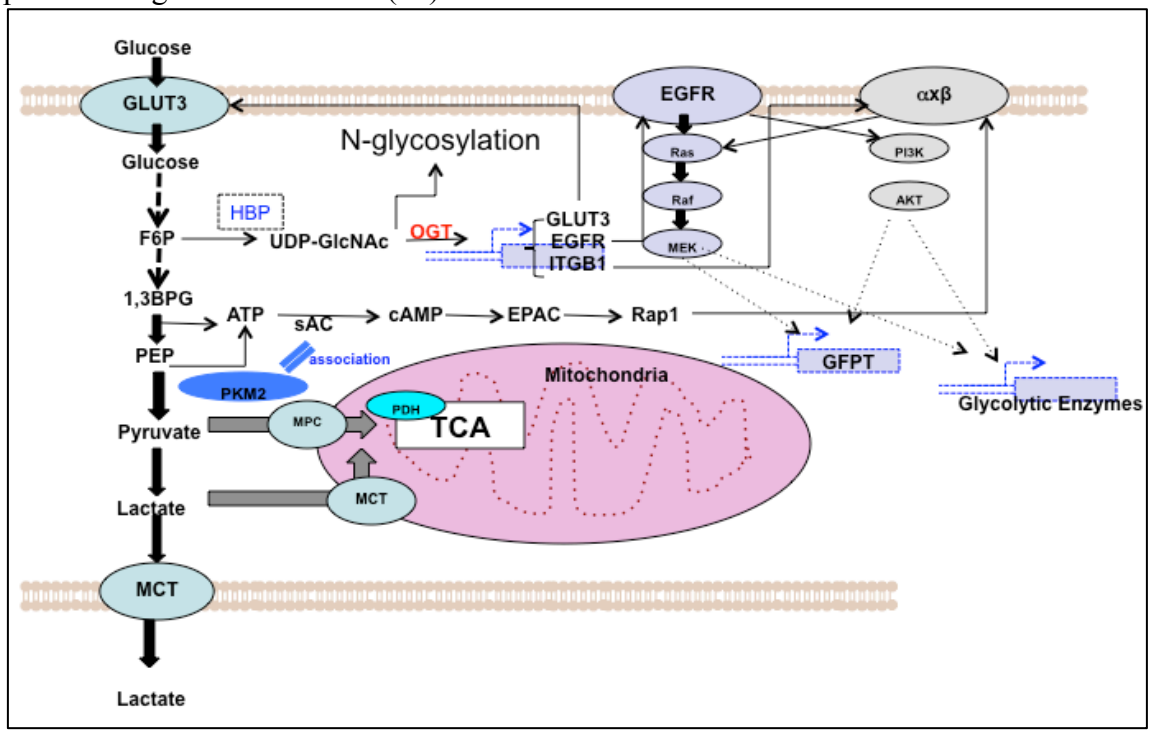

Figure 3: Adapted from Onodera et al. (40). Illustration shows how increased glucose uptake in 3D model of Human Mammary Epithelial Cells (HMECs) activates oncogenic signaling pathways, including epidermal growth factor receptor (EGFR), β1 integrin (αxβ), mitogen-activated protein kinase kinase (MEK), and protein kinase B (Akt) pathways. There are reciprocal interactions between glucose metabolism and the oncogenic signaling pathways. The sAC-EPAC-Rap1 pathway regulates β1 integrin positively via a direct link between ATP production in the glycolytic pathway and cAMP generation by sAC. The hexosamine biosynthetic pathway (HBP) is also upregulated through activation of oncogenic signaling. The downstream O-GlcNAcylation of target proteins regulates the expression of β1 integrin, EGFR, and GLUT3.
(ATP: Adenosine triphosphate, 1,3BPG: 1,3-Bisphosphoglycerate, cAMP: Cyclic adenosine monophosphate, EPAC: Exchange proteins activated by cAMP, F6P: Fructose-6-phosphate, GLUT3: Glucose transporter type 3, ITGB1: Gene encoding b 1 integrin protein, MCT: Monocarboxylate Transporters, MPC; Pyruvate transporters, OGT: O-linked N-acetylglucosamine transferase, PDH: Pyruvate dehydrogenase, PEP: Phosphoenolpyruvate, PKM2: Pyruvate kinase enzyme type M2, Rap1: Ras-related protein 1, sAC; Spindle assembly checkpoint protein, TCA: Tricarboxylic acid cycle, UDP-GLcNAc: Uridine diphosphate-N-acetylglucosamine)

To transport lactate, cancer cells have to rely on its transporters, the monocarboxylate transporters (MCTs), to move it either into mitochondria for oxidation

(23, 26), or outside the cells for recycling (21). The monocarboxylate transporters 1, 2, and 4 are the major lactate/pyruvate transporters between and within cells (21). The three MCTs (1, 2, and 4) differ in their affinity to lactate, with MCT2 having the highest affinity and MCT4 having the lowest affinity for substrates. The different affinities of lactate transporters have been correlated with the expression of these transporters on different types of cells based on their oxidative capacity. For example, glycolitic muscle cells, glia, and many cancer cells, which release large amounts of lactate, express MCT4, and the oxidative muscle cells, liver, and neurons, which take up large amounts of lactate, express MCT1 or MCT2 (Table 1) (21). Furthermore, the expression of different types of lactate transporters cause cells to respond differently to lactate exposure. The over-expression of MCT1 in pancreatic ß- cells causes those cells to release insulin upon exposure to lactate or pyruvate (27), and the re-expression of MCT1 in MDA-MB-231 breast cancer cells causes those cells to decrease lactate release (17).

TISSUE	DOMINANT LDH	DOMINANT MCT	TYPE
Liver	LDHA	MCT2 & MCT1	OXIDATIVE
Heart	LDHB	MCT1	OXIDATIVE
Muscle cells (SO type1)	LDHA	MCT1	OXIDATIVE
Muscle cells (FG type2)	LDHA	MCT4	GLYCOLYTIC

Table. 1. The expression of MCTs and LDHs in different tissues

The expression of specific MCTs in all cancer types has not been documented, but high expression of MCT4 has been reported in hypoxic areas of tumors (50), which may be due to the activation of MCT4's promoter under hypoxic conditions. A high expression of MCT1 was also found in basal-like highly dividing breast tissues (42), and was associated with low patient survival in gastrointestinal stromal tumors (2, 12). MCT1 can also be activated by hypoxia in cancer through the NF-KB pathway, but this activation depends on p53's status. The changes in MCT1 expression altered the way hypoxic p53-/- tumor cells took up or released lactate according to environmental conditions, and helped the cells to continue their proliferation in the high lactate environment by using lactate for mitochondrial respiration. The P53 protein and its co-repressor mSin-3A can bind to the promoter region of MCT1 genes during hypoxia (2).

The Promise of the Warburg Effect

The Warburg Effect has proven to be valuable in cancer detection, and still holds promise for treatment (15, 18, 28, 41, 65). Positron emission tomography (PET) scans use [^{18}F]fludeoxyglucose (FDG), a radioactive glucose analogue, to detect and visualize tumors in the human body based on cancer cells' higher glucose uptake relative to the rest of the body. The PET scan was developed more than 40 years ago and is still used in clinical diagnostic and research settings to study brain metablosim, cadiac function, and cancer (36, 53). Many anticancer drugs have been developed to target certain steps in glycolysis (18, 28, 41, 65) or lactate disposal in cancer cells (15), and some are currently in clinical trials (for example dichloroacetic acid and AT-101) (19, 41, 54). Table 2 shows some examples of anticancer drugs that target the Warburg Effect (15, 18, 28, 41, 65). Although such drugs have not yet been shown to be effective, there is hope that a complete understanding of the Warburg Effect may help us develop new effective drugs to target cancer cell metabolism without killing host cells.

Name of cancer drug	Target	Status
2-Deoxy-D-glucose (2DG)	A competitive inhibitor of glucose metabolism, inhibits hexokinase action, inhibits protein glycosylation (37, 41, 65).	Phase I/II clinical trial for prostate cancer: trial was terminated on November 2013 (ClinicalTrials.gov identifier: NCT00633087).
Phloretin	Glucose transporter (Glut1) (65)	In vitro and in vivo studies (9, 62)
Lonidamine	Inhibits hexokinase action on glucose (18, 41).	Phase II/III clinical trial for symptomatic benign prostatic hyperplasia: trial was terminated on 2006 (ClinicalTrials.gov identifier: NCT00435448).
Dichloroacetic acid (DCA)	Inhibits pyruvate dehydrogenase kinase (PDHK), thus activating pyruvate dehydrogenase enzyme (PDH) and increasing pyruvate oxidation (3, 47, 51, 52).	Phase I clinical trial for of metabolic reprogramming therapy for treatment of recurrent head and neck cancers (ClinicalTrials.gov identifier: NCT01163487) Phase II clinical trial for treatment of brain cancer (ClinicalTrials.gov identifier: NCT00540176). Trial completed in 2010. Phase I clinical trial for study of the safety and efficacy of Dichloroacetate (DCA) in Glioblastoma and other recurrent brain tumors (ClinicalTrials.gov identifier: NCT01111097).
α -Cyano-4-hydroxycinnamic acid (CHC)	Inhibits lactate transporters (MCTs) and the mitochondrial pyruvate carriers (MPCs) (50).	Animal study (50).
Gossypol (AT-101)	Inhibits LDHA a and LDHB (15, 54, 64)	Phase II clinical trial for Recurrent Adrenocortical Carcinoma; Stage III/IV Adrenocortical Carcinoma (ClinicalTrials.gov identifier: NCT00848016)
AZD3965	MCT1/MCT2 inhibitor (15)	A Phase I Trial in patients with advanced cancer (ClinicalTrials.gov identifier: NCT01791595)

Table. 2. Examples of some anticancer drugs that target the Warburg Effect in cancer cells.

In our next study I wanted to contribute to efforts to design better drugs for targeting breast cancer cells based on lactate transporters and LDH isoforms. I examined the distribution of lactate transporters in mitochondrial and plasma membranes in normal and cancerous epithelial cells. I examined available microarray (10) and MassArray data (39) to extend my findings to a larger set of breast cancer cell lines. I showed that MCT (1, 2, and 4), and LDH isoforms (A and B) are expressed in both normal and cancerous breast cells occupying both mitochondrial and extra-mitochondrial cell compartments. The expression of lactate shuttle proteins was different in each cell line, but their sub-cellular localizations were similar. The changes in the expression of lactate shuttle proteins were associated with decreased oxidative capacity and increased lactate accumulation within breast cancer cells. Our data support the existence of the previously reported lactate shuttle in cancer, and add a new explanation of its function (26). My study also added more detail to the understanding of the Warburg Effect, and provided a base for further study of the contribution of lactate transporters to this effect.

REFERENCES

1. Bluemlein K, Gruning NM, Feichtinger RG, Lehrach H, Kofler B, and Ralser M. No evidence for a shift in pyruvate kinase PKM1 to PKM2 expression during tumorigenesis. *Oncotarget* 2: 393-400, 2011.
2. Boidot R, Vegran F, Meulle A, Le Breton A, Dessy C, Sonveaux P, Lizard-Nacol S, and Feron O. Regulation of Monocarboxylate Transporter MCT1 Expression by p53 Mediates Inward and Outward Lactate Fluxes in Tumors. *Cancer research* 72: 939-948, 2012.
3. Bonnet S, Archer SL, Allalunis-Turner J, Haromy A, Beaulieu C, Thompson R, Lee CT, Lopaschuk GD, Puttagunta L, Bonnet S, Harry G, Hashimoto K, Porter CJ, Andrade MA, Thebaud B, and Michelakis ED. A mitochondria-K+ channel axis is suppressed in cancer and its normalization promotes apoptosis and inhibits cancer growth. *Cancer Cell* 11: 37-51, 2007.
4. Brooks GA. Cell-cell and intracellular lactate shuttles. *J Physiol* 587: 5591-5600, 2009.
5. Brooks GA. Intra- and extra-cellular lactate shuttles. *Med Sci Sports Exerc* 32: 790-799, 2000.
6. Brooks GA. Lactate shuttles in nature. *Biochem Soc Trans* 30: 258-264, 2002.
7. Cairns RA, Harris IS, and Mak TW. Regulation of cancer cell metabolism. *Nature reviews Cancer* 11: 85-95, 2011.
8. Cantor JR, and Sabatini DM. Cancer cell metabolism: one hallmark, many faces. *Cancer Discov* 2: 881-898, 2012.
9. Cao X, Fang L, Gibbs S, Huang Y, Dai Z, Wen P, Zheng X, Sadee W, and Sun D. Glucose uptake inhibitor sensitizes cancer cells to daunorubicin and overcomes drug resistance in hypoxia. *Cancer chemotherapy and pharmacology* 59: 495-505, 2007.
10. Charafe-Jauffret E, Ginestier C, Monville F, Finetti P, Adelaide J, Cervera N, Fekairi S, Xerri L, Jacquemier J, Birnbaum D, and Bertucci F. Gene expression profiling of breast cell lines identifies potential new basal markers. *Oncogene* 25: 2273-2284, 2006.
11. Dang CV, Kim JW, Gao P, and Yustein J. The interplay between MYC and HIF in cancer. *Nature reviews Cancer* 8: 51-56, 2008.
12. de Oliveira AT, Pinheiro C, Longatto-Filho A, Brito MJ, Martinho O, Matos D, Carvalho AL, Vazquez VL, Silva TB, Scapulatempo C, Saad SS, Reis RM, and Baltazar F. Co-expression of monocarboxylate transporter 1 (MCT1) and its chaperone (CD147) is associated with low survival in patients with gastrointestinal stromal tumors (GISTs). *J Bioenerg Biomembr* 2012.
13. DeBerardinis RJ. Is cancer a disease of abnormal cellular metabolism? New angles on an old idea. *Genet Med* 10: 767-777, 2008.
14. DeBerardinis RJ, Mancuso A, Daikhin E, Nissim I, Yudkoff M, Wehrli S, and Thompson CB. Beyond aerobic glycolysis: transformed cells can engage in glutamine metabolism that exceeds the requirement for protein and nucleotide synthesis. *Proc Natl Acad Sci U S A* 104: 19345-19350, 2007.
15. Doherty JR, and Cleveland JL. Targeting lactate metabolism for cancer therapeutics. *The Journal of clinical investigation* 123: 3685-3692, 2013.

16. Draoui N, and Feron O. Lactate shuttles at a glance: from physiological paradigms to anti-cancer treatments. *Dis Model Mech* 4: 727-732, 2011.
17. Garcia CK, Goldstein JL, Pathak RK, Anderson RG, and Brown MS. Molecular characterization of a membrane transporter for lactate, pyruvate, and other monocarboxylates: implications for the Cori cycle. *Cell* 76: 865-873, 1994.
18. Gatenby RA, and Gillies RJ. Glycolysis in cancer: a potential target for therapy. *The international journal of biochemistry & cell biology* 39: 1358-1366, 2007.
19. Granchi C, and Minutolo F. Anticancer agents that counteract tumor glycolysis. *ChemMedChem* 7: 1318-1350, 2012.
20. Groussard C, Morel I, Chevanne M, Monnier M, Cillard J, and Delamarche A. Free radical scavenging and antioxidant effects of lactate ion: an in vitro study. *J Appl Physiol* 89: 169-175, 2000.
21. Halestrap AP, and Meredith D. The SLC16 gene family-from monocarboxylate transporters (MCTs) to aromatic amino acid transporters and beyond. *Pflugers Arch* 447: 619-628, 2004.
22. Hanahan D, and Weinberg RA. Hallmarks of cancer: the next generation. *Cell* 144: 646-674, 2011.
23. Hashimoto T, Hussien R, and Brooks GA. Colocalization of MCT1, CD147, and LDH in mitochondrial inner membrane of L6 muscle cells: evidence of a mitochondrial lactate oxidation complex. *Am J Physiol Endocrinol Metab* 290: E1237-1244, 2006.
24. Hashimoto T, Hussien R, Oommen S, Gohil K, and Brooks GA. Lactate sensitive transcription factor network in L6 cells: activation of MCT1 and mitochondrial biogenesis. *Faseb J* 21: 2602-2612, 2007.
25. Hirschhaeuser F, Sattler UG, and Mueller-Klieser W. Lactate: a metabolic key player in cancer. *Cancer research* 71: 6921-6925, 2012.
26. Hussien R, and Brooks GA. Mitochondrial and plasma membrane lactate transporter and lactate dehydrogenase isoform expression in breast cancer cell lines. *Physiol Genomics* 43: 255-264, 2011.
27. Ishihara H, Wang H, Drewes LR, and Wollheim CB. Overexpression of monocarboxylate transporter and lactate dehydrogenase alters insulin secretory responses to pyruvate and lactate in beta cells. *The Journal of clinical investigation* 104: 1621-1629, 1999.
28. Jang M, Kim SS, and Lee J. Cancer cell metabolism: implications for therapeutic targets. *Experimental & molecular medicine* 45: e45, 2013.
29. Jiang P, Du W, and Yang X. p53 and regulation of tumor metabolism. *J Carcinog* 12: 21, 2013.
30. Kumar VB, Viji RI, Kiran MS, and Sudhakaran PR. Endothelial cell response to lactate: implication of PAR modification of VEGF. *J Cell Physiol* 211: 477-485, 2007.
31. Le Floch R, Chiche J, Marchiq I, Naiken T, Ilk K, Murray CM, Critchlow SE, Roux D, Simon MP, and Pouyssegur J. CD147 subunit of lactate/H+ symporters MCT1 and hypoxia-inducible MCT4 is critical for energetics and growth of glycolytic tumors. *Proc Natl Acad Sci U S A* 108: 16663-16668, 2011.
32. Levine AJ, and Puzio-Kuter AM. The control of the metabolic switch in cancers by oncogenes and tumor suppressor genes. *Science* 330: 1340-1344, 2010.
33. Liang Y, Liu J, and Feng Z. The regulation of cellular metabolism by tumor suppressor p53. *Cell Biosci* 3: 9, 2013.

34. Liu J, Zhang C, Hu W, and Feng Z. Tumor suppressor p53 and its mutants in cancer metabolism. *Cancer Lett* 2013.
35. Lu C, Ward PS, Kapoor GS, Rohle D, Turcan S, Abdel-Wahab O, Edwards CR, Khanin R, Figueroa ME, Melnick A, Wellen KE, O'Rourke DM, Berger SL, Chan TA, Levine RL, Mellinghoff IK, and Thompson CB. IDH mutation impairs histone demethylation and results in a block to cell differentiation. *Nature* 483: 474-478, 2012.
36. Maisey MN. Positron Emission Tomography in Clinical Medicine
. In: *Positron Emission Tomography*, edited by Bailey DL, Townsend, D.W., Valk, P.E., Maisey, M.N. . NJ: Springer, 2005.
37. Maschek G, Savaraj N, Priebe W, Braunschweiger P, Hamilton K, Tidmarsh GF, De Young LR, and Lampidis TJ. 2-deoxy-D-glucose increases the efficacy of adriamycin and paclitaxel in human osteosarcoma and non-small cell lung cancers in vivo. *Cancer research* 64: 31-34, 2004.
38. Mazurek S. Pyruvate kinase type M2: a key regulator within the tumour metabolome and a tool for metabolic profiling of tumours. *Ernst Schering Found Symp Proc* 99-124, 2007.
39. Novak P, Jensen TJ, Garbe JC, Stampfer MR, and Futscher BW. Stepwise DNA methylation changes are linked to escape from defined proliferation barriers and mammary epithelial cell immortalization. *Cancer research* 69: 5251-5258, 2009.
40. Onodera Y, Nam JM, and Bissell MJ. Increased sugar uptake promotes oncogenesis via EPAC/RAP1 and O-GlcNAc pathways. *The Journal of clinical investigation* 2013.
41. Pelicano H, Martin DS, Xu RH, and Huang P. Glycolysis inhibition for anticancer treatment. *Oncogene* 25: 4633-4646, 2006.
42. Pinheiro C, Albergaria A, Paredes J, Sousa B, Dufloth R, Vieira D, Schmitt F, and Baltazar F. Monocarboxylate transporter 1 is up-regulated in basal-like breast carcinoma. *Histopathology* 56: 860-867, 2010.
43. Pinheiro C, Longatto-Filho A, Nogueira R, Schmitt F, and Baltazar F. Lactate-induced IL-8 pathway in endothelial cells--letter. *Cancer research* 72: 1901-1902, 2012.
44. Sattler UG, Meyer SS, Quennet V, Hoerner C, Knoerzer H, Fabian C, Yaromina A, Zips D, Walenta S, Baumann M, and Mueller-Klieser W. Glycolytic metabolism and tumour response to fractionated irradiation. *Radiother Oncol* 94: 102-109, 2010.
45. Semenza G. Signal transduction to hypoxia-inducible factor 1. *Biochemical pharmacology* 64: 993-998, 2002.
46. Semenza GL. HIF-1 and human disease: one highly involved factor. *Genes Dev* 14: 1983-1991, 2000.
47. Semenza GL. HIF-1 mediates metabolic responses to intratumoral hypoxia and oncogenic mutations. *The Journal of clinical investigation* 123: 3664-3671, 2013.
48. Semenza GL. HIF-1: upstream and downstream of cancer metabolism. *Current opinion in genetics & development* 20: 51-56, 2010.
49. Soga T. Cancer metabolism: key players in metabolic reprogramming. *Cancer Sci* 104: 275-281, 2013.
50. Sonveaux P, Vegran F, Schroeder T, Wergin MC, Verrax J, Rabbani ZN, De Saedeleer CJ, Kennedy KM, Diepart C, Jordan BF, Kelley MJ, Gallez B, Wahl ML, Feron O, and Dewhirst MW. Targeting lactate-fueled respiration selectively kills hypoxic tumor cells in mice. *The Journal of clinical investigation* 118: 3930-3942, 2008.

51. Stacpoole PW. The pharmacology of dichloroacetate. *Metabolism* 38: 1124-1144, 1989.
52. Stacpoole PW, Kurtz TL, Han Z, and Langaee T. Role of dichloroacetate in the treatment of genetic mitochondrial diseases. *Advanced drug delivery reviews* 60: 1478-1487, 2008.
53. Ter-Pogossian MM, Phelps ME, Hoffman EJ, and Mullani NA. A positron-emission transaxial tomograph for nuclear imaging (PETT). *Radiology* 114: 89-98, 1975.
54. Vander Jagt DL, Deck LM, and Royer RE. Gossypol: prototype of inhibitors targeted to dinucleotide folds. *Current medicinal chemistry* 7: 479-498, 2000.
55. Vegran F, Boidot R, Michiels C, Sonveaux P, and Feron O. Lactate influx through the endothelial cell monocarboxylate transporter MCT1 supports an NF-kappaB/IL-8 pathway that drives tumor angiogenesis. *Cancer research* 71: 2550-2560, 2011.
56. Vousden KH, and Ryan KM. p53 and metabolism. *Nature reviews Cancer* 9: 691-700, 2009.
57. Walenta S, and Mueller-Klieser WF. Lactate: mirror and motor of tumor malignancy. *Semin Radiat Oncol* 14: 267-274, 2004.
58. Walenta S, Wetterling M, Lehrke M, Schwickert G, Sundfor K, Rofstad EK, and Mueller-Klieser W. High lactate levels predict likelihood of metastases, tumor recurrence, and restricted patient survival in human cervical cancers. *Cancer research* 60: 916-921, 2000.
59. Warburg O. On respiratory impairment in cancer cells. *Science* 124: 269-270, 1956.
60. Warburg O. On the origin of cancer cells. *Science* 123: 309-314, 1956.
61. Wong KK, Engelman JA, and Cantley LC. Targeting the PI3K signaling pathway in cancer. *Current opinion in genetics & development* 20: 87-90, 2010.
62. Wu CH, Ho YS, Tsai CY, Wang YJ, Tseng H, Wei PL, Lee CH, Liu RS, and Lin SY. In vitro and in vivo study of phloretin-induced apoptosis in human liver cancer cells involving inhibition of type II glucose transporter. *International journal of cancer Journal international du cancer* 124: 2210-2219, 2009.
63. Yang W, and Lu Z. Regulation and function of pyruvate kinase M2 in cancer. *Cancer Lett* 339: 153-158, 2013.
64. Yu Y, Deck JA, Hunsaker LA, Deck LM, Royer RE, Goldberg E, and Vander Jagt DL. Selective active site inhibitors of human lactate dehydrogenases A4, B4, and C4. *Biochemical pharmacology* 62: 81-89, 2001.
65. Zhao Y, Butler EB, and Tan M. Targeting cellular metabolism to improve cancer therapeutics. *Cell Death Dis* 4: e532, 2013.
66. Ziebart T, Walenta S, Kunkel M, Reichert TE, Wagner W, and Mueller-Klieser W. Metabolic and proteomic differentials in head and neck squamous cell carcinomas and normal gingival tissue. *J Cancer Res Clin Oncol* 137: 193-199, 2011.

CHAPTER 2

Mitochondrial and Plasma Membrane Lactate Transporter and Lactate Dehydrogenase Isoform Expression in Breast Cancer Cell Lines

This chapter was published in *The Journal of Physiological Genomics* (Physiol. Genomics March 1, 2011 vol. 43 no. 5 255-264)

ABSTRACT

We hypothesized that dysregulation of lactate/pyruvate (monocarboxylate) transporters (MCT), and lactate dehydrogenase (LDH) isoforms contribute to the Warburg Effect in cancer. Therefore, we assayed for the expression levels and the localizations of MCT (1, 2 and 4), and LDH (A and B) isoforms in breast cancer cell lines MCF-7 and MDA-MB-231, and compared results with those from a control, untransformed primary breast cell line, HMEC 184. Remarkably, MCT 1 is not expressed in MDA-MB-231, but MCT 1 is expressed in MCF-7 cells, where its abundance is less than in control HMEC 184 cells. When present in HMEC 184 and MCF-7 cells, MCT 1 is localized to the plasma membrane. MCT 2 and MCT 4 were expressed in all the cell lines studied. MCT 4 expression was higher in MDA-MB-231 compared to MCF-7 and HMEC 184 cells, whereas MCT 2 abundance was higher in MCF-7 compared to MDA-MB-231 and HMEC 184 cells. Unlike MCT 1, MCT 2 and MCT 4 were localized in mitochondria in addition to the plasma membrane. LDHA and LDHB were expressed in all the cell-lines, but abundances were higher in the two cancer cell-lines than in the control cells. MCF-7 cells expressed mainly LDHB, while MDA-MB-231 and control cells expressed mainly LDHA. LDH isoforms were localized in mitochondria in addition to the cytosol. These localization patterns were the same in cancerous and control cell lines. In conclusion, MCT and LDH isoforms have distinct expression patterns in two breast cancer cell lines. These differences may contribute to divergent lactate dynamics and oxidative capacities in these cells, and offer possibilities for targeting cancer cells.

INTRODUCTION

Most cancer cells display a Warburg Effect, a state of active glycolysis with lactate production under aerobic conditions (3, 18, 32, 39, 52). Studies of lactate metabolism in humans and rodents have shown that lactate is not only an end product of glycolysis, but is an important fuel for active muscles and other tissues, and may have hormone-like actions (7-9). The operation of lactate shuttles within and among cells, tissues, and organs such as retina, brain, testis, liver, and cardiac and skeletal muscle under fully aerobic conditions is well established (7-9). In skeletal muscle, the Cell-Cell Lactate Shuttle involves the exchange of lactate between glycolytic and oxidative fibers and cardiocytes that actively respire lactate. As well, during physical exercise, lactate released from working muscle and other tissues becomes the main precursor for hepatic gluconeogenesis (4). The Intracellular Lactate Shuttle plays an important role in maintaining the redox balance within cells (7, 9). After transport from cytosol to mitochondria, proximal to the inner membrane, lactate is reconverted to pyruvate, a process that generates NADH to be used by the mitochondrial electron transport chain (ETC), as well as pyruvate to be used by the TCA Cycle, again to produce reducing equivalents for the ETC (26). Functioning of the intracellular lactate shuttle in muscle may be facilitated by the presence of a mitochondrial lactate oxidation complex (mLOC) comprised of monocarboxylate transporter-1 (MCT1), it's chaperone basigin (CD147), lactate dehydrogenase (LDH), and cytochrome oxidase (COx) (26). More recent studies suggest that lactate may also be oxidized to pyruvate by an intermembrane space mitochondrial lactate oxidase and produce hydrogen peroxide (13), a reactive oxygen species with second messenger properties implicated in diverse cellular processes (19, 48, 55) including carcinogenesis (6, 11) and metastasis (36, 43).

While lactate accumulation is characteristic of cancer cells, there is no consensus on its cause. Some researchers postulate that lactate production by tumors is due to exaggerated glycolysis, while others suggest that lactate accumulation is due to limited clearance capacity imposed by impaired capability for oxidative phosphorylation (30, 41, 49). Lactate production has been proposed as a marker for malignancy in some human cancers and is associated with poor outcome (57). In normal- and patho-physiology, MCTs are the major gateways for lactate trafficking between and within cells (40, 42). The fact that cancer cells also express MCTs like normal cells suggests that these transporters might facilitate lactate exchange and be involved in cancer proliferation. However, little research has been done to detail the roles of MCTs and related proteins in cancer.

Breast tissue expresses lactate transporter proteins, and the plasma membrane abundances of these proteins change significantly in cancer. The MCT4 gene is upregulated in the breast cancer cell line MDA-MB-231 (21), and the MCT1 gene promoter is reported to be hypermethylated in 4 of 19 breast cancer tissues (1). The gene encoding the MCT chaperone, Basigin (CD147), is also upregulated in metastatic breast cancer cells, and has been shown to induce extracellular matrix metalloproteinase, and play a role with MCT4 in cancer cell invasion (21, 60). The intracellular localization of MCTs may also play a role transducing the changes in lactate concentrations. In healthy slow red oxidative myofibers, MCT1 exists in mitochondrial and plasma membranes (10, 15, 29). In skeletal muscle, peroxisomal membranes express MCT1 and MCT2 (38). In

fast-glycolytic fibers, MCT4 and MCT1 are localized to the plasma membrane, and mitochondrial abundance of MCT1 is low as the mitochondrial reticulum is sparse (29). Although MCT1 is the only monocarboxylate transporter in the MitoCarta (mitochondrial proteome list) (46), we have found that, depending on area in mammalian brain, either MCT1 or MCT2, or both, are the mitochondrial MCTs (mMCT) (27). However little is known about the distribution of lactate transporters in mitochondrial and plasma membranes in cancerous cells.

Given the recent realization of the crucial role of lactate exchange and metabolism in normal physiology and the prevalence of lactate in tumors, lactate shuttling and MCT proteins emerge as possible targets for cancer treatment. In neuroblastoma cells, blocking MCT1 activity was shown to cause acidosis inside those cells, leading to their apoptotic death. The same study showed that lactate transporters facilitate nutrient exchange, and thereby facilitate cancer cell growth (17). In a different study, MCT1 inhibition was shown to block lactate transport between glycolytic and oxidative regions within tumors of various cancer types, causing death in the centers of the tumors. Lactate transporters were suspected of playing another permissive role on cancer cells growth, that of transporting lactate from the center cells of tumors to be used as energy substrates by the peripheral tumor cells (54). Knowing the differential roles of lactate transporters in normal and cancer cells could offer opportunities for targeting the latter. Therefore, in the effort to extend knowledge of the role of lactate in cancer growth, we sought to identify differences in the expression of MCT and LDH isoforms in two breast cancer cell lines MCF-7 (a lumenal-like breast cell line, estrogen (ER) and progesterone (PGR) receptor positive, and weakly invasive *in vitro*), and MDA-MB-231 (a mesenchymal-like breast cell line, estrogen (ER) and progesterone (PGR) receptor negative, and highly invasive *in vitro*) (33), and the control primary breast cell line HMEC 184 (a 10-25% lumenal-like and 75-90% basal-like breast cell line, and pre-stasis with finite lifespan) (22). In addition, we examined available microarray (12) and MassArray data (44) to extend our findings to a larger set of breast cancer cell lines. Results of our study could contribute to efforts to design better strategies for targeting cancer cells based on lactate transporters and LDH isoforms. Knowing the localization and expression patterns of MCT and LDH may help in efforts to target the cancer cells specifically without killing the normal cells.

MATERIALS AND METHODS

Tissue culture

The human breast cancer cell lines (MCF-7, MDA-MB-231) were a gift from Dr. Gary Firestone, UC Berkeley, and the normal primary-human breast cell line (HMEC 184) was a gift from the Human Mammary Epithelial Cell (HMEC) Bank, Lawrence Berkeley National Laboratory (LBNL). The MCF-7 cell line was grown in high-glucose Dulbecco's Modified Eagle's Medium (DMEM) supplemented with 10% fetal bovine serum (FBS), 1% L-glutamine and 0.25% penicillin-streptomycin and (10 µg/ml) insulin. MDA-MB-231 cell line was grown in high-glucose Iscove Modified Eagle's Medium (IMEM) supplemented with 10% fetal bovine serum (FBS), 1% L-glutamine, and 0.25% penicillin-streptomycin. The HMEC 184 cell line (passage 5-8) was grown in M87A+CT+GFX medium prepared by the Human Mammary Epithelial Cell Bank, LBNL. The M87A+CT+GFX medium contained 50% Mammary Epithelial Basal Medium (MEBM) [supplemented with 5 mg/ml insulin, 70 µg/ml PBE, 0.5 µg/ml hydrocortisone, 5 ng/ml EGF, 5 µg/ml transferrin, 10^{-5} M isoproterenol, 2 nM glutamine)], and 50% DMEM/F12 [supplemented with 10 µg/ml insulin, 10 nM Tri-iodothyronine (T3), 1 nM ß-estradiol (E2), 0.1 µg/ml hydrocortisone, 0.5 % fetal calf serum (FCS), 5 ng/ml EGF, 2 mM glutamine, and 1 ng/ml cholera toxin (CT)], and 0.1 nM oxytocin (GEX) and 0.1% lipid rich bovine serum albumin (albuMaxI). Cells were grown in 5% CO2 atmosphere at 37ºC.

Materials

Chemicals were purchased from Sigma-Aldrich (St. Louis, MO). Tissue culture medium, serum, and reagents were purchased from Gibco (Carlsbad, CA).

Preparation of subcellular fractions and Immunoblots (IB)

Cells were grown in 15 cm dishes until they reached 80-90% confluence, washed with phosphate-buffer saline (PBS), and collected by scraping and brief centrifuging at 700g for 5 min. The subcellular fractions of whole homogenate, cytosolic-enriched and mitochondrial-enriched fractions were prepared as previously described (26). Briefly cells were homogenized in buffer A (250 mM sucrose, 5 mM NaN_3, 2 mM EGTA, 100 µM PMSF, 1 µM pepstatin A, 10 µM Leupeptin, 20 mM HEPES-Na, pH 7.4), using a loose-fitting Dunce (Teflon-glass) homogenizer. Homogenates were centrifuged at 600g for 10 min at 4ºC to remove nuclei and unbroken cells. The pellet was discarded and the supernatant (whole homogenate, WH) was removed, and some was saved for immunoblotting. The rest of the supernatant was centrifuged at 10,000g for 30 min at 4ºC. The supernatant was removed and saved for immunoblotting (Cytosolic fraction, Cyto). The pellet was washed with buffer A and repelleted by centrifuging at 10,000g for 30 min at 4ºC. This pellet was washed once in buffer C (1 mM EDTA and 10 mM Tris, pH 7.4), then resuspended in buffer C with 1% NP-40 (mitochondrial fraction, MI). Protein concentration was determined using a BCA protein assay kit (Pierce Biotechnology, Radford, IL). Western blotting was performed as previously described (26), and the same amount of total protein (30 µg) was loaded in each well. Briefly, samples were diluted with LDS sample buffer (Invitrogen, Grand Island, NY), and incubated in a 70 ºC water bath for 10 min. Samples and the molecular weight standard,

MagicMark XP (Invitrogen, Grand Island, NY) were separated on a SDS-PAGE gel, then transferred to a polyvinylidene fluoride membrane (GE Healthcare, Amersham, Piscataway, NJ). The membrane was blocked with 10% milk in TTBS buffer (0.1 M NaCl, 0.1 M Tris pH 7.5, 0.1 % Tween 20) for 1h, and then incubated with primary antibody with 10% milk in TTBS for 2h. Next, the membrane was washed 3 times with TTBS buffer, then incubated with a second antibody in 10% milk in TTBS for 1h. Finally, the membrane was washed 3 times with TTBS buffer, then incubated with a chemiluminescence reagent kit (ECL plus kit, GE Healthcare, Amersham, Piscataway, NJ) for 5 min, then exposed to X-ray film (GE Healthcare, Amersham, Piscataway, NJ). Primary antibodies used were rabbit anti-MCT1, and rabbit anti-MCT4 (Brooks, polyclonal custom antibody), rabbit anti-MCT2 (Chemicon International, Temecula, CA), rabbit and mouse anti- cytochrome oxidase subunit IV, and goat anti-LDH, that reacts with all LDH isoforms (Fig. 1E, Abcam, Cambridge, MA), rabbit anti-LDHA and rabbit anti-LDHB (Sigma- Aldrich, St. Louis, MO), goat anti-CD147 (Research Diagnosis, Flanders, NJ), rabbit anti-ß-actin, mouse anti-GAPDH (Imgenex, San Diego, CA), mouse anti-Na^+-K^+-ATPase-α (Upstate, Millipore Corporate, MA), rabbit anti-GLUT1, and rabbit anti-TGFß-R2 (Santa Cruz Biotechnology, Santa Cruz, CA). Band intensity was quantified by BioRad GS-700 Densitometer. The band used for densitometer quantification was marked by underlining the molecular weight standard that corresponded to its size in Fig 1.

Confocal Laser Scanning Microscopy (CLSM)

Cells grown on cover slips were washed with PBS and fixed with acetone on ice for 5 min. Cells were washed with PBS and permeabilized with 0.2% Trition X-100 for 5 min. Cells were blocked with 2% FBS for 1h, then incubated with primary antibodies overnight at 4°C. Cells were washed with PBS and incubated with secondary antibodies for 1h, then washed with PBS and H_2O and mounted using Vectashield (Vector laboratories, Burlingame, CA). The primary and secondary antibodies were used as previously described (26). Primary antibodies used were rabbit anti-MCT1, rabbit anti-MCT4, rabbit anti-MCT2, rabbit and mouse anti-cytochrome oxidase subunit IV, and goat anti-LDH (the same antibodies as described for Western blotting). The secondary antibodies were anti-rabbit Alexa fluor 488 conjugate secondary antibody (Molecular Probes), anti-mouse Cy3 (Chemicon International), and anti-goat Alexa fluor 546 conjugated secondary antibodies (Molecular Probes, Invitrogen, Grand Island, NY). An oil immersion objective on Zeiss 510 META (Zeiss 63x/1.4 numerical aperture) was used. Images represent optical slices of ~1 µm. Linear adjustments of contrast and brightness were not applied. Hence, images are not contrast enhanced.

Lactate measurements

Cells were seeded on 60 mm dishes at 4.6 x 10^5 cells/dish and allowed to grow for 3 days to reach 80-90% confluence. Cells were washed with PBS and incubated with IMDM without phenol red and supplemented with 10% fetal bovine serum (FBS), 1% L-glutamine and 0.25% penicillin-streptomycin, and with/without 10 mM oxamate (Oxa) [LDH inhibitor] and 50 µM iodoacetate (IAA) [glycolysis blocker]. The medium (350 µl) was collected and added to 100 µl of 7% perchloric acid (PCA) at time 0, 1, 2, 3, 4, and 5h. Cells were washed with PBS and collected by scraping and brief centrifuging, and

total protein concentration was measured by BCA protein assay kit (Pierce Biotechnology, Radford, IL). Lactate concentration (μM) was measured by spectrophotometry (24), and normalized to total protein concentration (μg). Lactate standards were made with sodium L-lactate in IMDM (without phenol red and supplemented as mentioned above). Lactate standards (350 μl) were added to 100 μl of 7% perchloric acid (PCA). Samples and lactate standards were centrifuged at 3000g for 10 min at 4ºC, and the pellets were discarded and the supernatants saved. Samples or lactate standards (25 μl) were incubated with 250 μl of reaction buffer (0.5 M glycine, 2 % hydrazine hydrate, pH 9, 2.6 units of L-lactate dehydrogenase, 3.0 mM nicotinamide adenine dinucleotide, NAD^+) for 40 min at 37°C in 96 wells plate. The plate was allowed to cool for 20 min, and then the absorbance was determined at 340 nm using a SPECTRA MAX spectrophotometer (Molecular Devices, Sunnyvale, CA).

Oxygen consumption measurements

Oxygen consumption of intact MCF-7, MDA-MB-231, and HMEC 184 cells was measured using a Clark-type oxygen electrode (Rank Brothers Ltd, Cambridge, England) and LabVIEW software (National Instruments, TX) was used to record the data as described previously (16). Briefly, Fresh medium was allowed to equilibrate in the sample chamber at 37°C before adding the trypsinized cells (5- 8 x 10^6 cells) from 10 mm dishes. The chamber was tightly closed and a record of endogenous oxygen consumption was obtained for 15 minutes. Carbonyl cyanide m-chlorophenylhydrazone (CCCP, 10, 5, 2.5 μM final concentration was added to MCF-7, HMEC 184, MDA-MB-231 cells, respectively), and a record of maximum uncoupled oxygen consumption was obtained for 10 minutes. CCCP was added to MDA-MB-231 cells by titration. Data were normalized to total cell number, which was determined by hemacytometer. One-way analyses of variance (ANOVA) were used to compare the means of the groups. If a significant F value ($p<0.05$) was obtained, a Dunnett's test was performed using HMEC 184 as the control while maintaining α at 0.05. As well, selected Student's t-tests were used to evaluate significance differences between cancer cell lines ($p<0.05$).

LDH isoforms analysis by electrophoresis

LDH isoforms in cytosolic (Cyto) and mitochondrial (MI) fractions from MCF-7, MDA-MB-231, and HMEC 184 cell lines were separated on 1% agarose gels as described previously (10). Briefly, 1% agarose gel was prepared and equilibrated in TAE electrophoresis buffer (40 mM Tris acetate, 1 mM EDTA) for 1h. Samples containing 12 mg of total protein were diluted in sample buffer (20% glycerol, 0.05% bromophenol blue, 80% TAE buffer). Samples and LDH marker (LDH Isotrol, Sigma) were separated by electrophoresis at 90 V for 30 min. The LDH bands were stained and visualized with colorimetric procedure (Sigma Procedure 705). The gel was fixed in methanol-acetic acid solution (5 parts acetic acid, 75 parts methanol, 20 parts water) for 30 min. The gel was washed with distilled water for 30 min, then dried for 15-30 min in a forced air incubator at 37°C, then scanned using a Bio-Rad GS-700 imaging Densitometer.

RESULTS

CD147, MCT, and LDH isoforms were detected by immunoblotting.

Figure 1 is a montage of images compiled from individual Western blot images of MCT1, MCT2, MCT4, LDHA, LDHB, and CD147 proteins. Relative protein abundances with the predicted MWs, identified by the specified antibodies, are shown to facilitate comparisons. Protein levels in whole homogenate and mitochondrial fractions were normalized to ß-actin expression, and their expression levels in the two cancer cell lines (MCF-7 and MDA-MB-231) were compared to those in the control cells HMEC 184 cell line; the fold changes of the examined proteins were reported in Figure 1H. To show relative abundances left- and right-hand plates show unsaturated and saturated autoradiograms, respectively. The MCT1 blot showed a single band at 40 KDa (Fig. 1A). MCT1 expression was lower in MCF-7 and MDA-MB-231 compared to HMEC 184 (Fig. 1H). The MCT2 blot shows multiple bands around 40 KDa (Fig. 1B). The mitochondrial fractions also showed two major bands of MCT2 at 50 KDa in all three cell lines; these mitochondrial bands were heavier than the MCT2 proteins that were localized to the plasma membrane. MCT 2 expression was higher in MCF-7 compared to MDA-MB-231 and HMEC 184 cells (Fig. 1H). MCT4 was expressed in higher amounts in MDA-MB-231 than in MCF-7 and HMEC 184 cells (Fig. 1H). MCT4 showed two unique bands at 40 and 25 KDa (Fig. 1C). CD147 was expressed in three cell lines and had two major bands at 40 and 60 KDa, which represent the core-glycosylated, and the fully glycosylated forms respectively (Fig. 1D). The CD147 protein was more highly expressed in MDA-MB-231 than in HMEC 184 and MCF-7 (Fig. 1H).

LDH was highly expressed in cancerous cell lines (Fig. 1E, 1H), but the LDHA protein was mainly expressed in MDA-MB-231 and HMEC 184 (Fig. 1G, 2), while the LDHB isoform was mainly expressed in MCF-7 (Fig. 1F, 2). LDH isoenzymes separated by electrophoresis on agarose gels confirmed this result (Fig. 2). Using an LDH antibody that reacts with all five LDH isoenzymes (Fig. 1E), LDH blots showed unique size bands in mitochondrial fractions of three cell lines, different from the cytosolic LDH, and MCF-7 showed a unique band of LDH at 28 KDa (Fig. 1E).

Subcellular assessments show mitochondrial fractions to contain Na^+-K^+-ATPase.

Whole homogenate (WH), cytosolic (Cyto), and mitochondrial (MI) cell fractions were isolated from human breast cancer cell lines (MCF-7, MDA-MB-231) and normal primary human breast cell line (HMEC 184). Figure 3 shows that the mitochondrial fractions were rich with mitochondrial protein COxIV. Despite our best efforts at mitochondrial isolation, probing mitochondrial fractions showed strong signals for the plasma membrane maker, Na^+-K^+-ATPase-α, a small, but observable signal for GLUT1 protein in the mitochondrial fraction of MDA-MB-231 cells, but no signal for TGFß-R2. Importantly, mitochondrial preparations were negative for the cytosol marker GAPDH. The absence of TGFß-R2, but variable presence of Na^+-K^+-ATPase and GLUT1 proteins in the mitochondrial fraction of MDA-MB-231 cells may have resulted from small and variable levels of plasma membrane fragments that coalesce with mitochondrial membranes during isolation. Alternatively, those plasma membrane marker proteins may be functionally associated with the mitochondrial reticulum, *in vivo*. We previously reported the presence of Na^+-K^+-ATPase in mitochondrial fractions of primary neuronal

cultures (27), and concluded that rather than indicating contamination, Na^+-K^+-ATPase may be connected to outer mitochondrial membranes. The same association was also reported by others (58). Seemingly, it would be an advantage for the endergonic Na^+-K^+-ATPase system, which maintains the plasma membrane cationic gradients, to be associated with the system for maintaining cellular ATP homeostasis. The contamination of mitochondrial fractions by other cell compartments was not tested for because MCT and LDH were mainly found in plasma membrane, mitochondria, and cytosol.

MCTs and LDH localization by confocal laser scanning microscopy (CLSM).

Using confocal laser scanning microscopy, we found that MCT1 was mainly expressed in the plasma membrane in HMEC 184 and MCF-7 cell lines (Fig. 4B, 5B). MCT2, MCT4, and LDH were found to be co-localized with COxIV antibody in the mitochondria of the three cell lines that were tested (Figs 4, 5, 6). The localizations of MCT1, MCT2, MCT4, and LDH in cancerous cells were similar to those in control cells (Fig. 4, 5, 6).

Lactate accumulation is higher in cancer cells, and the oxygen consumption is higher in control cells.

Lactate accumulation in HMEC 184, MCF-7, and MDA-MB-231 cell lines was measured (Fig. 7 A, B, C). Cells were incubated with IMDM media with or without 40 mM oxamate (Oxa), a LDH inhibitor, and 50μM iodoacetate (IAA), a blocker of glycolysis. Lactate accumulation was significantly lower in dishes that were incubated with IAA or oxamate compared to control, but higher in cancerous cell lines than control cell lines. Lactate accumulation was highest in the MCF-7 cell line, and lowest in the HMEC 184 cell line. Oxygen consumption measurements showed that the three cell lines have different basal (endogenous) and maximum (max) respiratory rates (Fig. 7 D, E, F). Interestingly, MCF-7 had a higher endogenous respiratory rate than did MDA-MB-231. The HMEC 184 cell line had the highest endogenous and max respiration rates. In aggregate, results suggest that cancer cells display both increased rates of lactate production and reduced capacities for oxidative disposal.

Available Microarray Databases

To expand our findings to a larger set of breast cancer cell lines, we examined the microarray data of Charafe-Jauffret *et al.* (12) for the expression of MCT and LDH isoforms, as well as the MassArray data of Novak *et al.* (44) for MCT methylation status in cancer cells. Two-fold changes were taken to be significant. Charafe-Jauffret *et al*. used 31 breast cell lines (BCL), in which all but three were cancerous: MCF-10A, which is derived from a fibrocystic disease, and HME-1 and 184B5, which were derived from normal mammary tissue. The expression profiles of MCT1, MCT4, LDHA, and LDHB were reported in their supplementary Table 1, but MCT2 and CD147 were not annotated. MCT1 was identified as one of 1,233 marker genes, which are differentially expressed between the luminal-like and the basal-like breast cell lines. MCT1 was highly expressed in basal-like breast cell lines. By comparing the MCT1 mRNA expression levels of all cancerous cell lines to the three normal cell lines in the data of Charafe-Jauffret *et al.*, we found a significant decrease in MCT1 mRNA expression level in cancer cell lines compared to the there normal cell lines. MCT4 also showed a trend of lower expression

in cancerous cell lines in the data of Charafe-Jauffret *et al*., but there were some exceptions such as MDA-MB-231 and five other cell lines, which showed increased mRNA expression levels. MCT2 was not found in Supplemental Table 1 of Charafe-Jauffret *et al*., but MCT2 was one of the marker genes that were highly expressed in mesenchymal-like cell lines compared to luminal-like cell lines. LDHA showed little change in cancerous cells that did not pass the two-fold limit set to assess significance. LDHB expression was lower in many cancerous cells compared to the three normal cell lines, and appeared to be a marker gene that was highly expressed in the mesenchymal breast cell lines compared to luminal-like cancer cell lines.

Novak *et al.* had exposed three primary breast cell lines (48RT, 184D, 240LD) to different treatments or genetic manipulations that allow them to pass stasis and telomere dysfunction barriers to acquire immortality. By examining MassArray data in their Supplemental Table 2, we saw that MCT1 promoter hypermethylation appeared in an early stage of cancer development after passing the stasis barrier in some cell lines (48RS and 184B), and MCT1 promoter hypermethylation was significant after passing the telomere dysfunction barrier (184B5, 184AA2, 184A1-RF, 184B5ME, 184ZNMY3, 184ZNMY3-N). No change in MCT2 and MCT4 methylation status was seen in any of the cell lines used in the MassArray data of Novak *et al*.

DISCUSSION

In this study, the expression and the localization of MCT and LDH isoforms in two breast cancer cell lines, MCF-7 and MDA-MB-231, and the control primary breast cell line, HMEC 184, were examined. We show that MCT (1, 2, and 4), and LDH isoforms (A and B) are expressed in both control and cancerous breast cells occupying both mitochondrial and extra-mitochondrial cell compartments. Our results generated three main conclusions that are discussed in more detail below: 1) breast cancer appears to change the expression of lactate shuttle proteins, but not their sub-cellular localizations; 2) changes in the expression lactate shuttle proteins are associated with decreased oxidative capacity and an increased lactate accumulation within breast cancer cells, and 3) our data and those of others indicate that MCT1 expression is down-regulated in breast cancer cells in general.

Breast cancer appears to change the expression of lactate shuttle proteins, but not their sub-cellular localizations

The existence of MCT and LDH proteins in mitochondria in different healthy tissues was reported previously by us (10, 26), and others (2, 5, 35), and supported by the MitoCarta list (46). However, for first time we report on the presence of MCT and LDH isoforms in the mitochondrial reticula of breast cell lines. Our data show that MCT (1, 2, and 4), and LDH (A and B) isoforms are expressed in both control and cancerous breast cells occupying both mitochondrial and extra-mitochondrial cell compartments. An exception is that MDA-MB-231 did not express MCT1 as determined by either of two methods (Figs. 1A and 6). The expression of MCT and LDH isoforms in each cell line was unique. MCT1 was highly expressed in the primary-human breast cell line HMEC 184 (Fig. 1A), MCT2 was highly expressed in MCF-7 cell lines (Fig. 1B), MCT4 was highly expressed in MDA-MB-231 cell lines (Fig. 1C), and LDH was highly expressed in both cancerous cell lines (Fig. 1E). The localization of MCT and LDH isoforms in cancerous and normal cell lines was the same. MCT2, MCT4, and LDH were localized in mitochondria in addition to their localization in plasma membrane and cytosol, respectively (Figs 4, 5 and 6), whereas MCT1 was mainly localized in plasma membrane.

The mechanism of the translocation of MCT and LDH proteins to mitochondria is unclear. MCT1 is the only candidate lactate/pyruvate transporter in the MitoCarta list; further, of the LDH isoforms annotated in the MitoCarta only *LDHAL6B* and *LDH-D* have a mitochondrial TargetP signal. While we know of no report showing MCT1 or MCT4 splice variants, our data show that splicing variants might explain the existence of LDH and MCT2 proteins in mitochondria (Figs 1E and 1B). In skeletal muscle (26), and neurons of some brain areas (27), we have found MCT1 to be expressed in both plasma and mitochondrial membranes. Our new result is that MCT1 is either not found at all in breast cancer cells (e.g., MDA-MB-231), or if found, MCT1 is localized mainly to the plasma membrane as in MCF-7 cells, with only trace amounts in the mitochondrial web. The unique localization of MCT1 mainly in plasma membrane may make it the main facilitator of lactate flow between tumor and stroma cells in breast tissue.

The three cell lines expressed MCT2 and MCT4, which were localized in the mitochondria (Figs 1, 4, 5, and 6). The localizations of MCT1 mainly to plasma membrane, and MCT2 and MCT4 to plasma as well as mitochondrial membranes, is

unique for breast cells. MCT2, which was first found in the liver, has a high affinity for substrates (k_m of 0.1 mM for pyruvate, and k_m of 0.7 mM for lactate), while MCT4, which is highly expressed in highly glycolytic cells, has a low affinity for substrates (k_m of 150 mM for pyruvate, and k_m of 28 mM for lactate) (25). It may be that MCT2 and MCT4 serve to import lactate and pyruvate into mitochondria for oxidation, whereas one or both transporters act to extrude substrate from mitochondria for use in other pathways. In this context, DeBeradinis *et al*., who incubated glioblastoma cells with [1,6-^{13}C2]glucose and [3-^{13}C]glutamate, showed that entries of lactate and pyruvate into the TCA cycle were accompanied by export of labeled citrate, presumably to support fatty acid synthesis, and glutamine was used to replenish the TCA cycle compensating for citrate export (14). Such a pathway in breast cells may exist, and therefore requires further investigation.

Contrary to our expectations, our data do not show changes in LDH or MCT isoform expression or intracellular distribution unique to cancer; rather, the changes we observed appear consistent with the glycolytic and oxidative capacities of cells (26). We discuss our findings within the context of targeting and killing cancer cells *in vivo*.

Changes in the expression of lactate shuttle proteins are associated with decreased oxidative capacity and an increased lactate accumulation within breast cancer cells

The three breast cell lines we studied had different basal endogenous and maximum respiration rates (Fig. 7D, 7E, 7F), with the control HMEC 184 cell line having the highest endogenous and maximum (uncoupler-stimulated) respiration rates, and with MCF-7 having a higher endogenous respiration than MDA-MB-231. Cells of all types responded to CCCP, indicating coupling of oxidative phosphorylation; however, respiration was less well-coupled in both cancer cell lines than the HMEC 184 control cell line (Fig. 7F). As expected from their high LDH expression levels, the two cancer cell lines accumulated more lactate and used less oxygen than did the control cell line HMEC 184. In contrast, the control cell line HMEC 184 had lower LDH and higher MCT1 expression levels than the cancer cell lines. Lactate accumulation in the two cancer cell lines is indicative of high lactate production, low oxidative capacity, or some combination of both factors. Lactate production was also significantly lower in media when cells were incubated with IAA or oxamate compared to control, but higher in cancer than normal cell lines (Fig. 7A, 7B, and 7C). This may mean that lactate production in all the cell lines was mainly generated through glycolysis, but that there were downstream, i.e., mitochondrial defects that disrupt oxidative lactate disposal of lactate. Alternatively, pathways other than glycolysis contribute to high lactate production in cancerous cells lines. For example, enhanced glutamine metabolism has been associated with increased lactate production in cancerous cell lines (14). However, the mechanism of such an effect is undefined.

Our data may be useful in explaining some of the observations of Sonveaux *et al.* (54), who showed that cancer cells express different MCT isoforms and substrates use patterns depending on their localization in a tumor mass. Our result of a lower expression of MCT1 in breast cancerous cells compared to normal cells may be an early-programmed cancer strategy, allowing hypoxic tumor cells to utilize glucose without competing with control cells. The MCT1 inhibitor, α-cyano-4-hydroxycinnamate (CHC), used by us previously to block sarcolemmal lactate transport (50, 51), was used by

Sonveaux *et al.* (54) to reduce tumor volume. We suspect that by blocking MCT1 in normal control cells, Sonveaux *et al*. forced control cells peripheral to the tumor mass to become glycolytic and compete with cancer cells for glucose. We suspect that by virtue of their peripheral location close to the microcirculation, control cells out-competed transformed cancer cells in the tumor core. Our data suggest the possible hypothesis that the high amount of lactate produced by cancer cells acts as a signaling molecule that increases the expression of MCT1 and causes mitochondrial biogenesis in stroma cells surrounding tumors. As with endurance training of muscle, the increased MCT1 expression and oxidative capacity of stroma cells would encourage them to use lactate as their energy source, and spare the glucose for the tumor cells. MCT4 expression in the tumor cells would be up-regulated by hypoxia (56), which increases lactate transport from the cancer cells to the stroma cells. An increase of 10% to 15% in pyruvate and lactate uptake was seen in the cancer cell line MDA-MB-231 when transfected with plasmid containing MCT1 gene (23), and this uptake was accelerated at acidic pH and with an increase in lactate or pyruvate concentration in the incubation media (23). In this way, lactate contributes to the seed and soil hypothesis of Paget (45), by optimizing the microenvironment for tumor growth. That lactate acts as a paracrine signal in carcinogenesis was also proposed by others (30), and the idea is supported by the results of the experiments we now describe. We showed that incubation of rat muscle cell line L6 with lactate increased the expression of MCT1 and COx 4, and 100 genes involved in ROS signaling and mitochondrial biogenesis (28). Lu *et al*. (37) showed that lactate and pyruvate stimulated the accumulation of HIF-1α, and increased the expression of Aldo-A, VEGF, and GLUT-3 in many cancerous cell lines. Fukumura *et al.* (20) showed that VEGF expression increased with acidosis in brain tumor cells, and that this increase was independent of hypoxia.

Our data and Micro- and MassArray data from much larger sets of breast cell lines indicate that MCT1 expression is down-regulated in breast cancer cells in general

To expand our findings to a larger set of breast cancer cell lines, we examined the available microarray data in Charafe-Jauffret *et al*. (12). Charafe-Jauffret *et al*. used 31 breast cell lines (BCL), all of which were cancerous except three: MCF-10A, which is derived from a fibrocystic disease, and HME-1 and 184B5, which were derived from normal mammary tissue. We found that the MCT1 mRNA expression levels in cancer cell lines are lower than those of three control cell lines (184B5, HME-1, MCF-10A). This finding is consistent with our protein expression data, which compared the control primary breast cell line HMEC 184 to the two cancerous cell lines MDA-MB-231 and MCF-7 (Fig. 1H). One limitation of this comparison is that the three normal control breast cell lines used in microarray comparisons were basal-like breast cell lines, which may exaggerate this reduction, as MCT1 is identified by Charafe-Jauffret *et al*. and others (47) as a basal-like breast cell line marker.

MCT4 also showed a trend of lower expression in most cancerous cell lines in Charafe-Jauffret *et al*., but there were some exceptions, such as the MDA-MB-231 cell line and five other cell lines that showed an increase in mRNA expression levels. This result was consistent with the MCT4 protein expression levels we observed in MDA-MB-231 (Fig. 1H), and in other studies (21). MCT4 expression was reported to be upregulated by hypoxia through HIF-1α (56), which may explain its increased expression in some

cancer cells lines. MCT2 was not found in the Supplemental Table 1 of Charafe-Jauffret *et al*., but surprisingly *MCT2* was one of the marker genes that were highly expressed in the mesenchymal cell line as compared with lumenal cells in their Supplemental Table 3. Our results show that in the lumenal-like cell line MCF-7, MCT2 was highly expressed compared to HMEC 184 and MDA-MB-231 (Fig. 1H). In this respect our results are different from those reported by Charafe-Jauffret *et al*.

Our results with two cancerous cell lines showed differences in LDH isoform expression (Fig. 1H), with LDHA mainly expressed in MDA-MB-231, and LDHB mainly expressed in MCF-7 (Fig. 2). These results were inconsistent with those of Charafe-Jauffret *et al*. who showed no significant (i.e., > 2-fold) change in LDHA, but instead observed a reduction in LDHB expression. Transcriptional and post-transcriptional regulation of LDHA mRNA has been previously reported (31, 53), and may explain the differences in LDHA expression observed by Charafe-Jauffret *et al*. and by us. In addition, Charafe-Jauffret *et al*. reported high expression of LDHB in the mesenchymal compared to lumenal-like cell lines, which is inconsistent with our data. LDHA was proposed as a targeting therapy in many cancerous cells (34). However, the data of Charafe-Jauffret *et al*. show that lower expression of LDHB is more characteristic of cancer cells than is the increase in LDHA.

The MCT1 gene is silenced by hypermethylation in MDA-MB-231 cells as well as in 4 of 19 other breast cancer tissues (1). We asked the question whether this hypermethylation occurred in an early or a late stage in cancer development. Novak *et al*. (44) had exposed three primary breast cell lines (48RT, 184D, 240LD) to different treatments or genetic manipulations that allowed them to pass stasis and telomere dysfunction barriers to acquire immortality. By examining their MassArray data in their Supplemental Table 2, we found that MCT1 promoter hypermethylation appeared in an early stage of cancer development after passing the stasis barrier in two of 7 manipulated cell lines (48RS, 184B), and *MCT1* hypermethylation was clearer after cells passed the telomere dysfunction barrier in 6 of 7 manipulated cell lines (184B5, 184AA2, 184A1-RF, 184B5ME, 184ZNMY3, 184ZNMY3-N). However, this early-stage hypermethylation was not associated with MCT1 silencing, as is seen in the 184B5 cell line in the data of Charafe-Jauffret *et al*. That result tells us that MCT1 silencing or reduction is an early programmed step in many breast cancer cells, and not due to random events.

The three cell lines used in this study along with those used by Charafe-Jauffret *et al*. (12), and Novak *et al*. (44), were grown in optimized culture media. However, those culture conditions may not reflect those *in situ*, so a concern is that the *ex vivo* conditions used in research may have affected the observed morphological and genetic changes. In this respect however, Wistuba *et al*. (59) compared the properties of 18 human breast cancer cell lines and their corresponding tumor tissue, and showed a strong correlation between the two groups after 25 months of culture (12).

MCT inhibition provides a promising treatment for cancer. Nevertheless, we caution that inhibition of either MCT or LDH isoforms needs further investigation, and should be regarded with caution because all cells in the body express MCT and LDH isoforms. Importantly also, our data show that MCT and LDH isoforms are localized in mitochondrial fraction in both cancer and normal cells, and that this localization is not changed in cancer. These results are consistent with our previous findings (26, 27) which

showed that MCT and LDH exist in mitochondria of muscle and brain cells. Hence, inhibiting lactate shuttle proteins would effect the normal function of mitochondria of may cell types including neurons. As far as targeting Lactate Shuttle proteins as a means to disrupt tumor cells is concerned, we conclude that development of effective means to kill cancer cells by interfering with lactate shuttling *in vivo* will require better understanding of the unique roles of MCTs and other mLOC proteins in cancer.

ACKNOWLEDGEMENTS

We thank Dr. Kishorchandra Gohil and Xiying Fan for their comments on our paper. We thank our undergraduate students Tina Xu and Michael Krugly for their help with tissue culture work. We thank Dr. Gary Firestone for the gift of cancer cell lines and Drs Martha Stampfer and James Garbe for their advice on culturing primary-human breast cell lines. We thank Holly Aaron for assistance in microscopy. Images were taken at the Molecular Imaging Center facility in the Cancer Research Laboratory at UC Berkeley. This work was supported by NIH grant AR050459 and a gift from CytoSport, Inc.

FIGURES

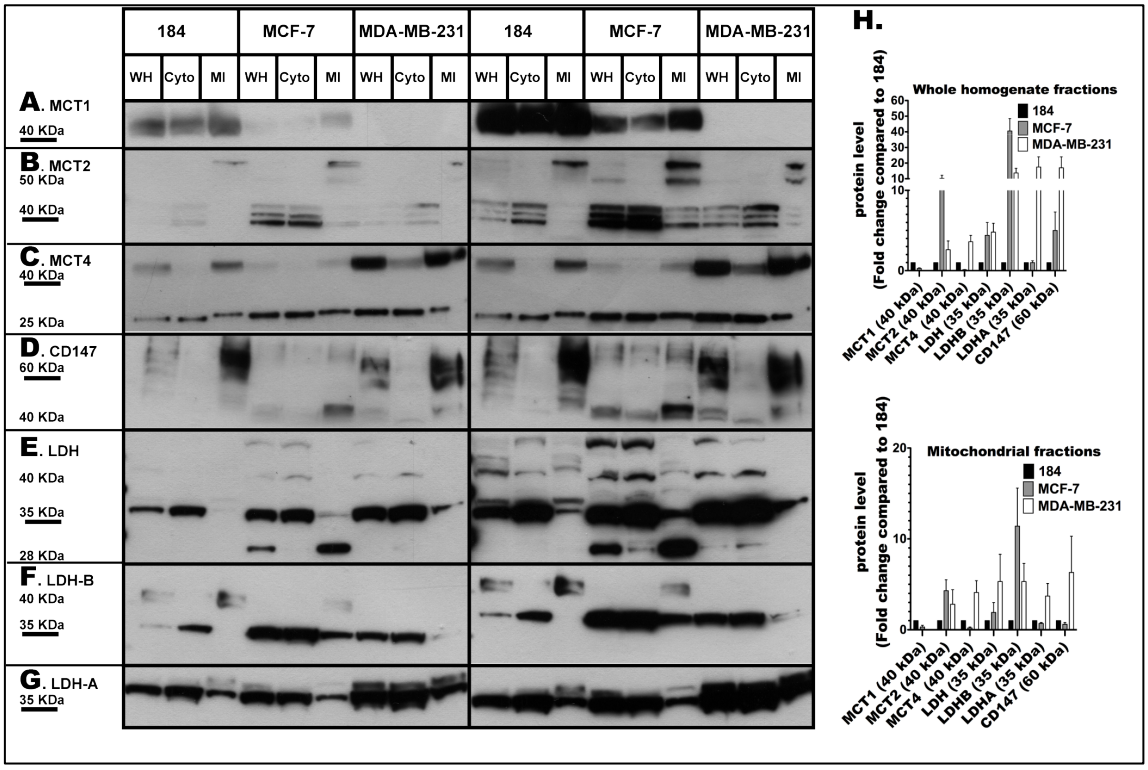

Figure 1. Expression of CD147 and MCT and LDH isoforms detected by immunoblotting. To show relative abundances left- and right-hand plates show unsaturated and saturated autoradiograms, respectively. The expression of MCT1 (A), MCT2 (B), MCT4 (C), CD147 (D), total LDH (E), LDHB (F), and LDHA (G) in whole homogenates (WH), cytosolic fractions (Cyto), and mitochondrial fractions (MI) from one control (HMEC 184), and two cancerous breast cell lines (MCF-7, MDA-MB-231). All cell lines expressed lactate transporters (MCT1, 2, 4) in WH and MI fractions except MDA-MB-231, which did not express MCT1. An LDH antibody that reacts with all LDH isoforms was used in (E). LDH was found in both Cyto and MI fractions of all cell lines. The same amount of total protein was loaded (30 μg) in each well. The fold changes in the expression levels of lactate shuttle proteins in whole homogenate fraction and mitochondrial fraction in the two cancerous cell lines were compared to the control cell line (H). The band of interest that was used for densitometer quantification was marked by underlining the molecular weight standard that corresponded to its size in (A, B, C, D, E, F, G), and was reported in (H). Data are derived from the average of four different experiments ±SEM.

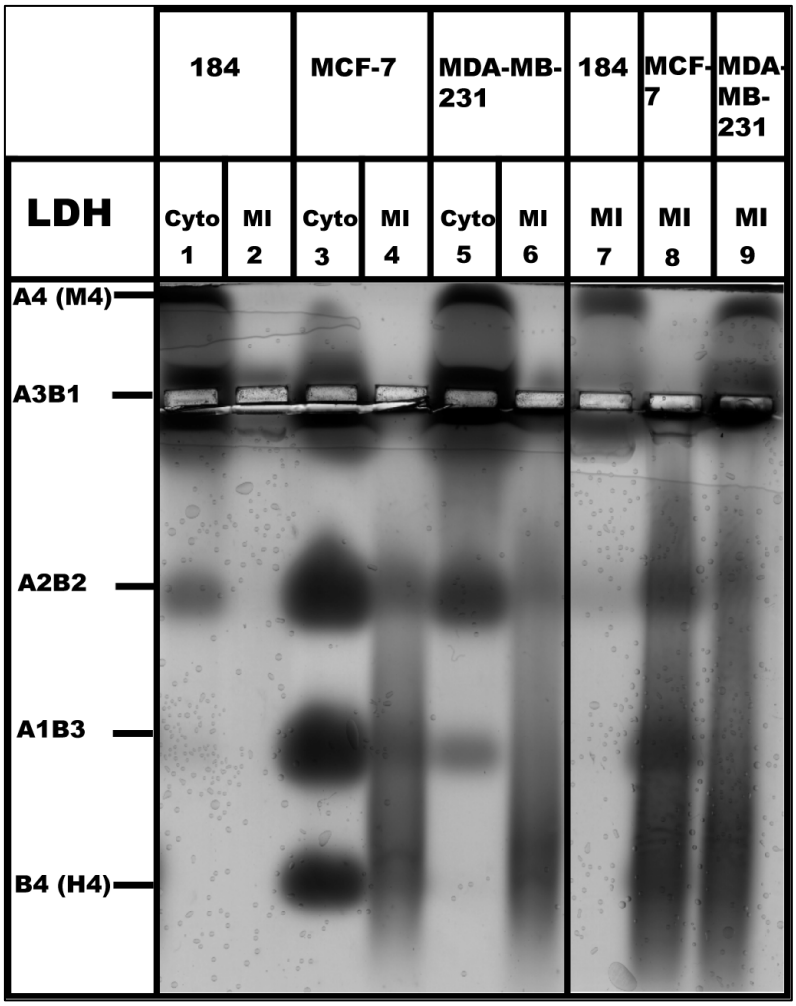

Figure 2. Gel electrophoresis analysis of LDH isoforms. LDH isoforms from cytosolic fractions (Cyto) and mitochondrial fractions (MI) in control primary breast cell line (HMEC 184), and breast cancer cell lines (MCF-7, MDA-MB-231) were separated by agarose gel electrophoresis. Total protein of 12 µg was loaded in wells (1, 2, 3, 4, 5, and 6), and 48 µg in wells (7, 8, and 9). The MCF-7 cell line expressed mainly LDHB, an LDH isoform found in oxidative cell lines. The HMEC 184 and MDA-MB-231 cell lines expressed mainly LDHA, an LDH isoform found in glycolytic cell lines. Data are from two different experiments.

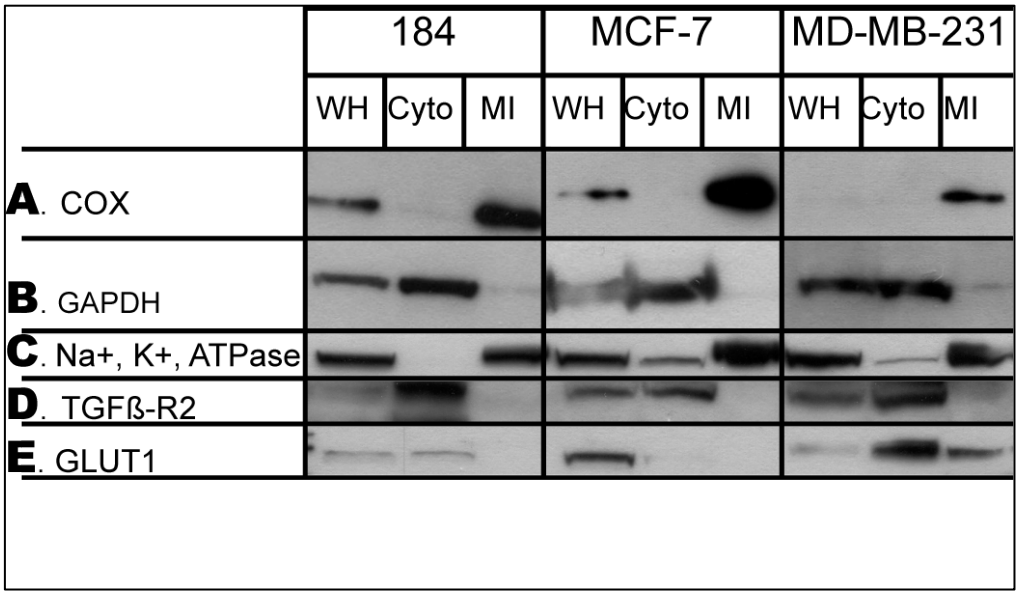

Figure 3. Assessment of subcellular contamination. Representative Immunoblots showing expressions of (A) COx, (B) GAPDH, (C) Na^{+}-K^{+}-ATPase-α, (D) TGFß-R2, and (E) GLUT1 in whole homogenates (WH), cytosolic fractions (Cyto) and mitochondrial fractions (MI) from normal primary breast cell line (HMEC 184) and breast cancer cell lines (MCF-7, MDA-MB-231). Mitochondrial fractions (MI) were rich with the mitochondrial marker COx-IV, and showed the presence of plasma membrane marker Na^{+}-K^{+}-ATPase-α in all mitochondrial fractions, and the presence of plasma membrane marker GLUT1 in the mitochondrial fraction of MDA-MB-231 cells, but no signal of plasma membrane marker TGFß-R2. There were undetectable amounts of the cytosolic marker GAPDH in mitochondrial fractions.

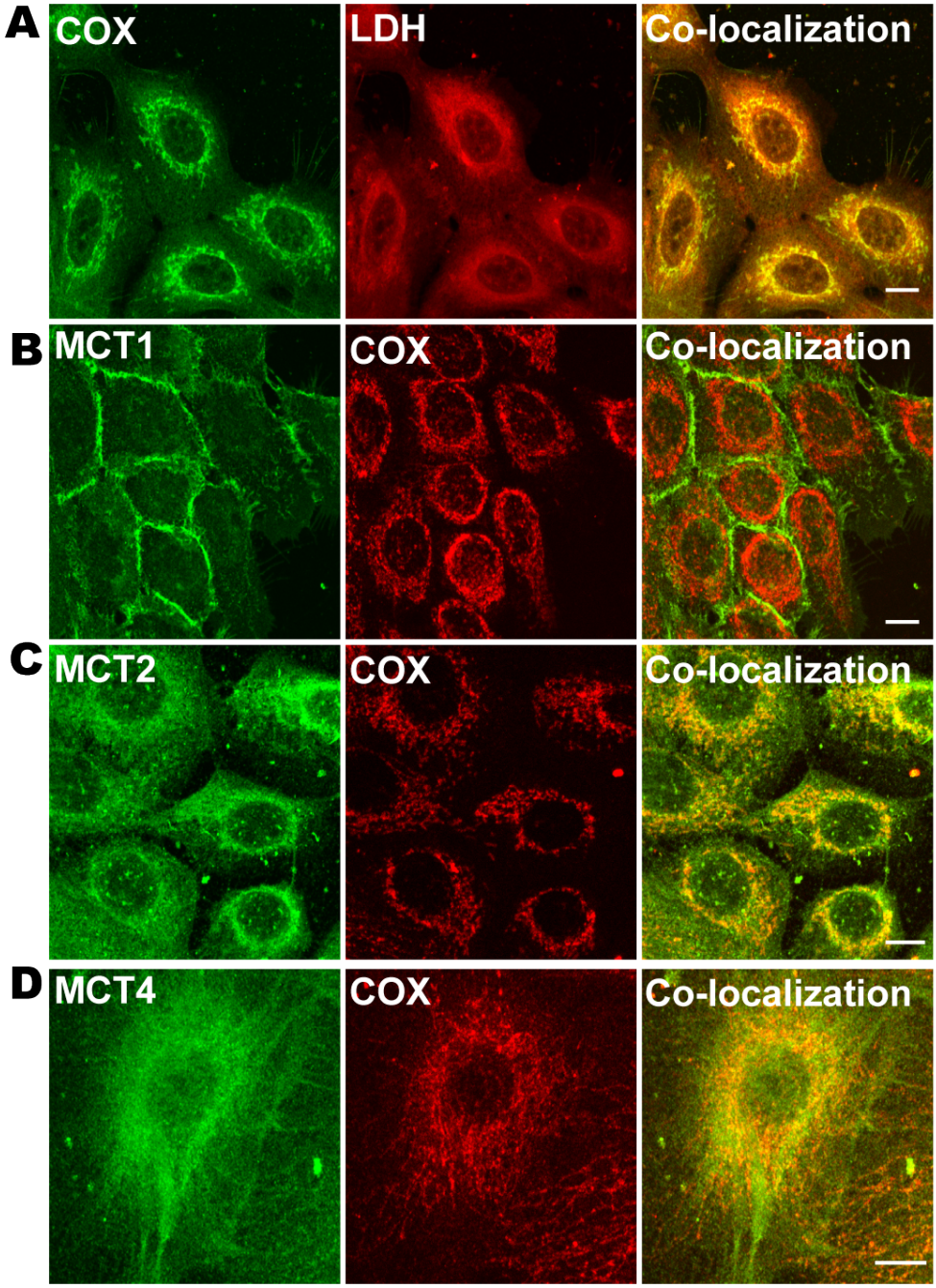

Figure 4. Immunohistochemical detection of MCT, LDH isoforms, and COx in control breast cell line HMEC 184. LDH isoforms, MCT2, and MCT4 were co-localized with mitochondrial protein marker COx (A, C, D), but MCT1 was not, and was localized mainly in the plasma membrane (B). The thickness of the optical section ~ 1 μm, scale bar = 10 μm.

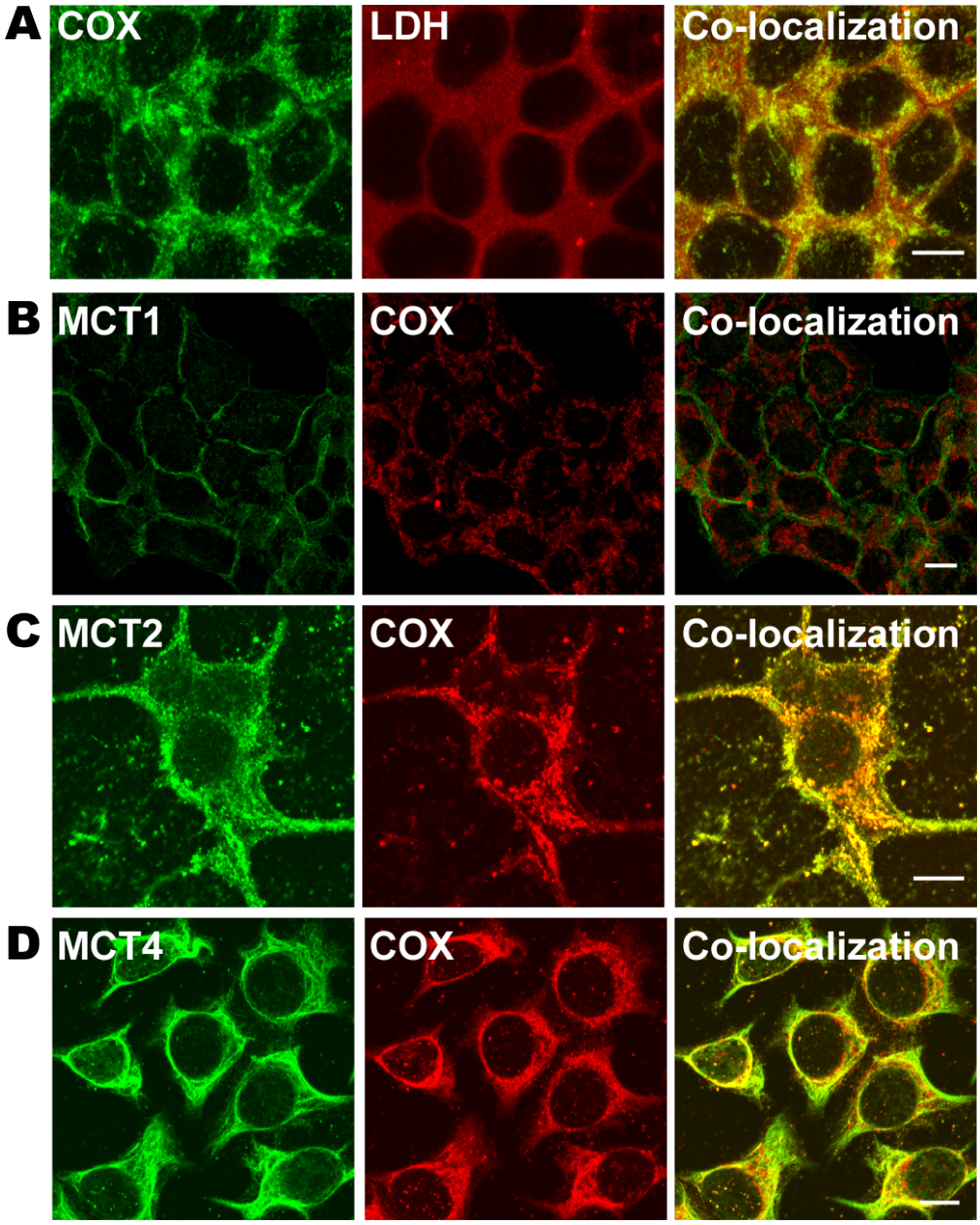

Figure 5. Immunohistochemical detection of MCT, LDH isoforms, and COx in breast cancer cell line MCF-7. LDH isoforms, MCT2, and MCT4 were co-localized with mitochondrial protein marker COx (A, C, D), but MCT1 was not, and was localized to the plasma membrane (B). The thickness of the optical section ~ 1 μm, scale bar = 10 μm.

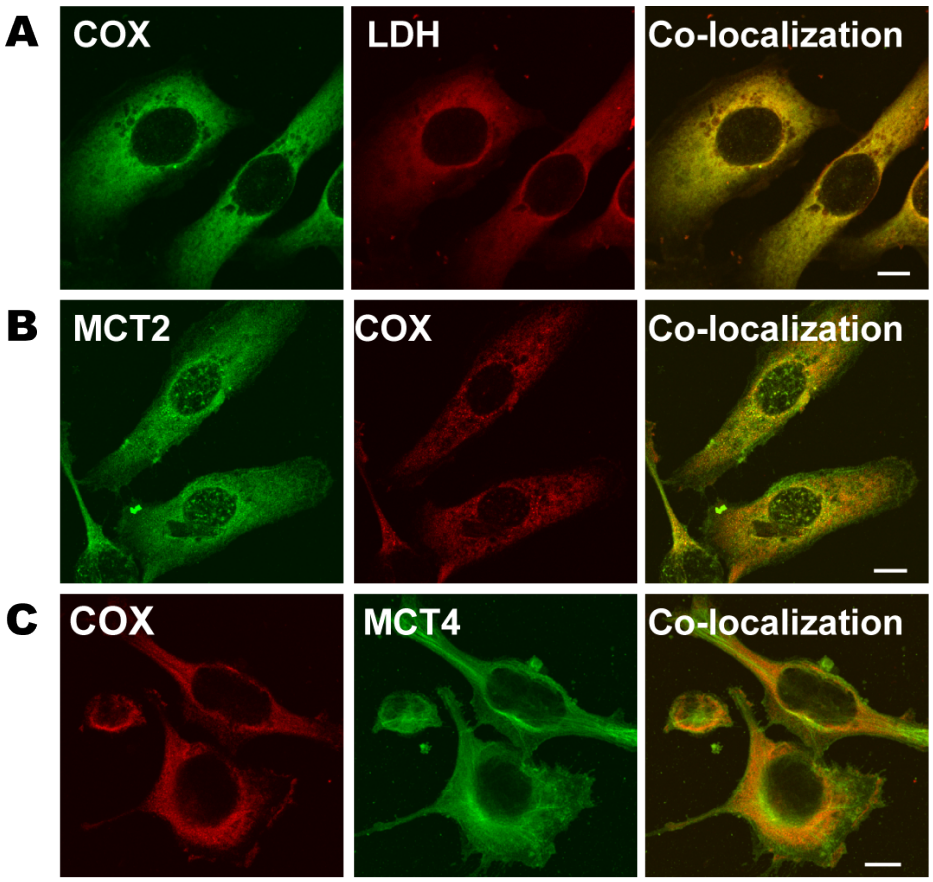

Figure 6. Immunohistochemical detection of MCT, LDH isoforms, and COx in breast cancer cell line MDA-MB-231. LDH isoforms, MCT2, and MCT4 were co-localized with mitochondrial protein marker COx (A, C, D). MCT 1 was not expressed in MDA-MB-231 cells. The thickness of the optical section ~ 1 μm, scale bar = 10 μm.

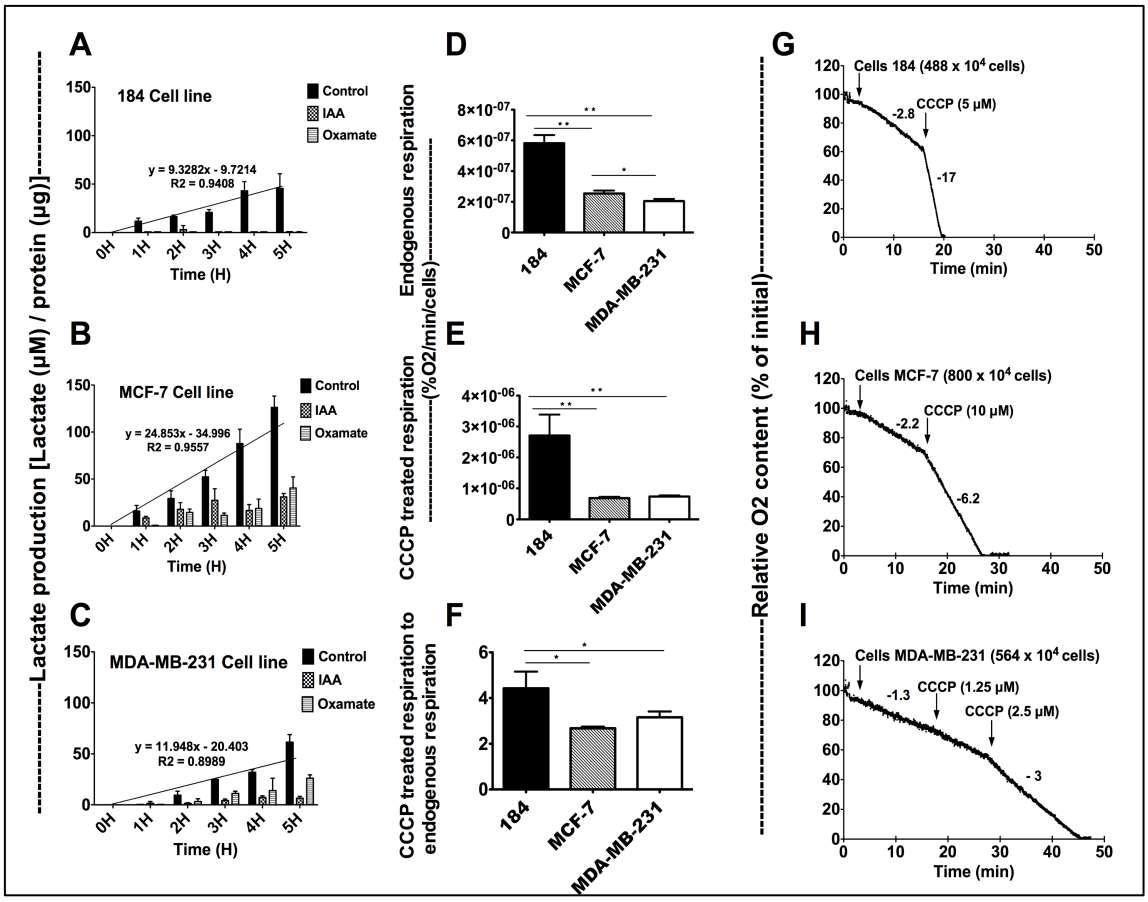

Figure 7. Lactate production is higher in cancer cells, and the oxygen consumption is higher in control cells. Lactate production (µM) per hour in HMEC 184 (A), MCF-7 (B), and MDA-MB-231(C) cell lines was normalized to total protein concentration (µg). Lactate production rates are represented by histogram bars and diagonal slope. Cells were incubated with media with and without 40 mM oxamate (Oxa), a LDH inhibitor, and 50 µM iodoacetate (IAA), a glycolysis blocker. Lactate production was higher in control, IAA, and oxamate dishes of cancerous cell lines compared to the control cell line. The respiration in control and cancerous cell lines were measured (A, B, C). The endogenous respiration (D), CCCP (uncoupler) treated respiration (E), and CCCP treated respiration to endogenous respiration ratio (F) were calculated by measuring the oxygen consumption in HMEC 184 (G), MCF-7 (H), and MDA-MB-231 (I) cell lines. The MCF-7 cell line had higher endogenous respiration rate than did MDA-MB-231. The HMEC 184 cell line has the highest endogenous and max respiration rates. Data are mean ± SEM. * Significantly different between groups. * $P < 0.05$, **$P < 0.001$.

REFERENCES

1. Asada K, Miyamoto K, Fukutomi T, Tsuda H, Yagi Y, Wakazono K, Oishi S, Fukui H, Sugimura T, and Ushijima T. Reduced expression of GNA11 and silencing of MCT1 in human breast cancers. *Oncology* 64: 380-388, 2003.
2. Baba N, and Sharma HM. Histochemistry of lactic dehydrogenase in heart and pectoralis muscles of rat. *J Cell Biol* 51: 621-635, 1971.
3. Bayley JP, and Devilee P. Warburg tumours and the mechanisms of mitochondrial tumour suppressor genes. Barking up the right tree? *Curr Opin Genet Dev* 20: 324-329, 2010.
4. Bergman BC, Horning MA, Casazza GA, Wolfel EE, Butterfield GE, and Brooks GA. Endurance training increases gluconeogenesis during rest and exercise in men. *Am J Physiol Endocrinol Metab* 278: E244-251, 2000.
5. Brandt RB, Laux JE, Spainhour SE, and Kline ES. Lactate dehydrogenase in rat mitochondria. *Arch Biochem Biophys* 259: 412-422, 1987.
6. Brigelius-Flohe R, and Kipp A. Glutathione peroxidases in different stages of carcinogenesis. *Biochim Biophys Acta* 1790: 1555-1568, 2009.
7. Brooks GA. Cell-cell and intracellular lactate shuttles. *J Physiol* 587: 5591-5600, 2009.
8. Brooks GA. Intra- and extra-cellular lactate shuttles. *Med Sci Sports Exerc* 32: 790-799, 2000.
9. Brooks GA. Lactate shuttles in nature. *Biochem Soc Trans* 30: 258-264, 2002.
10. Brooks GA, Dubouchaud H, Brown M, Sicurello JP, and Butz CE. Role of mitochondrial lactate dehydrogenase and lactate oxidation in the intracellular lactate shuttle. *Proc Natl Acad Sci U S A* 96: 1129-1134, 1999.
11. Cerutti PA. Prooxidant states and tumor promotion. *Science* 227: 375-381, 1985.
12. Charafe-Jauffret E, Ginestier C, Monville F, Finetti P, Adelaide J, Cervera N, Fekairi S, Xerri L, Jacquemier J, Birnbaum D, and Bertucci F. Gene expression profiling of breast cell lines identifies potential new basal markers. *Oncogene* 25: 2273-2284, 2006.
13. de Bari L, Valenti D, Atlante A, and Passarella S. L-lactate generates hydrogen peroxide in purified rat liver mitochondria due to the putative L-lactate oxidase localized in the intermembrane space. *FEBS Lett* 584: 2285-2290, 2010.
14. DeBerardinis RJ, Mancuso A, Daikhin E, Nissim I, Yudkoff M, Wehrli S, and Thompson CB. Beyond aerobic glycolysis: transformed cells can engage in glutamine metabolism that exceeds the requirement for protein and nucleotide synthesis. *Proc Natl Acad Sci U S A* 104: 19345-19350, 2007.
15. Dubouchaud H, Butterfield GE, Wolfel EE, Bergman BC, and Brooks GA. Endurance training, expression, and physiology of LDH, MCT1, and MCT4 in human skeletal muscle. *Am J Physiol Endocrinol Metab* 278: E571-579, 2000.
16. Fan X, Hussien R, and Brooks GA. H2O2-induced mitochondrial fragmentation in C2C12 myocytes. *Free Radic Biol Med* 49: 1646-1654, 2010.
17. Fang J, Quinones QJ, Holman TL, Morowitz MJ, Wang Q, Zhao H, Sivo F, Maris JM, and Wahl ML. The H+-linked monocarboxylate transporter (MCT1/SLC16A1): a potential therapeutic target for high-risk neuroblastoma. *Mol Pharmacol* 70: 2108-2115, 2006.

18. Feron O. Pyruvate into lactate and back: from the Warburg effect to symbiotic energy fuel exchange in cancer cells. *Radiother Oncol* 92: 329-333, 2009.
19. Forman HJ, Maiorino M, and Ursini F. Signaling functions of reactive oxygen species. *Biochemistry* 49: 835-842, 2010.
20. Fukumura D, Xu L, Chen Y, Gohongi T, Seed B, and Jain RK. Hypoxia and acidosis independently up-regulate vascular endothelial growth factor transcription in brain tumors in vivo. *Cancer Res* 61: 6020-6024, 2001.
21. Gallagher SM, Castorino JJ, Wang D, and Philp NJ. Monocarboxylate transporter 4 regulates maturation and trafficking of CD147 to the plasma membrane in the metastatic breast cancer cell line MDA-MB-231. *Cancer Res* 67: 4182-4189, 2007.
22. Garbe JC, Bhattacharya S, Merchant B, Bassett E, Swisshelm K, Feiler HS, Wyrobek AJ, and Stampfer MR. Molecular distinctions between stasis and telomere attrition senescence barriers shown by long-term culture of normal human mammary epithelial cells. *Cancer Res* 69: 7557-7568, 2009.
23. Garcia CK, Goldstein JL, Pathak RK, Anderson RG, and Brown MS. Molecular characterization of a membrane transporter for lactate, pyruvate, and other monocarboxylates: implications for the Cori cycle. *Cell* 76: 865-873, 1994.
24. Gutmann I, and Wahlefeld A. *L-(+)-lactate determination with lactate dehydrogenase and NAD. In Methods of Enzymatic Analysis.(Bergmeyer, H.U., eds.)*. New York, NY, USA: Academic, 1974, p. pp. 1464-1472.
25. Halestrap AP, and Meredith D. The SLC16 gene family-from monocarboxylate transporters (MCTs) to aromatic amino acid transporters and beyond. *Pflugers Arch* 447: 619-628, 2004.
26. Hashimoto T, Hussien R, and Brooks GA. Colocalization of MCT1, CD147, and LDH in mitochondrial inner membrane of L6 muscle cells: evidence of a mitochondrial lactate oxidation complex. *Am J Physiol Endocrinol Metab* 290: E1237-1244, 2006.
27. Hashimoto T, Hussien R, Cho HS, Kaufer D, and Brooks GA. Evidence for the mitochondrial lactate oxidation complex in rat neurons: demonstration of an essential component of brain lactate shuttles. *PLoS One* 3: e2915, 2008.
28. Hashimoto T, Hussien R, Oommen S, Gohil K, and Brooks GA. Lactate sensitive transcription factor network in L6 cells: activation of MCT1 and mitochondrial biogenesis. *Faseb J* 21: 2602-2612, 2007.
29. Hashimoto T, Masuda S, Taguchi S, and Brooks GA. Immunohistochemical analysis of MCT1, MCT2 and MCT4 expression in rat plantaris muscle. *J Physiol* 567: 121-129, 2005.
30. Hsu PP, and Sabatini DM. Cancer cell metabolism: Warburg and beyond. *Cell* 134: 703-707, 2008.
31. Jungmann RA, and Kiryukhina O. Cyclic AMP and AKAP-mediated targeting of protein kinase A regulates lactate dehydrogenase subunit A mRNA stability. *J Biol Chem* 280: 25170-25177, 2005.
32. Kuhn KS, Muscaritoli M, Wischmeyer P, and Stehle P. Glutamine as indispensable nutrient in oncology: experimental and clinical evidence. *Eur J Nutr* 49: 197-210, 2010.
33. Lacroix M, and Leclercq G. Relevance of breast cancer cell lines as models for breast tumours: an update. *Breast Cancer Res Treat* 83: 249-289, 2004.

34. Le A, Cooper CR, Gouw AM, Dinavahi R, Maitra A, Deck LM, Royer RE, Vander Jagt DL, Semenza GL, and Dang CV. Inhibition of lactate dehydrogenase A induces oxidative stress and inhibits tumor progression. *Proc Natl Acad Sci U S A* 107: 2037-2042, 2010.
35. Lemire J, Mailloux RJ, and Appanna VD. Mitochondrial lactate dehydrogenase is involved in oxidative-energy metabolism in human astrocytoma cells (CCF-STTG1). *PLoS One* 3: e1550, 2008.
36. Lopez-Lazaro M. Why do tumors metastasize? *Cancer Biol Ther* 6: 141-144, 2007.
37. Lu H, Forbes RA, and Verma A. Hypoxia-inducible factor 1 activation by aerobic glycolysis implicates the Warburg effect in carcinogenesis. *J Biol Chem* 277: 23111-23115, 2002.
38. McClelland GB, Khanna S, Gonzalez GF, Butz CE, and Brooks GA. Peroxisomal membrane monocarboxylate transporters: evidence for a redox shuttle system? *Biochem Biophys Res Commun* 304: 130-135, 2003.
39. Menendez JA. Fine-tuning the lipogenic/lipolytic balance to optimize the metabolic requirements of cancer cell growth: molecular mechanisms and therapeutic perspectives. *Biochim Biophys Acta* 1801: 381-391, 2010.
40. Merezhinskaya N, and Fishbein WN. Monocarboxylate transporters: past, present, and future. *Histol Histopathol* 24: 243-264, 2009.
41. Moreno-Sanchez R, Rodriguez-Enriquez S, Marin-Hernandez A, and Saavedra E. Energy metabolism in tumor cells. *Febs J* 274: 1393-1418, 2007.
42. Morris ME, and Felmlee MA. Overview of the proton-coupled MCT (SLC16A) family of transporters: characterization, function and role in the transport of the drug of abuse gamma-hydroxybutyric acid. *Aaps J* 10: 311-321, 2008.
43. Nishikawa M, and Hashida M. Inhibition of tumour metastasis by targeted delivery of antioxidant enzymes. *Expert Opin Drug Deliv* 3: 355-369, 2006.
44. Novak P, Jensen TJ, Garbe JC, Stampfer MR, and Futscher BW. Stepwise DNA methylation changes are linked to escape from defined proliferation barriers and mammary epithelial cell immortalization. *Cancer Res* 69: 5251-5258, 2009.
45. Paget S. The distribution of secondary growths in cancer of the breast. 1889. *Cancer Metastasis Rev* 8: 98-101, 1989.
46. Pagliarini DJ, Calvo SE, Chang B, Sheth SA, Vafai SB, Ong SE, Walford GA, Sugiana C, Boneh A, Chen WK, Hill DE, Vidal M, Evans JG, Thorburn DR, Carr SA, and Mootha VK. A mitochondrial protein compendium elucidates complex I disease biology. *Cell* 134: 112-123, 2008.
47. Pinheiro C, Albergaria A, Paredes J, Sousa B, Dufloth R, Vieira D, Schmitt F, and Baltazar F. Monocarboxylate transporter 1 is up-regulated in basal-like breast carcinoma. *Histopathology* 56: 860-867, 2010.
48. Rhee SG, Kang SW, Jeong W, Chang TS, Yang KS, and Woo HA. Intracellular messenger function of hydrogen peroxide and its regulation by peroxiredoxins. *Curr Opin Cell Biol* 17: 183-189, 2005.
49. Ristow M. Oxidative metabolism in cancer growth. *Curr Opin Clin Nutr Metab Care* 9: 339-345, 2006.

50. Roth DA, and Brooks GA. Lactate and pyruvate transport is dominated by a pH gradient-sensitive carrier in rat skeletal muscle sarcolemmal vesicles. *Arch Biochem Biophys* 279: 386-394, 1990.
51. Roth DA, and Brooks GA. Lactate transport is mediated by a membrane-bound carrier in rat skeletal muscle sarcolemmal vesicles. *Arch Biochem Biophys* 279: 377-385, 1990.
52. Seyfried TN, and Shelton LM. Cancer as a metabolic disease. *Nutr Metab (Lond)* 7: 7, 2010.
53. Short S, Tian D, Short ML, and Jungmann RA. Structural determinants for post-transcriptional stabilization of lactate dehydrogenase A mRNA by the protein kinase C signal pathway. *J Biol Chem* 275: 12963-12969, 2000.
54. Sonveaux P, Vegran F, Schroeder T, Wergin MC, Verrax J, Rabbani ZN, De Saedeleer CJ, Kennedy KM, Diepart C, Jordan BF, Kelley MJ, Gallez B, Wahl ML, Feron O, and Dewhirst MW. Targeting lactate-fueled respiration selectively kills hypoxic tumor cells in mice. *J Clin Invest* 118: 3930-3942, 2008.
55. Stone JR, and Yang S. Hydrogen peroxide: a signaling messenger. *Antioxid Redox Signal* 8: 243-270, 2006.
56. Ullah MS, Davies AJ, and Halestrap AP. The plasma membrane lactate transporter MCT4, but not MCT1, is up-regulated by hypoxia through a HIF-1alpha-dependent mechanism. *J Biol Chem* 281: 9030-9037, 2006.
57. Walenta S, Wetterling M, Lehrke M, Schwickert G, Sundfor K, Rofstad EK, and Mueller-Klieser W. High lactate levels predict likelihood of metastases, tumor recurrence, and restricted patient survival in human cervical cancers. *Cancer Res* 60: 916-921, 2000.
58. Wimmer VC, Horstmann H, Groh A, and Kuner T. Donut-like topology of synaptic vesicles with a central cluster of mitochondria wrapped into membrane protrusions: a novel structure-function module of the adult calyx of Held. *J Neurosci* 26: 109-116, 2006.
59. Wistuba, II, Behrens C, Milchgrub S, Syed S, Ahmadian M, Virmani AK, Kurvari V, Cunningham TH, Ashfaq R, Minna JD, and Gazdar AF. Comparison of features of human breast cancer cell lines and their corresponding tumors. *Clin Cancer Res* 4: 2931-2938, 1998.
60. Yan L, Zucker S, and Toole BP. Roles of the multifunctional glycoprotein, emmprin (basigin; CD147), in tumour progression. *Thromb Haemost* 93: 199-204, 2005.

CHAPTER 3

Introduction to Nanoparticle Research

Though there has been a controversy about the history of who started the field of nanoparticles (32), many believe that the idea of creating nano-scale materials was first introduced by the Nobel laureate Richard Feynman in 1959 in his talk, "There's Plenty of Room at the Bottom," at the American Physical Society meeting at Caltech (9), and that it was later fueled by Erick Drexler's work in 1980 and his 1986 book "Engines of Creation" (5, 6, 14, 27). Practical nanoparticle science became feasible with the development of high-resolution microscopy, including scanning tunneling microscopy (STM) in 1982 (3) and atomic Force microscopy (AFM) in 1986 (2) (both developed by the Nobel laureates Gerd Binnig and Heinrich Rohrer), and the discovery of carbon nanotubes in 1985 by the Nobel laureates Harry Kroto, Richard Smalley, and Robert Curl (11, 13). Some credit for supporting research in this field in the US goes to president Bill Clinton for launching the National Nanotechnology Initiative (NNI) in 2000 (http://nano.gov/about-nni) (14). The NNI brought twenty departments and agencies together to advance research, development, education, and regulation of nanoscale technology in the US. Since 2000 research in nanoparticles has grown rapidly, as seen in the increase of the number of articles published and distributed in pubmed (http://www.ncbi.nlm.nih.gov/pubmed) with the keyword "nanoparticles" (from 287 in 2000 to 14,169 in 2013 (Figure 1)).

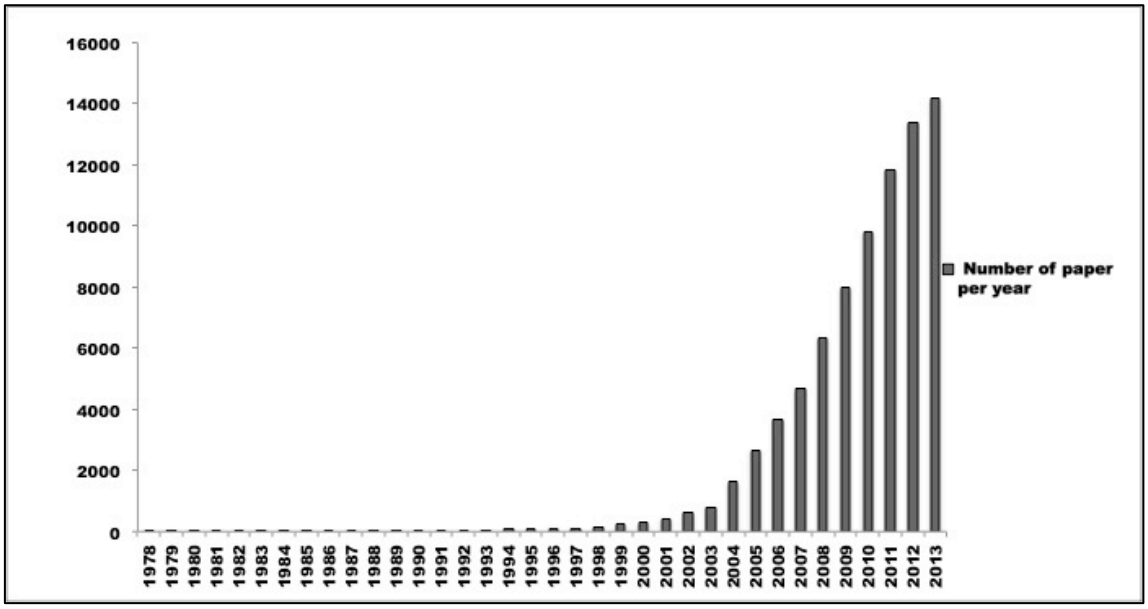

Figure 1. The number of publications related to nanoparticles appearing in Pubmed.

Research in nanoparticles generated new subfields such as nanotechnology, nanomedicine, nanotoxicology, and nano-ecotoxicology. Nanotechnology is the manipulation of materials or the building of novel materials atom by atom to create small-scale objects called nanoparticles. Nanoparticles (or what were also known as ultrafine particles, or UFP) are objects that measure less than 100 nm in one dimension or more (15, 27). Nanoparticles' specific properties are exploited in different ways in many fields (7, 15). Nanoparticles (NPs) are not strictly new, but have existed in nature and have been used by humans in glass and pottery work since the early ninth century (26). The discovery thirty years ago of the unique properties differentiating nanoparticles from

larger objects of the same material brought them to the forefront of research (15). A material's physical, chemical, kinetic, thermodynamic, magnetic, electronic, and optical properties all change significantly when nano-sized objects are produced from them (15).

Nanomedicine is based on the incorporation of nanotechnology to create imaging and diagnostic agents or carriers for drugs of nano-scale size (31). The use of nanoparticles to detect or treat cancer is one of the most promising areas of nanomedicine. Researchers are hoping to use nanoparticles to develop devices or imaging agents that detect cancer at early stages, and deliver chemotherapy drugs to kill specifically cancer cells without killing healthy cells (25). The nanoparticles used in encapsulation drugs can be made from organic or inorganic materials such as liposome and carbon nanotubes, respectively. The unique physiochemical properties of nanoparticles can help reduce toxicity at the same time as they increase the bioavailability, stability, and action of nano-formulated chemotherapeutic agents (27, 29, 33). The first use of nanoparticle drugs in treating cancer was through the repacking of previously known cancer drugs into simple carriers such as polymeric and liposomal nanoparticles. For example, Doxil is the drug Doxorubcin repacked in polyethyl glycol (PEG) liposomal nanoparticles for the treatment of AIDS-associated Kaposi Sarcoma. Likewise, Abraxane is the drug Paclitaxel repacked in albumin polymeric nanoparticles and used to treat breast cancer (25, 31). The enhanced permeability and retention effect (EPR) found in tumor vasculature helps these simple nanoparticle-formulated drugs accumulate in the tumor mass. More sophisticated delivery methods were later developed, including the anchoring of nanoparticle-formulated drugs to antibodies, single strand RNA or DNA, or oligopeptide tags to direct the drugs specifically to tumor masses within the body. MBP-426, for example, is the drug Oxaliplatin repacked in N-glutaryl phosphatidylethanolamine (NGPE) liposome nanoparticles with a Transferrin-targeting ligand. This drug is now in phase 2 clinical trials to treat advanced or metastatic solid cancer (www.clinicalTrials. gov) (31).

A cause for concern is that the same properties of engineered nanoparticles that make them attractive for use in medicine and technology may have negative consequences on human health and environments if their use is not carefully controlled (14, 18). Research and epidemiological studies of similar size objects such as ultrafine aerosols showed negative effects on respiratory tracts of animals (8, 20, 35), and adverse impacts on human health (4, 28). Similarly, carbon nanotubes and carbon fullerenes have been shown to cause inflammatory responses in rat lungs and lipid peroxidation in the brains and gills of largemouth bass (17, 27, 34).

Engineered nanoparticles, not found in nature, are now produced in great numbers. Human bodies have evolved to protect themselves from naturally occurring nanoparticles, but there is no clear understanding as to how our bodies will handle these newly introduced nanoparticles. Each engineered nanoparticle has particular physicochemical characteristics (size, charge, composition, and shape), and acts as a whole independent unit. Their bio-kinetics and their effects inside living organisms are hard to predict (21, 22). For these reasons concerns have been raised about the ability of existing methodologies to detect and characterize the potential risks of nanotechologies, since we still do not understand the mechanisms and kinetics that govern their uptake and release. While naturally occurring nanoparticles interacted with the human body through respiration or skin contact, medicinal nanoparticles are now introduced through new

routes of entry that have not been previously studied. Research has shown that nanoparticles can be transported far from their entry site to other vital organs, cells, and their organelles, and can even pass through tight junctions and blood-brain barrier (Figure 2) (1, 19, 23). This raises more concerns about nanoparticles' long-term effects on vital organs and the nervous system.

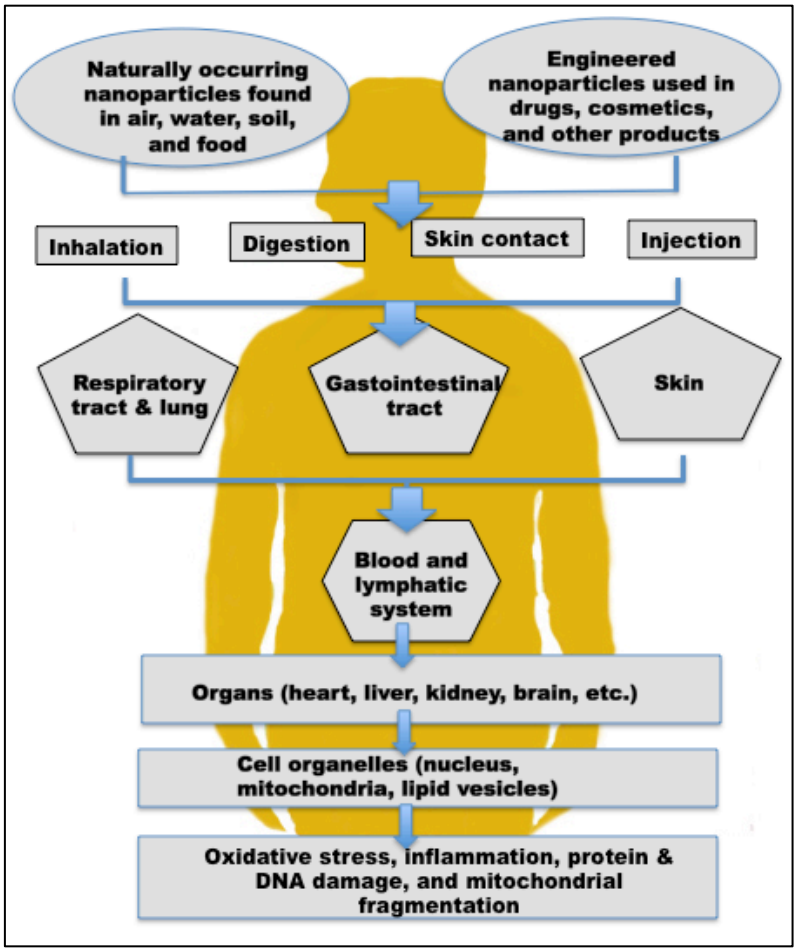

Figure 2. Naturally occurring and engineered nanoparticles enter the human body through inhalation, digestion, skin contact, and injection. Within the body they are transported to different organs and their organelles. Each engineered nanoparticle has specific physiochemical characteristics (size, charge, composition, and shape), and acts as a whole independent unit. Depending on their size, shape, and surface reactivity, some nanoparticles can cause serious harm to the body appearing as oxidative stress, inflammation, protein and DNA damage, and mitochondrial fragmentation.

All the above concerns have generated the new subfields of nanotoxicology and nanoecotoxicology. Nanotoxicology examines the toxicokinetics and toxicodynamics of engineered nanomaterial and its effects on human health (14, 31), and nanoecotoxicology assesses the risk of engineered nanoparticles on ecosystems and the environment (12). The main challenge in these new fields is the lag between this research and the more rapid adoption of nanoparticles in industry, technology, and medicine. The Project on Emerging Nanotechnologies (http://www.nanotechproject.org/cpi/products/) reported that as of February 2014 there are 1,854 consumer products containing nanoparticles. These products ranged from general products such as furniture and paint to personal products such as sunscreens, cosmetics, clothes, and food. The city of Berkeley is the first city in the USA to pass laws regulating nanoparticle use and disposal, possibly due to the large involvement of UC Berkeley and Lawrence Berkeley in nano-research (16). The hope is that more regulation of nanotechnology (longer approval time to add them to products, and clear labeling of nanoparticle-containing goods) will give scientists more time to

conduct research to understand the effects of different particles on human health and on the environment.

In the following study we examined the effects of unloaded Eudragit nanoparticles (ENP) on three mammary epithelial cell lines (two cancerous and one normal) to assess their effect on epithelial cells when used in drugs delivery. Eudragit RS is a ethylacrylate and methylmetacrylate copolymer that is PH-sensitive (Figure 3), and has been used widely to encapsulate drugs to protect them from gastric fluids (24). The use of Eudragit as a nanoparticle carrier for cancer drugs has been claimed to increase the bio-availability of cancer drugs with poor-water solubility, such as Genistein (30). Our study shows that Eudragit nanoparticles increase the metabolic activity and growth, and decrease the proliferation of epithelial cells without any signs of cytotoxicity. These effects were found to be the result of these particles' binding to tissue culture serum proteins and growth factors, then delivering them closer to cellular surfaces. Our study presents a novel effect of Eudragit RS nanoparticles on epithelial cells, and opens doors for new use of those particles in medicine (10).

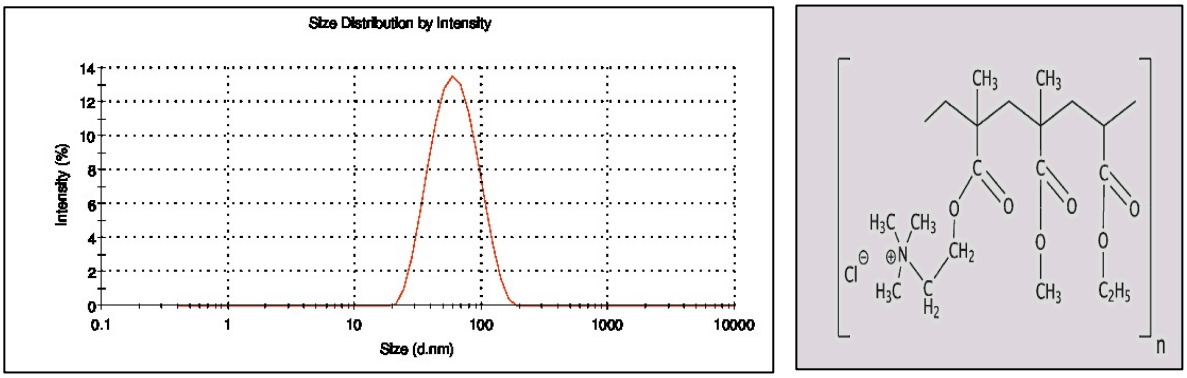

Figure 3. Size distribution of Eudragit RS® NP (left), and chemical structure of the polymer patented by Evonik Industries (Essen, Germany) (right).

REFERENCE

1. Agarwal A, Lariya N, Saraogi G, Dubey N, Agrawal H, and Agrawal GP. Nanoparticles as novel carrier for brain delivery: a review. *Curr Pharm Des* 15: 917-925, 2009.
2. Binnig G, Quate CF, and Gerber C. Atomic force microscope. *Phys Rev Lett* 56: 930-933, 1986.
3. Binnig G, Rohrer H, Gerber C, and Weibel E. Surface studies by scanning tunneling microscopy. *Applied Physics Letters* 40: 1982.
4. Dockery DW, Pope CA, 3rd, Xu X, Spengler JD, Ware JH, Fay ME, Ferris BG, Jr., and Speizer FE. An association between air pollution and mortality in six U.S. cities. *N Engl J Med* 329: 1753-1759, 1993.
5. Drexler E, K. *Engines of Creation: The Coming Era of Nanotechnology*. New York: Anchor books, 1986.
6. Drexler E, K. Molecular engineering: An approach to the development of general capabilities for molecular manipulation. *Proc Natl Acad Sci USA* 78: 5275-5278, 1981.
7. Drexler E, K. *Nanosystems: Molecular Machinery, Manufacturing, and Computation*. New York: John Wiley & Sons, 1992.
8. Ferin J, Oberdorster G, Penney DP, Soderholm SC, Gelein R, and Piper HC. Increased pulmonary toxicity of ultrafine particles 1.Particle clearance, translocation, morphology. *J Aerosol Sci* 21: 381–384, 1990.
9. Feynman RP. There's plenty of room at the Bottom. *Eng Sci* 23: 22-36, 1960.
10. Hussien R, Rihn BH, Eidi H, Ronzani C, Joubert O, Ferrari L, Vazquez O, Kaufer D, and Brooks GA. Unique growth pattern of human mammary epithelial cells induced by polymeric nanoparticles. *Physiol Rep* 1: e00027, 2013.
11. Iijima S. Helical microtubules of graphitic carbon. *Nature* 354: 56-58, 1991.
12. Kahru A, and Dubourguier HC. From ecotoxicology to nanoecotoxicology. *Toxicology* 269: 105-119, 2010.
13. Kroto HW, Heath JR, O'Brien SC, Curl RF, and Smalley RE. C60: Buckminsterfullerene. *Nature* 318: 162-163, 1985.
14. Maynard AD, Warheit DB, and Philbert MA. The new toxicology of sophisticated materials: nanotoxicology and beyond. *Toxicol Sci* 120 Suppl 1: S109-129, 2011.
15. Mukhopadhyay SM. Key Attributes of Nanoscale Materials and Special Functionalities Emerging from them. In: *Nanoscale Multifunctional Materials: Science and Applications*, edited by Mukhopadhyay SM. Hoboken, NJ, USA: John Wiley & Sons, p. 4-28, 2011.
16. O'Brian FP. An overview of the law of nanotechnology In: *The Nanotechnology Challenge: Creating Legal Institutions for Uncertain Risks*, edited by Dana DCambridge University Press, 2012.
17. Oberdorster G. Pulmonary effects of inhaled ultrafine particles. *Int Arch Occup Environ Health* 74: 1-8, 2001.
18. Oberdorster G. Safety assessment for nanotechnology and nanomedicine: concepts of nanotoxicology. *J Intern Med* 267: 89-105, 2010.
19. Oberdorster G, Elder A, and Rinderknecht A. Nanoparticles and the brain: cause for concern? *J Nanosci Nanotechnol* 9: 4996-5007, 2009.

20. Oberdorster G, Ferin J, Gelein R, Soderholm SC, and Finkelstein J. Role of the alveolar macrophage in lung injury: studies with ultrafine particles. *Environ Health Perspect* 97: 193-199, 1992.
21. Oberdorster G, Maynard A, Donaldson K, Castranova V, Fitzpatrick J, Ausman K, Carter J, Karn B, Kreyling W, Lai D, Olin S, Monteiro-Riviere N, Warheit D, and Yang H. Principles for characterizing the potential human health effects from exposure to nanomaterials: elements of a screening strategy. *Part Fibre Toxicol* 2: 8, 2005.
22. Oberdorster G, Oberdorster E, and Oberdorster J. Nanotoxicology: an emerging discipline evolving from studies of ultrafine particles. *Environ Health Perspect* 113: 823-839, 2005.
23. Pehlivan SB. Nanotechnology-based drug delivery systems for targeting, imaging and diagnosis of neurodegenerative diseases. *Pharm Res* 30: 2499-2511, 2013.
24. Pignatello R, Bucolo C, Ferrara P, Maltese A, Puleo A, and Puglisi G. Eudragit RS100 nanosuspensions for the ophthalmic controlled delivery of ibuprofen. *Eur J Pharm Sci* 16: 53-61, 2002.
25. Prud'homme R, and Svenson S. Introduction: Benefits and Challenges for Multifunctional Nanoparticles in Medicine. In: *Multifunctional Nanoparticles for Drug Delivery Applications*
Nanostructure Science and Technology edited by Robert k, Prud'homme, and Svenson SSpringer US, 2012.
26. Reiss Gn, and Hütten A. Magnetic Nanoparticles In: *Handbook of Nanophysics: Nanoparticles and Quantum Dots*, edited by Sattler KDCRC Press, 2010.
27. Santamaria A. Historical overview of nanotechnology and nanotoxicology. *Methods Mol Biol* 926: 1-12, 2012.
28. Seaton A, MacNee W, Donaldson K, and Godden D. Particulate air pollution and acute health effects. *Lancet* 345: 176-178, 1995.
29. Swami A, Shi J, Gadde S, Votruba AR, Kolishetti N, and Farokhzad OC. Nanoparticles for targeted and temporally controlled drug delivery. In: *Multifunctional Nanoparticles for Drug Delivery Applications*Springer US, 2012.
30. Tang J, Xu N, Ji H, Liu H, Wang Z, and Wu L. Eudragit nanoparticles containing genistein: formulation, development, and bioavailability assessment. *Int J Nanomedicine* 6: 2429-2435, 2011.
31. Tong R, Tang L, and Cheng J. Development and Application of Anticancer Nanomedicine. In: *Multifunctional Nanoparticles for Drug Delivery Applications*, edited by Svenson S, and Prud'homme RK. New York: Springer 2012.
32. Toumey C. Plenty of room, plenty of history. *Nat Nanotechnol* 4: 783-784, 2009.
33. Waite CL, and Roth CM. Nanoscale drug delivery systems for enhanced drug penetration into solid tumors: current progress and opportunities. *Crit Rev Biomed Eng* 40: 21-41, 2012.
34. Warheit DB, Laurence BR, Reed KL, Roach DH, Reynolds GA, and Webb TR. Comparative pulmonary toxicity assessment of single-wall carbon nanotubes in rats. *Toxicol Sci* 77: 117-125, 2004.
35. Wilson FJ, Jr., Hiller FC, Wilson JD, and Bone RC. Quantitative deposition of ultrafine stable particles in the human respiratory tract. *J Appl Physiol* 58: 223-229, 1985.

CHAPTER 4

Unique Growth Pattern of Human Mammary Epithelial Cells Induced by Polymeric Nanoparticles

This chapter was published in *The Journal of Physiological Reports* (Physiol. Reports September 10, 2013; 1(4): e00027.)

ABSTRACT

Due to their unique properties, engineered nanoparticles have found broad use in industry, technology, and medicine, including as a vehicle for drug delivery. However, the understanding of nanoparticles' interaction with different types of mammalian cells lags significantly behind their increasing adoption in drug delivery. In this study, we show unique responses of human epithelial breast cells when exposed to polymeric Eudragit® RS (ENPs) for 1 to 3 days. Cells displayed dose-dependent increases in metabolic activity and growth, but lower proliferation rates, than control cells, as evidenced in tetrazolium salt (WST-1) and 5-bromo-2'-deoxyuridine (BrdU) assays, respectively. Those effects did not affect cell death or mitochondrial fragmentation. We attribute the increase in metabolic activity and growth of cells culture with ENPs to three factors: (1) high affinity of proteins present in the serum for ENPs, (2) adhesion of ENPs to cells, and (3) activation of proliferation and growth pathways. The proteins and genes responsible for stimulating cell adhesion and growth were identified by mass spectrometry and Micrroarry analyses. We demonstrate a novel property of Eudragit® RS nanoparticles, which act to increase cell metabolic activity and growth and organize epithelial cells in the epithelium as determined by Microarray analysis.

INTRODUCTION

The size, penetrative, carrier, and other properties of nanoparticles (NPs) allow them to enter the human body through inhalation, digestion, injection, and skin contact (21, 23). Within the body, NPs can be transported to organs, tissues and cells far from the site of exposure, where NPs cross anatomical barriers and penetrate live cells and their organelles (23). The nanoparticulated forms of drugs and growth factors have potential to increase bioavailability, stability, and action of those agents while at the same time decrease toxicity and delivery variability associated with dosiometry (25). Accordingly, among the diverse potential uses of NPs are their potential for targeted effects, including chemotherapy (32). However, because the interactions between unloaded nanoparticles and different types of mammalian cells are poorly understood we undertook this investigation.

Eudragit® RS nanoparticles are a non-biodegradable, positively charged copolymer (8), and have been used for *per os* administration of drugs such as ibuprofen, cyclosporine, and indomethacin (3, 9, 22). Recent work by Eidi et al. (9) on the effect of unloaded Eudragit® RS nanoparticles on rat macrophages caused concern among researchers when results showed cytotoxic effects that included apoptosis, autophagy, and possible mitochondrial fragmentation. Concerns over toxicity of NP treatment emerged when studies demonstrated that some engineered nanoparticles, including carbon nanotubes, titanium dioxide, and aluminum oxide, caused inflammatory responses in rat lungs. Similarly, carbon fullerenes have been shown to cause lipid peroxidation in the brain and gills of largemouth bass (19, 20, 25, 34), and polyacrylate ester, one component of ENPs, was shown to cause pleural effusion, pulmonary fibrosis, and granuloma in humans (28). Hence, in retrospect the effect of ENPs on macrophages in Eidi et al. may not be surprising because macrophages are designed to induce phagocytosis of living as well as inert materials, such as ENPs. Despite the expected behavior of macrophages, the study of Eidi et al. showed the need for further research to clarify the effect of unloaded ENPs on the growth of different types of cells before attempting drug delivery to cells, tissues, and organisms.

The few studies that have been performed with Eudragit or its constitutive polymers have produced contradictory results on its effect on cell growth. Eudragit RL stimulated the growth of fibroblasts (4), while Eudragit RS 100 slowed the growth of hepatocytes while activating their differentiation (11). The constitutive polymers of Eudragit, poly(methylmethacrylate)-poly(methacrylic acid) copolymer, displayed no effect on the viability of neural cells (7). However, none of the above studies used ENPs, nor did they report the effect of ENPs on cell metabolic activity or the growth of epithelial cells.

Given uncertainties about the effect of NPs, in general, and Eudragit® RS nanoparticles in particular, the goal of our study was to evaluate the effect of unloaded ENPs on the metabolic activity, growth and proliferation of epithelial cells in culture. A range of 3 to 200 ug/ml of ENPs for 2000 cells per well of a 96-well plate was selected to compare our data to the data of Eidi et al., who used a similar range of ENP concentration. The use of different amounts of ENPs is important in our study, because it reflects the possibility of various actual direct and indirect exposure levels.

MATERIALS AND METHODS

Preparation of Eudragit™ RS nanoparticles

The Eudragit® RS 100 copolymer used in this study was purchased from Evonik Industries, and is a co-polymer of ethylacrylate and methylmethacrylate, with low methacrylic acid ester content with quaternary ammonium groups. Eudragit® RS nanoparticles (ENPs) were prepared as described previously (8) by dissolving a co-polymer of ethylacrylate and methylmethacrylate in acetone (20 mg/mL). The organic solution was poured in a syringe, flowed under stirring in 40 mL of a Pluronic® F68 (0.5%, w/v) aqueous phase. The solvent was removed by rotary evaporation under vacuum at 40° C to a final polymer concentration of 7.5 mg/mL. The obtained nanoparticles displayed a monodispersed distribution at 65.0±26.3 nm and a Z-average of +51.04 mV. Their refractive index was 1.59, the viscosity was 0.8872 cP, and the relative density (d_{20}^{20}) ranged from 0.816 to 0.836 (data not shown). The concentration of Pluronic F68 was 0.0008% for 200 µg/ml concentration of polymer. The potential effect of this concentration of Pluronic F68 on cells was evaluated, and none was observed (data not shown).

Cell proliferation assay WST-1

Human breast cancer cell lines (MCF-7, MDA- MB-231) and the primary human breast cell line (HMEC 184) were grown in their respective media as described previously (15). Cells were seeded at 2,000 per well and grown at 37°C in an air/CO_2 atmosphere (95/5 v/v) for 24, 48, and 72h in the presence of 0, 3.1, 6.2, 12.5, 25, 50, 100, or 200 µg/mL ENPs in 200 µl of their respective media. At each time point, the medium was discarded, cells were washed with PBS 1x, and DMEM medium without phenol red (supplemented with 10% FBS (fetal bovine serum), 1% L-glutamine, and 0.25% penicillin-streptomycin) but containing WST-1 (Cell Proliferation Reagent, Roche, Germany), was added and cells were incubated for 1 to 5h. The 96-well plates were then read by spectrophotometry at 450 nm.

BrdU and EdU cell proliferation assays

Cells were seeded in 96-well plates at 2,000 per well and grown in a T.C. incubator at 37°C and 5% CO_2 for 24h in the presence of ENPs in 200 µl of their respective media. 5-bromo-2'-deoxyuridine (BrdU) was used to label proliferating cells with a BrdU cell proliferation assay (Calbiochem, Darmstadt, Germany). Cells were incubated with BrdU for 6h, then fixed with fixing/denaturing solution. The BrdU-labeled DNA was detected with a BrdU Mouse mAb kit using the manufacturer's protocol. The absorbance in each plate was measured using a spectrophotometer at dual wavelengths of (450-540 nm). To quantify the percentage of proliferating cells and total cell count after 24h, HMEC 184 cells were seeded (5,000 per chamber) in an eight-chamber slide (Lab-tek, PA, USA) and treated with 0, 6, 25, and 100 µg/ml ENPs for 24h. Cells were incubated with 5-ethynyl-2´-deoxyuridine (EdU) (30 µM) from Invitrogen for 6h, and then washed twice with PBS and fixed with 4% paraformaldehyde. Cells were permeabilized with 0.1% Triton-X 100 in PBS for 5 min, then incubated with 5% NDS blocking buffer for 2h. Incorporated EdU was detected with a copper-catalyzed fluorescent azide reaction (Click-iT, Invitrogen), after which slides were washed with

PBS and mounted on cover slips with mounting medium containing DAPI (Vector, Burlingame, CA, USA). Nuclei and EdU positive nuclei were counted using the (20x/0.8 NA) air objective of an Axio Observer.Z1 fluorescence microscope (Zeiss, Germany) with Metamorph software (Molecular Devices, CA, USA).

Confocal Laser Scanning Microscopy and phase-contrast microscopy

ENPs were conjugated with Nile red (nominal diameter = 73 nm, zeta potential = +47 and polydispersity index = 0.34) according to a method described previously (37). Nuclei were stained with Hoechst 33342 (Sigma), mitochondria were stained with MitoTracker Deep Red 633 (Invitrogen/Molecular Probes, Eugene, OR), and the membranes were stained with Wheat Germ Agglutinin Alexa Fluor 488 conjugate, WGA (Invitrogen). Cells were observed with a (20x/1.0 NA) water-dipping objective in a Zeiss LSM 780 microscope. A 3D movie of HMEC 184 cells incubated for 3 days with Nile red-ENPs was generated using Imaris software (Bitplane, Zurich, Switzerland). ImageJ software was used to find ENPs localized with mitochondria (Wayne Rasband, NIH, Bethesda, MD, USA). The average mitochondrial volume of single HMEC 184 cells stained with Mito Tracker was measured using Imaris software from 3D images.

Total protein measurement and immunoblots

Cells were washed twice with PBS and then solubilized with 5% NP-40. Total protein concentration was determined using a BCA protein assay kit (Pierce Biotechnology, Radford, IL). Western blotting was performed as previously described (15). Primary antibodies used were rabbit anti-cytochrome oxidase subunit IV, mouse anti-β-actin, and mouse anti-VDAC (Abcam, Cambridge, MA). Band intensity was quantified as previously described (15).

Purification and identification of serum proteins coated on ENPs with proteomic mass spectrometry

A mixture of serum and ENPs was centrifuged at 2,500 g for 10 min and the obtained pellet was washed twice with PBS and exposed to organic extraction with dichloromethane. The organic phase was examined on thin layer chromatography (TLC), and the aqueous phase was examined with UV/VIS spectrometry. To identify the proteins attached to ENPs, FBS (5.9 mL, approx. 21.44 mg of proteins) containing 780 μg/mL of ENPs was centrifuged at 10,000 g for 3.5 min. The pellet was washed twice with an equal volume of PBS x1, then resuspended in 1 mL of either glycine•HCl (100 mM, pH = 3), Tris•HCl/NaCl (50 mM/5 M, pH = 8), or guanidine thiocyanate (6M). The three samples were run on SDS (sodium dodecyl sulfate) gel electrophoresis and stained with Coomassie Brilliant Blue. Seven bands from the SDS gel of guanidine thiocyanate were examined with MALDI-TOF mass spectrometry, which identified 290 non-redundant proteins belonging to *Bos Taurus,* and nine human contaminant cytokeratins. A total of 178 proteins were identified and analyzed for name of product in *Bos taurus* (as they appeared in Unigene (www.ncbi.nlm.nih.gov/UniGene/), name of gene in *Homo sapiens* counterpart, name of human counterpart protein (www.uniprot.org/uniprot/), and plasma levels in human and InterPRO domains if applicable (http://www.genecards.org/). A total of 69 proteins were cited only by their *Bos taurus* name and were not included in data analysis because either (*i*) their relative abundance (RA) was very low (1 to 10), (*ii*) their

identified peptides span less than 3% of the protein sequence, or (*iii*) they were isoforms of, or closely related to, already analyzed proteins. Proteins were ranked according to their (*i*) abundance (A), namely the ratio of spectrum count/length, and (*ii*) sequence coverage (SC), namely the percentage of the entire sequence that was expressed in the peptides found in trypsin hydrolysate. The relative abundance (RA) was calculated as the ratio of the most abundant protein to the least abundant protein. The InterPro domains (http://www.ebi.ac.uk/interpro/) of 178 proteins were retrievedand were submitted to the STRING database (http://string-db.org/).

Total RNA extraction and microarray analysis

Total RNA was extracted from HMEC 184 cells (50% and 90% confluence) incubated with 25 µg/mL ENPs for 24h, and without incubation (control). The quality of RNA extracted with RiboPure kit (Ambion, Austin, TX) was determined with spectrophotometry and capillary electrophoresis, using RNA 6000 Nano® (Agilent 2100 Bioanalyser™). cDNA synthesis, cRNA synthesis, Cy3-dye labeling, and microarray hybridization were carried out using 100 ng of total RNA according to manufacturer protocol (One-Color Microarray-Based Gene Expression Analysis, version 6.6). Microarray slides (SurePrint G3 Human GE v2 8x60K, Agilent technologies) were scanned with an Agilent DNA microarray scanner. The acquisition, quantification of array images, and primary data analysis were performed using Agilent Feature Extraction Software. Data were first normalized with quantile method and stringent filtering criteria were next used to identify genes whose expression level was significantly changed, with a modified Student t-test ($p \leq 0.001$) and FC (fold change) ≥ 2.0 . FC of mean of three replicates (for each ENP exposure and cell condition) on control were calculated. The selected genes display acceptable False Discovery Rate (<15%) according to Benjamini et al. (2). The Database for Annotation, Visualization, and Integrated Discovery (DAVID; http://david.abcc.ncifcrf.gov) was then used to analyze and extract (*i*) relevant GO terms (http://godatabase.org) (*ii*) functions and expression data on Genecard (http://www.genecards.org) and (*iii*) known and predicted protein-protein interactions (http://string-db.org) for selected genes (12). The raw data of our microarrays are available on http://www.ncbi.nlm.nih.gov/geo/, using the GSE45598 and GSE45869 access number.

Statistical analysis

Testing for significant differences between groups at $p<0.05$ was done either by the student's t test, one-way ANOVA analysis with Tukey's post test (comparing all groups), or Dunnett's post test (comparing all groups vs. control) using RLPlot or Prism software.

RESULTS

Dose-dependent increases in metabolic activity of epithelial cells exposed to ENPs

Human mammary epithelial cells (HMEC 184) (~40% confluent) exposed to ENPs from 3.1 to 200 μg/mL for 24, 48, and 72h showed a dose-dependent increase in metabolic activity, as measured by the WST-1 assay (Figures 1a, 1b, 1c). The increase in WST-1 indicates an increase in the activity of mitochondrial succinate dehydrogenase (18). Using HMEC 184 confluent cells (~90% confluent), ENPs induced a dose-dependent increase in metabolic activity (data not shown). Two human epithelial breast cancer cell lines (MCF-7 and MDA-MB- 231) grown in different media were also incubated with varying doses of ENPs for 24h; again, results showed a dose-dependent increase in metabolic activity (Figures 1d, 1e). In a separate experiment, ENPs were mixed with culture media (3.1 to 200 μg/mL) and added to 96-well plates, either 24h before seeding the HMEC 184 cells or at the same time as cell seeding, and a WST-1 assay was performed 2 days later. A similar trend of dose-dependent increased metabolic activity was seen in both cases (Supplementary Figure 1). Because a false-negative toxicity has been reported previously with MTT-formazan in interacting with NPs, but not with the WST-1 assay (35), additional control cells were subjected to WST-1 to rule out the possibility of reagent interaction with ENPs (Figure 1f).

Dose-dependent decrease in cell proliferation of epithelial cells exposed to ENPs

A dose-dependent decrease in cell proliferation, measured with a 5-bromo-2'-deoxyuridine (BrdU) ELISA assay, was observed in the HMEC 184 cells after 24h incubation with ENPs (Figure 2a). The decrease in proliferation was further confirmed with a proliferation assay that quantified proliferating HMEC 184 cells labeled with 5-ethynyl-2′-deoxyuridine (EdU) using a fluorescent azide reaction (Figure 2b). An increase in total protein content in the HMEC 184 cells, measured with a BCA assay, was observed after 24h of incubation with ENPs (Figure 2c), and a decrease in total cell count was seen only in those cells incubated with a high dose of ENPs (100 μg/mL), as measured with DAPI stain (Figure 2d). Additional control cells were subjected to BrdU assays to rule out the possibility of reagent interaction with ENPs (Figure 2e). Neural progenitor cells (NPC) were treated with 0 to 200 μg/mL ENPs to test whether results were specific to epithelial cells. A similar dose-dependent increase in metabolic activity and dose-dependent decrease in cell proliferation were seen in those cells (Supplementary Figure 2).

ENPs formed a visible network with serum proteins that adhered to cells in culture. ENPs entered the cells and caused an increase in total mitochondrial volume without an increase in mitochondrial biogenesis

An opalescent flocculate was visible when ENPs were added to HMEC 184, MDA-MB-231, and MCF-7 culture media. No flocculate was observed with the addition of ENPs to serum-free medium or PBS. Labeling of ENPs with Nile red fluorescent congregated dye and examination with confocal microscopy showed that ENPs entered the cells (Figure 3 & Supplementary movie 1), but the majority of ENPs aggregated into clumps with proteins that formed a clearly visible network closely attached to cells. Colocalization analysis in ImageJ showed that some ENPs are localized with

mitochondria (Figure 3g). No fragmentation was seen in mitochondrial networks in HMEC 184, MDA-MB-231, and MCF-7 cells treated with ENPs at 25 μg/mL for 24 and 72h (data not shown). There was an increase in the total mitochondrial volume in HMEC 184 cells treated with 25 μg/mL ENPs, when compared to untreated control cells as measured with Imaris software (Figure 4a). However, a decrease in Cox4 and VDAC proteins was seen with Western blotting, but neither was a significant change (Figure 4b). This implies an increase in cell size without a corresponding increase in mitochondrial biogenesis.

Proteomic mass spectrometry showed that the ENP-serum protein network contains proteins sharing common InterPro domains and exhibiting protease, antiprotease, epidermal growth factor, adhesion, and binding properties

To identify the nature of the visible flocculate, the pellet generated from centrifugation of a mixture of serum and ENPs was washed twice with PBS and exposed to organic extraction. No lipids were seen in the organic phase on TLC, but the aqueous phase showed a peak at 280 nm and an increased absorbance at 240 nm, with the UV/VIS spectrum suggesting the presence of proteins (data not shown). The pellet was examined with SDS-PAGE and MALDI-TOF mass spectrometry, which identified 290 non-redundant proteins belonging to *Bos taurus* and 9 human cytokeratins. From MALDI-TOF MS, 178 proteins were identified and analyzed (Supplementary Table 1). Sequence coverage varied from 79.2% for albumin to 0.4% for titin. The relative abundances (RAs) were calculated as the ratio of the most abundant to the least abundant protein, varied between 2,581 and 1.

Regression analysis at a 95% confidence level showed a linear correlation between protein abundance in mass spectrometry and the protein concentration in plasma (Supplementary Figure 3). However, notable exceptions were seen later in the InterPro analysis. Because the coefficient of correlation (r) was only 0.66, and because some proteins were present at concentrations less than 1 nmol in plasma (e.g., kininogen-2 isoform II, actins, periostin, and serpinA 3-3), but were abundant in the mass spectrometry chromatograms (Supplementary Table 1), we believe that proteins were not randomly fixed on ENPs according to their abundance in FBS. Therefore, we retrieved the InterPro domains of most of the 178 proteins we analyzed. The most frequently shared InterPro domain was "IPR006210:EGF-like," shared by 18 different proteins (Table 1). Approximately 120 of 170 analyzed proteins (70%) shared at least 2 common domains. A high number of proteins belonging to InterPro domains are known to be involved in endopeptidase inhibitor activity, proteolytic activity or its regulation, protein binding, calcium binding, cell adhesion, and signaling, or have certain structural motifs like leucine- rich or immunoglobulin domains (Table 1). By calculating the mean of relative abundance at the domain level, but not at the entire protein level, we found that proteins were coated not only due to their relative amounts in FBS, but also due to their affinities for ENPs, reflecting their composition in domains rather than the structure of the entire protein (Supplementary Table 2). When submitting 178 genes to the STRING database, 169 protein encoding genes were recognized, and more than 80% of these showed interactions, either at evidence, confidence, or action levels. Seemingly, the purified proteins were also isolated by interactions between and among themselves (e.g., by protease inhibitor/protease interactions, or known binding properties of individual

proteins). Serpins, proteases, and coagulation factors were found at the central core around which proteins involved in cell adhesion, growth, differentiation, and migration clustered (Supplementary Figure 4).

Microarray analysis for HMEC 184 cells treated with 25 µg/mL ENPs showed activation of proliferation and growth pathways

Microarray analysis was performed on HMEC 184 treated cells to identify the pathways induced by ENP treatment. HMEC 184 treated cells indicated 38 and 287 genes (50% and 90% confluence, respectively) whose expression was significantly altered when compared to control. The stringency of transcriptomic analysis was higher in the 90% confluence series ($p < 0.001$) than the 50% confluence series ($p < 0.05$). Few genes were downregulated in either cell-culture condition: 3 and 4 genes for the 50 and 90% confluence series, respectively (Supplementary Table 3).

Several of the up-regulated genes were genes involved in pathways of proliferation, growth, and transformation. These genes included *PIM-1,* which contributes to cell proliferation and survival; *VTCN1,* which promotes epithelial cell transformation; *ADRA1B* (up-regulated in the 50% confluence dishes, data not shown), which activates mitogenic responses and has been found in normal and cancerous breast cell lines (31); *LCN2*, described as a gene involved in breast tumor progression (36); *ELF3*, an ETS domain transcription factor that is epithelial-specific and is known to transactivate alone, or synergistically with other genes also upregulated in our experiment (such as *CLND7*, *FLG*, *KRT8*, *SPRR1A*, *MMP1*, *MM9,* and *TGM3)*, epithelial cell differentiation; and *NDRG2,* which is involved in WNT signaling pathway (17, 27).

The functional annotation using DAVID revealed GO terms such as epithelial cell differentiation, epidermis development, response to wounding, and ectoderm development with a highly significant probability ($p<10E-12$, FC> 10). These GO terms indicate that ENP action caused a spatial organization of breast epithelium (Supplementary Table 4). The effect of ENP on epithelial cell organization was also seen in significant changes within genes involved in apicolateral plasma membrane organization, cell-cell junction, cell-cell adhesion, and apical junction complex organization. These genes included *CLDN4*, *CLDN3*, *CGN*, *CLDN7*, *DSG4*, and *CDSN* (Supplementary Table 3).

Differentially expressed genes at a level of $p < 10E-03$ were detected in breast tissues by Illumina Body Map, indicating a strong relationship in expression pattern between HMEC 184 cell line and human breast tissue. Only 9 of 84 genes (~11%) displayed no expression in human breast tissue: *IL36RN*, *IL36G*, *CDSN*, *CWH43*, *ATP12A*, *NLRP10*, *IGFL2*, *KRT34*, and *MMP1*. Eighteen of the upregulated genes were described by Toulza et al. (30) as upregulated genes in epidermal barrier function: *A2ML1, ADAM8, BNIPL, CDSN, CLDN3, CLDN4, CLDN7, DSG4, FLG, IGFL2, KLK6, KRT23, KRT24, KRT34, KRT80, LIPH, SERPINB2,* and *SPRR1A*.

Several genes upregulated in macrophages after exposure to nanoparticles (9) were also upregulated in HMEC 184 cells when exposed to ENPs. These genes were (*i*) *TLR1 & 2*, which recognize bacterial proteins or lipopeptides, and are activated by *IL8* (IL8 was also upregulated); (*ii*) *MARCO,* which binds to Gram (+) and (-) bacteria; and (*iii*) S100A12, which binds to ANXA1 (both were upregulated), and displays antibacterial activity against *E coli* and *P aeruginosa*. The upregulation of genes such as

RAB11FIP1, *SPON2*, *MYO5B*, and *MAL2* indicates that the presence of ENPs with HMEC 184 cells allows those cells to acquire macrophage functions involved in endocytosis and potentializing MARCO.

Some of the induced genes code products that use proteins adsorbed on ENP as substrate, such as *MMP8*, *MMP9*, and *LCN2*, all of which activate procollagenase, and cleave collagene IV & VI, which bind to ENP. *MMP9* and *SERPINB2* degrade fibronectin and vitronectin, both adsorbed on ENP. *KK6* displayed hydrolytic activity against extracellular matrix proteins adsorbed on ENP, such as fibronectin, laminin, vitronectin and collagen.

Forty-one of the 84 genes in the 90% confluence series recognized by the String database (http://string-db.org) were linked at confidence, evidence or action level (Figure 5). Regarding the action level, some relevant catalysis involve: (*i*) initial activation of proMMP9 by MMP1, (*ii*) proMMP-9 activation by MMP-10, (*iii*) CEACAM1&6 heterodimer, (*iv*) MMP9 potentializing IL8, and (*v*) complex-forming of serum amyloid A protein with upregulated TLR genes, SAA1/TLR2/TLR1.

DISCUSSION

We examined the effect of ENPs on metabolic activities and proliferation rates of epithelial in culture. We show here: 1) an increase in metabolic activity and growth of epithelial cells after incubation with ENPs, 2) an activation of proliferation and growth genes in epithlial cells treated with ENPs, and 3) an effect of ENPs extracting from media and delivering to cell surfaces specific FBS plasma proteins involved in cell growth and metabolic activity of cells grown in culture. These results are discussed in more detail below.

An increase in metabolic activity and growth of epithelial cells after incubation with ENPs

Contrary to the results obtained by Eidi at el. (9), who showed a cytotoxic effect of unloaded ENPs on macrophages, we show here no cytotoxicity effect of unloaded ENPs; in contrast, we show a dose-dependent increase in the metabolic activity of epithelial cells that was accompanied by a small, but significant dose-dependent decrease in cell proliferation. The overall effect was a small, but significant decrease in the total cell count when compared to ENP-untreated control cells. We attribute the increase in metabolic activity to an increase in cell size and total mitochondrial volume and activity. Eudragit® RS nanoparticles or similar products have been used by several groups on many type of cells for different reasons (4, 5, 7, 9, 11), but outcomes similar to the changes in metabolic activity and cell proliferation rate we found have not been reported. Differences may result from the use of different nanoparticles or cell types by other groups. For example, ENPs used in this study were the same as those used by Eidi at el., so the differences in results are attributable to cell type. Macrophages are naturally designed to induce phagocytosis of inert or living particles, so it is not surprising that ENPs displayed cytotoxic effect on macrophages that were attributable to enhanced nanoparticle uptake and macrophage overload. In addition, the ENPs precipitated with FBS plasma proteins in the bottom of the culture dishes after ~2h, which may have reduced the amount of nutrients available for cells in suspension, such as macrophages, and may have increased the amount of nutrients available to adherent cells such as epithelial cells. Further research will be required to understand the contradictory results, but a similar trend was seen when neural stem cells were treated with ENPs, and so the newly described property of ENPs may effect multiple cell types.

An activation of proliferation and growth genes in epithelial cells treated with ENPs

The observed effects of ENPs decreasing cell proliferation rates while increasing metabolic activity (measured with Brdu and WST-1, respectively) were unexpected. The microarray data showed an activation of proliferation and growth pathways in HMEC 184 cells treated with ENPs, but we only found an increase in growth and metabolic activity in those cells. Further research will be required to understand what prevented cell proliferation. It is possible that cells invested energy in metabolism and growth more than in proliferation. However, we saw no significant decrease in proliferation at lower levels of ENP treatment, which means that the lower ENP exposure has a positive effect on cell growth without an associated effect on proliferation. A similar result was obtained by Cui et al. (6) who used gold nanoparticles (Au NPs). Cui et al. showed that small Au NPs

enter HeLa cells and cause a cytotoxic effect, but that large aggregated Au NPs adhere to the cell surface and cause an increase in cell growth.

Our data showed that ENPs caused an increase in cell metabolic activity in the three epithelial cells that were tested, the normal (HMEC 184) and the cancerous (MCF-7 and MDA-MB- 231) cells. However, our results with the cancerous cells gives cause for concern regarding the use of ENPs as a cancer drug delivery system, because increasing the access of cancer cells to nutrients would be counter productive even if ENPs targeted those cells and carried cytotoxic substances to them. On the other hand, stimulating growth in cells subjected to targeted chemotherapy could overstress normal cells leading to apoptosis. The effect of ENP treatment in increasing cancer cell metabolic activity has not been reported previously, and further research is needed to address the potentially counter-productive effect of ENP increasing cancer cell activity.

ENP extracts and delivers to cell surfaces specific FBS plasma proteins that are crucial for cell growth and metabolic activity of cells grown in culture

At present it is premature to speculate about the mechanisms by which Eudragit RS served to increase metabolism in cells. However, through its dual function of "polyaffinity nanochromatography" (i.e., aggregating numerous factors that promote metabolism and growth) and adherence to cells, Eudragit RS in effect concentrates stimuli for cell growth on cell surfaces.

To date, other NPs, such as magnetic nanoparticles coated with antibodies, ligands, or receptors, have been used to extract proteins from sera and other media (10, 24). Eudragit RS 100 was reported by some teams for the purification of proteins from bacteria and yeast [such as protein A (16), *beta*-glucosidase (1), and xylanase (26)], the immobilization of enzymes [such as amylosucrase of *Nesseira* (33)], and in affinity chromatography for MAB purification (29). Eudragit RS 100 was also used by some groups to refold fibroblast growth factor (FGF) and lyzozyme (13). The same proposed mechanism was also reported with TGF-*beta* and KGF-2 (14). Interestingly, the proteins extracted by the process described by those groups belong to an InterPro Domain, "TGF-*beta*," that is closely related to the protein TGF-*beta* that refolds well in an Eudragit buffer.

Sharma and Gupta (26) were the first to use the term "macroaffinity," and to link it to use of the Eudragit RS 100 polymer. Following their lead we named our method "polyaffinity nanochromatography." The methods we developed here allow the isolation of proteins that are closely related by structure, activity, and interactions, and that are not randomly distributed. In addition, the protocol we describe may allow the extraction and isolation of a select group of proteins for diagnostic purposes from animal and human fluids (serum, plasma, cerebrospinal fluid, urine, exudates, and transudates), as the proteins described here may also be present in those fluids in physiological or pathological conditions. Hence, the 45 proteins highlighted in Supplementary Table 1 were either never described in plasma or are present in plasma in pathological conditions. On the other hand, further research is required if ENPs are to be used increasingly in drug delivery, especially in light of their absorption of many important proteins and growth factors.

CONCLUSION

Our data show that ENPs can be used to increase the metabolic activity and growth of epithelial cells in a dose-dependent manner. The mechanism for this behavior stems from the ability of ENPs to bind to certain proteins in culture media and to bring them closer to the surface of cells. Those proteins are involved in cell adhesion, growth, differentiation, and migration. The observed behaviors of ENPs suggest new uses of ENPs beyond drug coating.

ACKNOWLEDGEMENTS

We thank Drs. Gary Firestone, Martha Stampfer, and James Garbe for their gifts of epithelial cell lines. We thank Dr. Alain Le Faou for his comments on our paper. Images were taken at the Molecular Imaging Center facility in the Cancer Research Laboratory at UC Berkeley. MALDI-TOF mass spectrometry analysis was performed at the proteomic mass spectrometry laboratory under direction of Dr. Lori Kohlstaedt at UC Berkeley. We thank our students Maxine Nanthavong, Phedre Rihn, and Tabya Sultan for their help. This work was supported by a gift from CytoSport, Inc. BR was supported by National Academy of Medicine and a grant from NanoSNO (France). RH was supported by the National Science Foundation (USA).

FIGURES AND TABLES

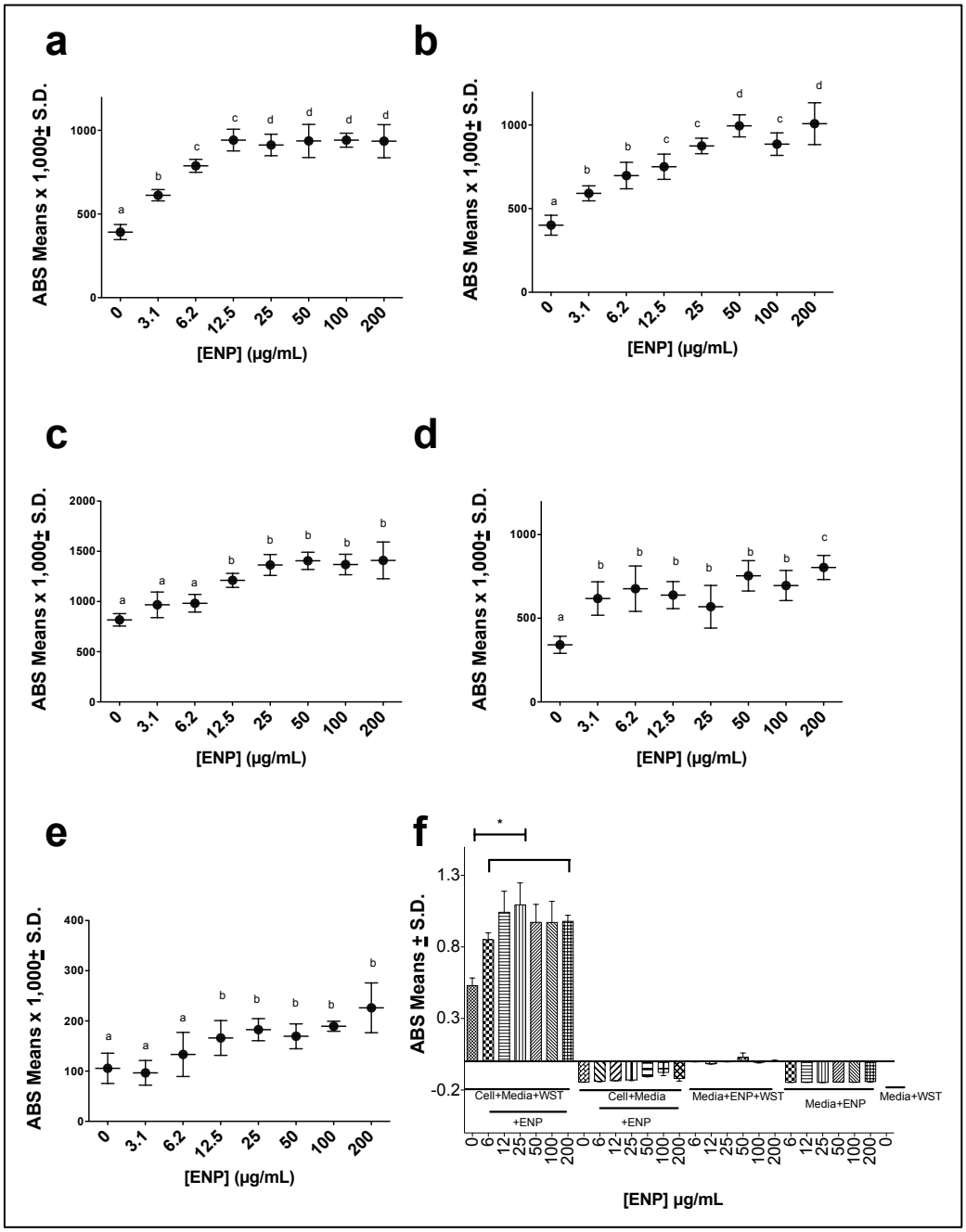

Figure 1. Metabolic activity of HMEC 184 cells (a, b, c), MDA-MB-231 (d), and MCF-7 (e) following 24 (a, d, e), 48 (b), and 72h (c) exposure to various doses of ENPs (µg/mL). Different controls were tested in HMEC 184 cells to examine the effect of ENPs on the accuracy of the WST-1 assay (f). Data are means ± SD. Groups not sharing the same letter are different at the 95% level according to ANOVA analysis ($p < 0.0001$, Tukey's honest significant difference). ***** Significantly different (comparing all groups vs. control, Dunnett's post test).

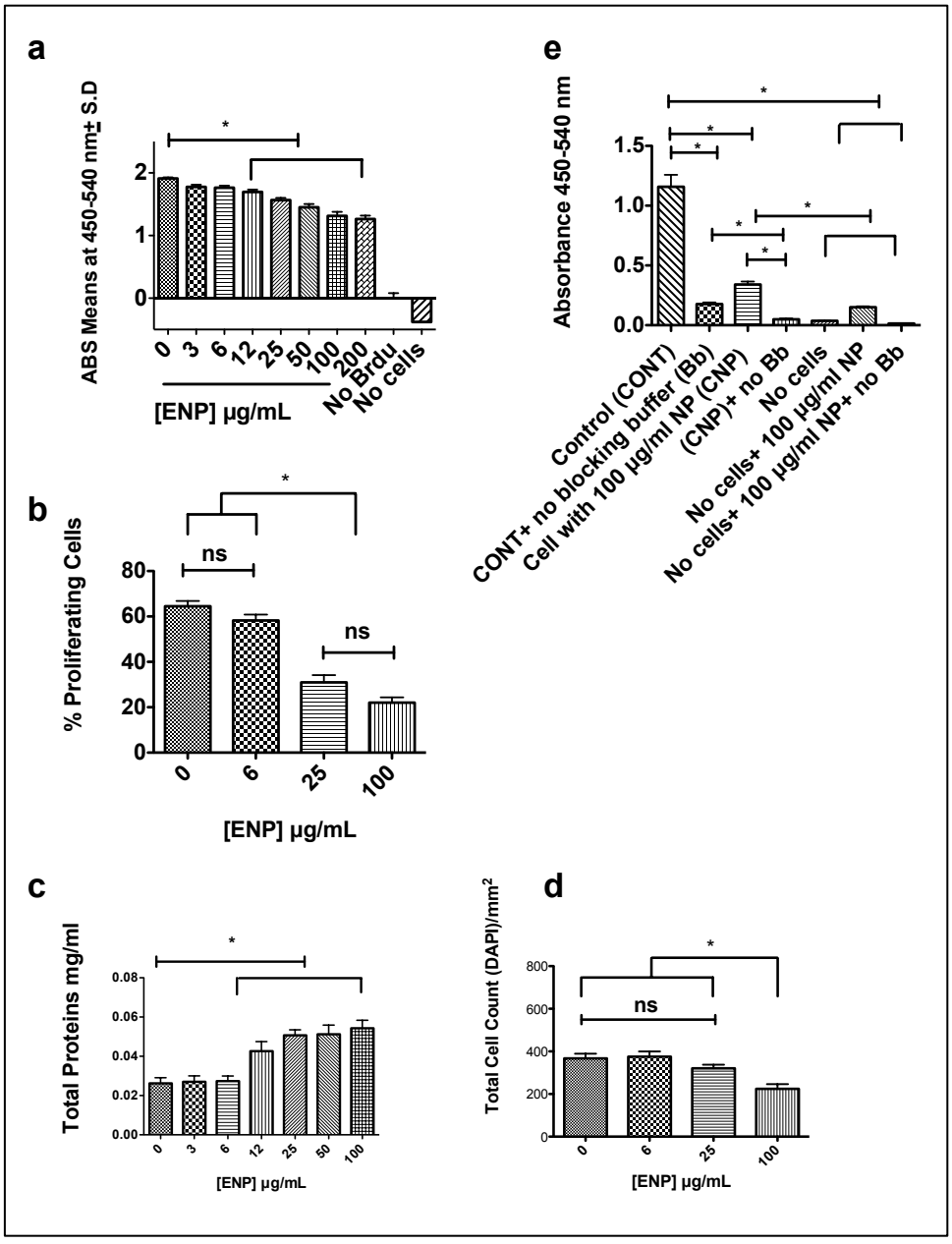

Figure 2. Cell Proliferation (a, b), total proteins (c), and cell count (d) in HMEC 184 cells following 24h exposure to ENPs (µg/mL). Cell proliferation (a) was measured with 5-bromo-2'-deoxyuridine (BrdU) incorporated into cellular DNA for 6h, and a BrdU mouse mAb used to detect the BrdU-labeled DNA. A 5-ethynyl-2´-deoxyuridine (EdU) cell proliferation assay (b) demonstrated that ENPs decrease the percent of proliferation of HMEC 184 cells in culture in a dose-dependent manner. Different controls were tested in HMEC 184 cells to examine the effect of ENPs or blocking buffer on the accuracy of the BrdU assay (e). Data are means ± SD. ***** Significantly different at the 95% level according to ANOVA analysis (comparing all groups vs. control, Dunnett's post test).

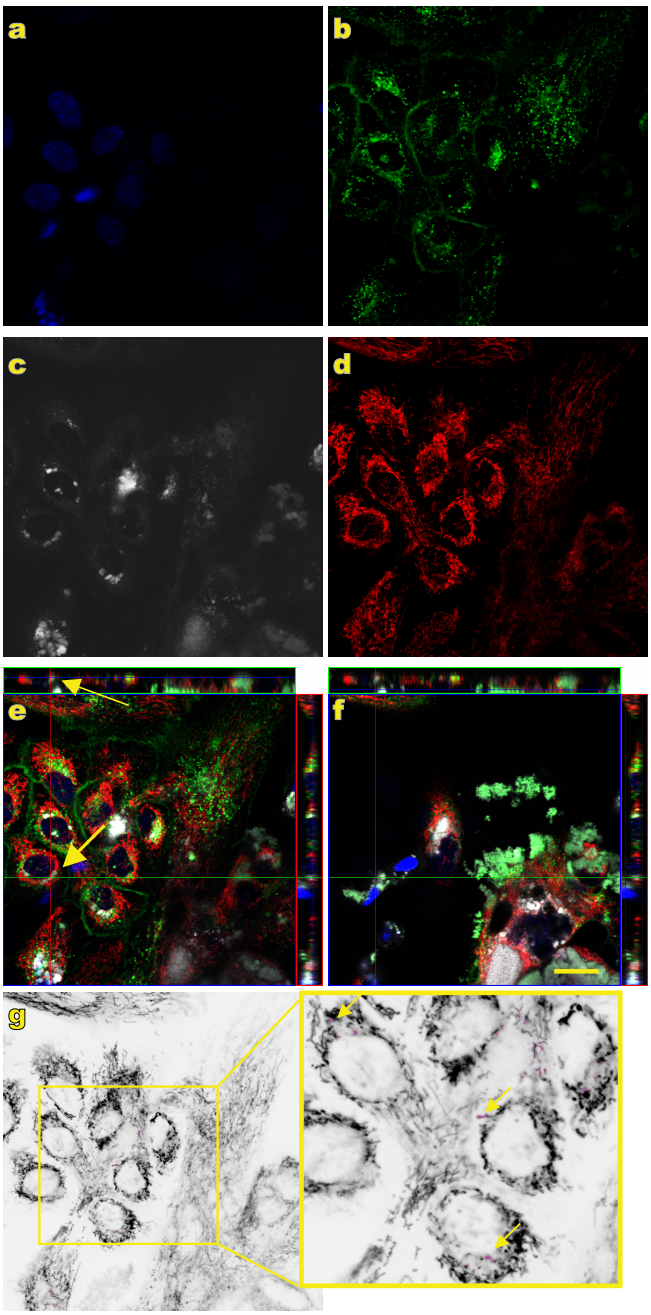

Figure 3. HMEC 184 cells after 3-day exposure to Nile red-ENP (25 µg/mL) as observed with a Zeiss LSM 780 confocal microscope. Nuclei were stained with 33342 Hoechst dye (a), membranes were stained with wheat germ agglutinin (b), ENPs were conjugated to Nile red (c), and mitochondria were stained with MitoTracker (d). Ortho-view of the z-stack shows that some ENPs are inside the cells (e) and some are aggregated on top of the cells (f). Colocalization analysis in ImageJ shows that some ENPs are colocalized with mitochondria (purple dot) (g). Whole images were contrast-enhanced using ImageJ software. Scale bar = 20 µm.

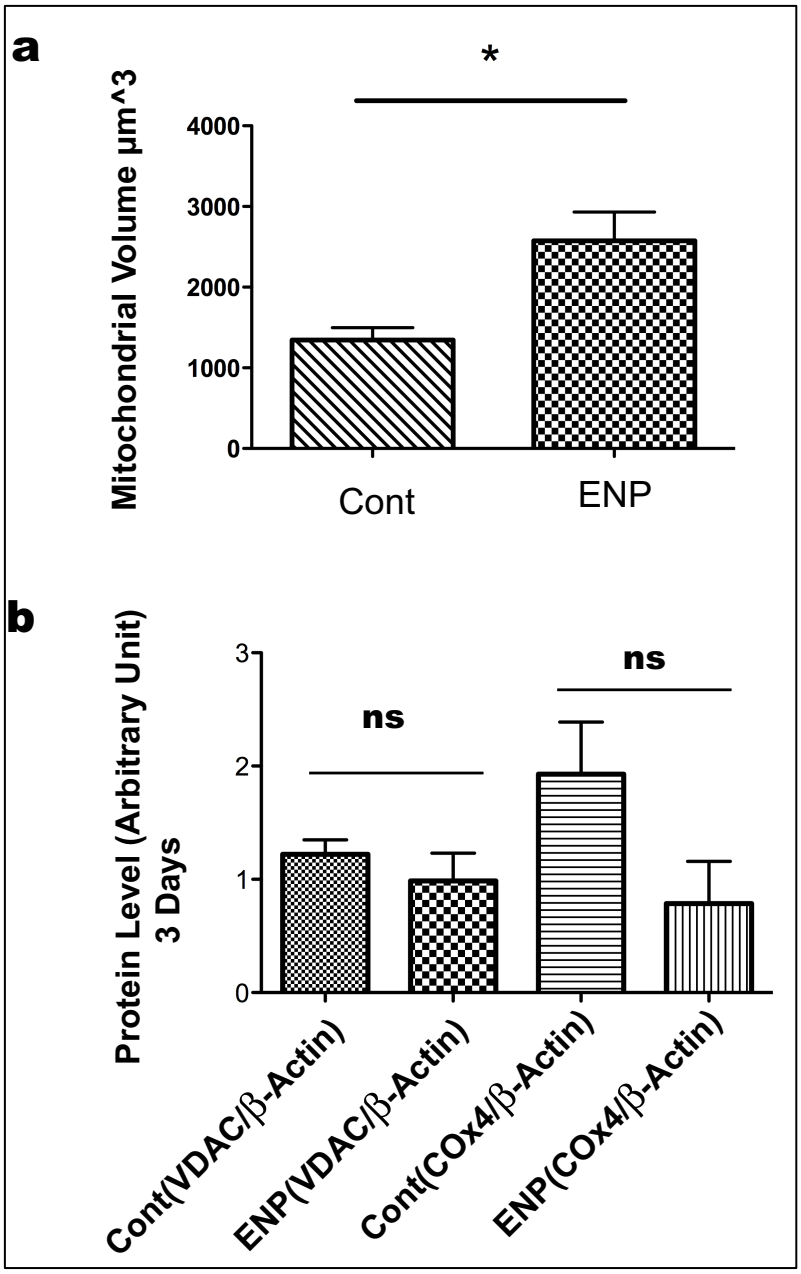

Figure 4. Mitochondrial volume (a) and protein content (b) in HMEC 184 cells after 3-day exposure to ENPs (25 µg/mL). Mitochondria were stained with MitoTracker, and mitochondrial volumes (µm^3) were measured with Imaris software. There was an increase in mitochondrial volume in cells treated with ENPs as compared to control cells. A decrease in Cox4 and VDAC proteins was seen with Western blotting, but neither was a significant change. Data are means ± SD. *Significantly different at the 95% level according to ANOVA analysis (comparing all groups vs. control, Dunnett's post test).

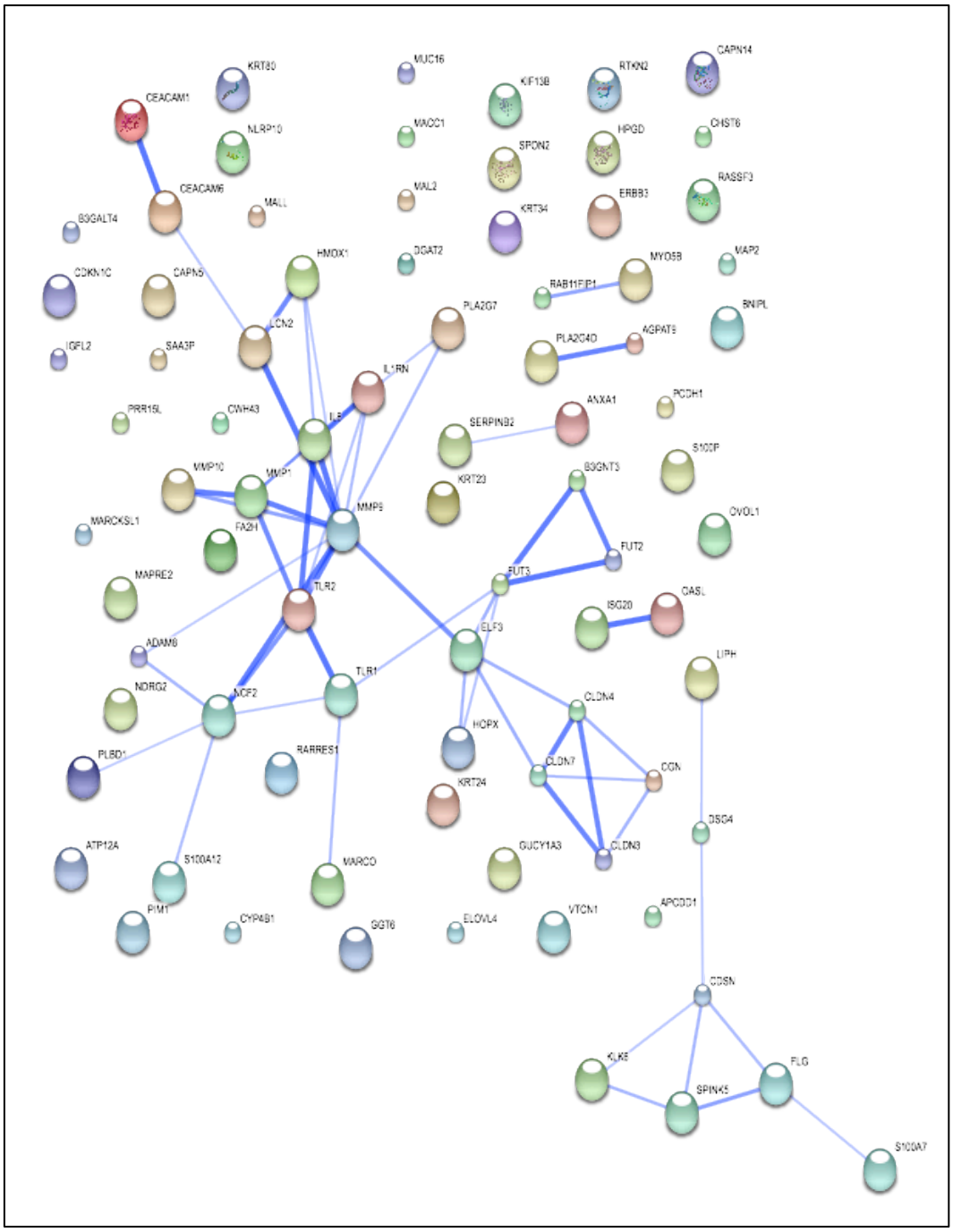

Figure 5. Protein/protein interactions of 84 overexpressed genes in HMEC 184 cells, as retrieved from String database. HMEC 184 cells (90% confluence) were incubated with and without 25 µg/ml ENPs for 24h. Total RNA was extracted and analyzed with microarray. There were 287 genes whose expression was significantly altered when compared to control. Forty-one of 84 genes recognized by String database were linked at the confidence, evidence or action level.

Table 1.

Commonly shared domains of proteins purified by ENPs. The InterPro domains were retrieved form (http://www.ebi.ac.uk/interpro/). About 120 of 170 analyzed proteins (70 %) shared at least 2 domains.

InterPro Name	**Number**
IPR006210:EGF-like	18
IPR000215:Protease_inhib_I4_serpin	13
IPR013783:Ig-like_fold	12
IPR016060:Complement_control_module	9
IPR001254:Peptidase_S1_S6	9
IPR001611:Leu-rich_rpt	9
IPR006209:EGF	9
IPR008985:ConA-like_lec_gl	8
IPR000436:Sushi_SCR_CCP	8
IPR009003:Pept_cys/ser_Trypsin-like	7
IPR018039:Intermediate_filament_CS	7
IPR011992:EF-hand-like_dom	6
PR002035:VWF_A	6
IPR001599:Macroglobln_a2	5
IPR000859:CUB	5
IPR008160:Collagen	5
IPR003961:Fibronectin_type3	5
IPR004001:Actin_CS	4
IPR000264:Serumumin	4
IPR000001:Kringle	4
IPR017857:Coagulation_fac_subgr_Gla_dom	4
IPR009053:Prefoldin	4
IPR018056:Kringle_CS	4
IPR000719:Prot_kinase_cat_dom	4
IPR001791:Laminin_G	4
IPR000010:Prot_inh_cystat	3
IPR000884:Thrombospondin_1_rpt	3
IPR012674:Calycin	3
IPR008979:Galactose-bd-like	3
IPR020837:Fibrinogen_CS	3
IPR001304:C-type_lectin	3
IPR002223:Prot_inh_Kunz-m	3
IPR017441:Protein_kinase_ATP_BS	3

SUPPLEMENTARY DATA

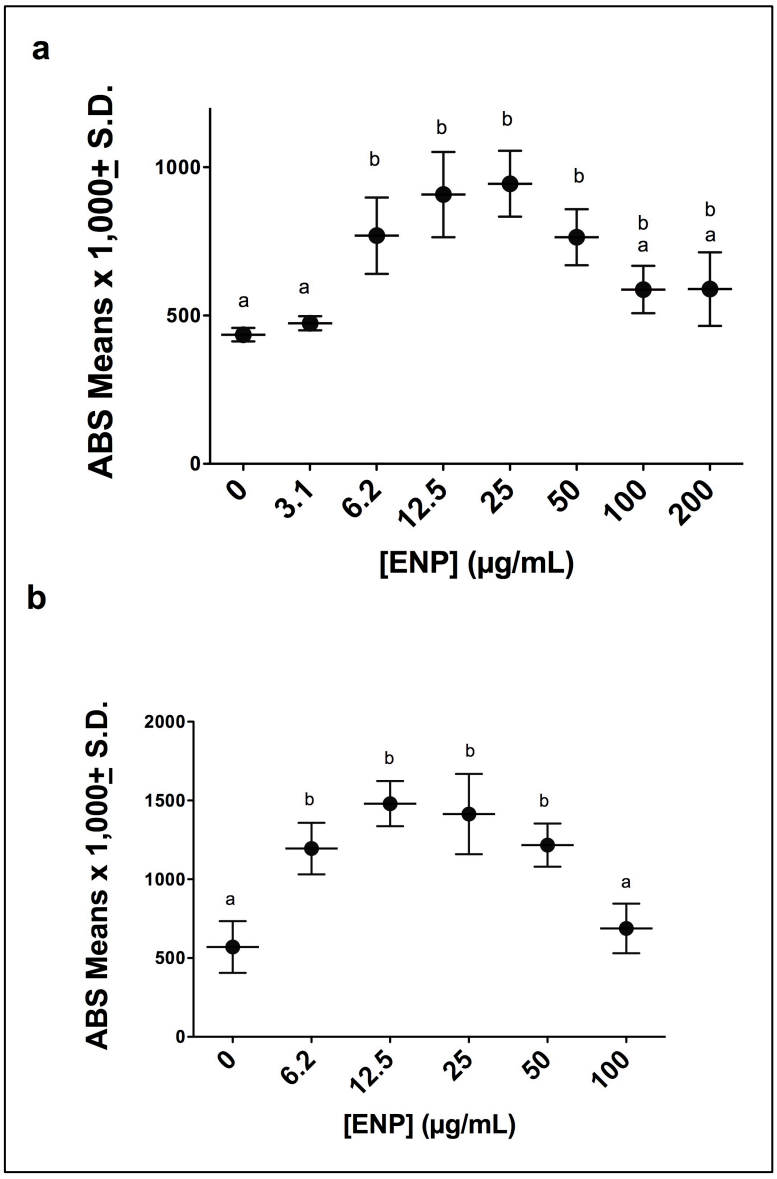

Supplementary Figure 1. Metabolic activity of HMEC 184 cells following 48h exposure to ENPs. ENPs (µg/mL) were pre-incubated for 24h in plates with culture media at different concentrations before cells were seeded and incubated for 48h (a). Cells were incubated for 48h with ENPs (µg/mL) at different concentrations at the same time as cell seeding (b). Groups not sharing the same letter are different at the 95% level according to ANOVA analysis ($p < 0.0001$, Tukey's honest significant difference).

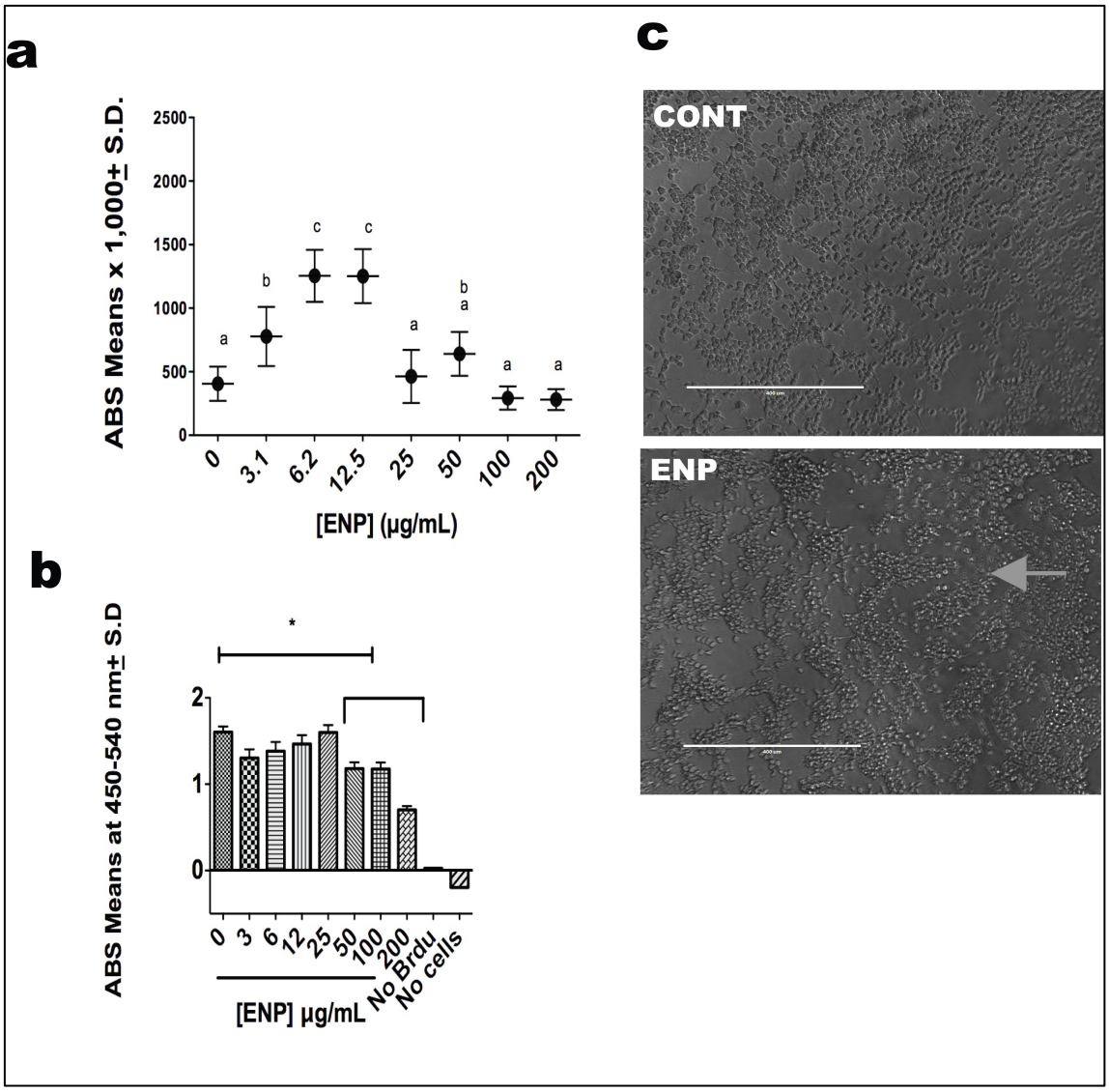

Supplementary Figure 2. Metabolic activity (a) and cell proliferation (b) in neural progenitor cells (NPC) following 24h exposure to ENPs (µg/mL). Metabolic activity and cell proliferation were measured with WST-1 and BrdU assays. A dose-dependent increase in metabolic activity and dose-dependent decrease in cell proliferation were seen in this cell line. ENPs formed a visible network with NPC media that adhered to cells in culture (c).

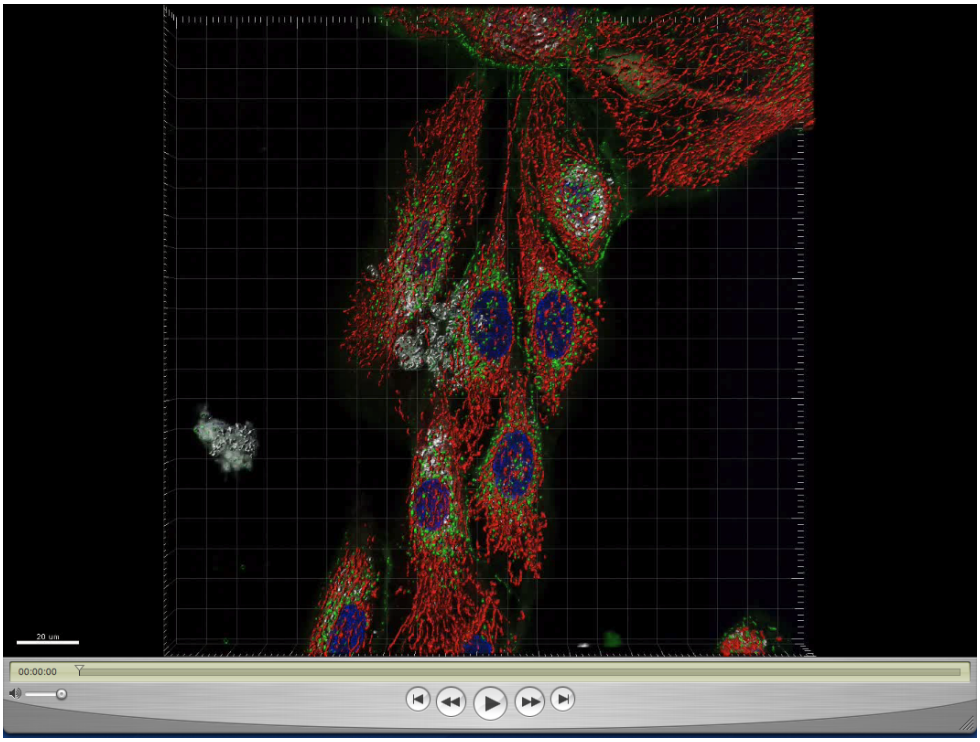

Supplementary Movie 1. A 3D movie of HMEC 184 cells after 3-day exposure to ENPs (25 µg/mL) as observed with a Zeiss LSM 780 confocal microscope. Nuclei were stained with Hoechst (blue), membranes were stained with wheat germ agglutinin (green), ENPs were conjugated to Nile red (white), and mitochondria were stained with MitoTracker Deep Red (red). ENPs were observed inside the cells and some were aggregated atop of the cells. https://docs.google.com/file/d/0B6TwZrW3wcudbkVaTklLd0U4eVE/edit?usp=sharing

Supplementary Table 1[1]. A list of proteins from FBS purified by ENPs and identified with MALDI-TOF mass spectrometry. Mass spectrometry analysis identified ~299 proteins from FBS that were attached to ENPs. Of these, 178 proteins are listed here and were identified and analyzed for: name of product in *Bos taurus* (as appeared in Unigene), name of gene in *Homo sapiens* counterpart, name of human counterpart protein, and levels in human plasma. A notable fraction of those proteins (~45, highlighted in gray) were either never described in plasma or are present in plasma in pathological conditions. Proteins are ranked according to their abundance (RA) and sequence coverage (SC). Sequence coverage varied from 79.2% for albumin to 0.4% for titin.

"GENE_ID"	"PROT_ID"	"Name"	"A"	"[Plasma]"	"RA "	"Rank RA"	"Rank SC"
ALB	P02768	serum albumin	0.9259	3500	2581.0	1	1
APOA1	P02647	apolipoprotein A-I	0.7585	2500	2114.4	2	4
SERPINA1	P01009	alpha-1-antiproteinase	0.4351	2000	1212.9	3	16
SERPINC1	P01008	antithrombin-III	0.3290	900	917.2	4	10
ITIH3	Q06033	inter-alpha-trypsin inhibitor heavy chain H3	0.3064	60	854.1	5	9
ACTA2	P62736	actin alpha cardiac muscle	0.2747	20	765.7	6	3
HBB	P68871	hemoglobin fetal subunit beta	0.2690	200	749.8	7	2
ITIH2	P19823	inter-alpha-trypsin inhibitor heavy chain H2	0.2072	400	577.6	8	25
A2M	P01023	alpha-2-macroglobulin	0.1927	1000	537.2	9	5
LUM	P51884	lumican	0.1725	150	480.9	10	12
ACTBL2	Q562R1	actin beta-like 2	0.1489	8	415.2	11	50
C4BPA	P04003	C4b-binding protein alpha chain	0.1385	300	386.0	12	8
F2	P00734	prothrombin	0.1376	800	383.6	13	45
HBA	P69905	hemoglobin subunit alpha	0.1338	150	373.0	14	7
ACTG1	P63261	actin gamma-enteric smooth muscle	0.1277	0	355.9	15	19
LGALS3BP	Q08380	galectin-3-binding protein	0.1261	20	351.6	16	23
ACTA2L	nd	uncharacterized protein LOC782051	0.1228	0	342.3	17	54
KNG2	P01045	kininogen-2 isoform II	0.1228	0	342.3	18	17
APOA4	P06727	apolipoprotein A-IV	0.1184	800	330.1	19	6
AMBP	P02760	protein AMBP	0.1165	200	324.7	20	38

[1] "GENE_ID" : Gene ID of the human counterpart as found in Genecard,
"PROT_ID" : Protein ID of the human counterpart as found in the Uniprot database,
"Name" : Name of the protein in *Bos taurus*,
"A" : Abundancy in mass spectrometry = spectrum count/length,
"[Plasma]" : Plasma level (nmol),
"RA " : Relative Abundancy,
"Rank RA" : Rank by Relative Abundancy,
"Rank SC" : Rank by Sequence Coverage,
ND : Non Determined in Genecard database.
SC : The percentage of the entire sequence that was expressed in the peptides found in trypsin hydrolysate.

VTN	P04004	vitronectin	0.1092	400	304.5	21	57
GC	P02774	vitamin D-binding protein	0.0949	1000	264.7	22	18
FBLN1	P23142	fibulin-1	0.0949	25	264.6	23	34
SERPIND1	P05546	heparin cofactor 2	0.0706	200	196.7	24	37
SPARCL1	Q14515	SPARC-like protein 1	0.0673	20	187.5	25	11
CLU	P10909	clusterin preproprotein	0.0638	300	177.8	26	21
C3	P01024	complement C3 preproprotein	0.0620	1100	172.9	27	13
SERPINA3	P01011	plasma serine protease inhibitor	0.0619	2000	172.5	28	28
C4BPB	P20851	uncharacterized protein LOC510860	0.0612	70	170.7	29	31
IGLL1	P15814	immunoglobulin lambda-like polypeptide 1	0.0553	6	154.2	30	30
FETUB	Q9UGM5	fetuin-B	0.0543	40	151.3	31	35
AHSG	P02765	alpha-2-HS-glycoprotein	0.0529	900	147.5	32	48
F13B	P05160	coagulation factor XIII B polypeptide	0.0514	70	143.4	33	33
F8	P00451	coagulation factor XIII B chain	0.0514	0.8	143.4	34	36
SERPINF2	P08697	alpha-2-antiplasmin	0.0508	300	141.6	35	27
SERPINA3_3	nd	serpin A3-3	0.0487	0	135.7	36	58
TTR	P02766	transthyretin	0.0476	1100	132.7	37	14
POSTN	Q15063	periostin	0.0475	1	132.4	38	15
TRFE	P02787	serotransferrin	0.0469	900	130.7	39	20
ITIH1	P19827	inter-alpha-trypsin inhibitor heavy chain H1	0.0464	400	129.2	40	22
KRT1	P04264	keratin type II cytoskeletal 1	0.0462	200	128.8	41	94
KRT2	P35908	keratin type II cytoskeletal 2	0.0446	50	124.2	42	102
KRT10	P13645	keratin type I cytoskeletal 10	0.0442	100	123.1	43	81
PLTP	P55058	phospholipid transfer protein	0.0431	8	120.3	44	46
SERPINA3_5	A2I7N1	serpin A3-5	0.0414	0	115.3	45	72
CD109	Q6YHK3	CD109 antigen	0.0408	1	113.8	46	39
AFM	P43652	afamin	0.0397	200	110.8	47	41
CD40LG	P29965	CD40 ligand	0.0383	0	106.8	48	124
APOB	P04114	apolipoprotein B-100	0.0373	200	104.1	49	32
GPX3	P22352	glutathione peroxidase	0.0354	50	98.7	50	44
FMOD	Q06828	fibromodulin	0.0347	0.9	96.6	51	53
FGA	P02671	fibrinogen alpha chain	0.0341	800	95.2	52	64
CLEC11A	Q9Y240	C-type lectin domain family 11 member A	0.0340	0	94.6	53	29
HPX	P02790	hemopexin	0.0327	2500	91.1	54	43
TLN1	Q9Y490	talin-1	0.0327	0	91.1	55	26
THBS1	P07996	thrombospondin-1	0.0316	30	88.2	56	40
PROC	P04070	vitamin K-dependent protein C	0.0313	11	87.1	57	52
ITIH4	Q14624	inter-alpha-trypsin inhibitor heavy chain H4	0.0306	800	85.2	58	55
APOA2	P02652	apolipoprotein A-II	0.0300	1500	83.6	59	42

FGB	P02675	fibrinogen beta chain	0.0283	800	78.8	60	86
HVM63	P84751	Ig heavy chain Mem5-like partial	0.0263	0	73.4	61	74
CHST3	Q7LGC8	carbohydrate sulfotransferase 3	0.0251	0.8	69.8	62	70
ORM1	P02763	alpha-1-acid glycoprotein	0.0248	2500	69.0	63	79
NRP2	O60462	neuropilin-2	0.0227	2	63.2	64	67
GPLD1	P80108	phosphatidylinositol-glycan-specific phospholipase D precurso	0.0226	20	63.1	65	47
SERPINA10	Q9UK55	protein Z-dependent protease inhibitor	0.0221	20	61.7	66	49
HSP90AA1	P07900	heat shock protein HSP 90-alpha	0.0218	10	60.8	67	68
FN1	P02751	fibronectin	0.0218	200	60.7	68	56
SERPINA3_8	A6QPQ2	SERPINA3-8	0.0215	0	60.0	69	164
IGLL5	B9A064	immunoglobulin lambda-like polypeptide 5-like	0.0214	300	59.6	70	78
S100A10	P60903	protein S100-A10	0.0206	0	57.5	71	99
C1S	P09871	complement C1s subcomponent	0.0201	200	56.2	72	93
TSP4	P35443	thrombospondin-4	0.0198	8	55.1	73	59
MTFP1	Q9UDX5	mitochondrial fission 1 protein	0.0197	0	55.0	74	51
HABP2	Q14520	hyaluronan-binding protein 2	0.0197	50	55.0	75	98
F12AI/ SERPING1	P50448	factor XIIa inhibitor (~SERPING1)	0.0192	700	53.6	76	61
OMD	Q99983	osteomodulin	0.0190	5	52.8	77	113
KRT3	P12035	keratin type II cytoskeletal 3	0.0173	3	48.3	78	108
HSPB1	P04792	heat shock protein HSP 90-beta	0.0166	6	46.2	79	76
SMPD1	P17405	sphingomyelin phosphodiesterase	0.0160	0	44.6	80	89
VWF	P04275	von Willebrand factor	0.0157	9	43.7	81	97
CTSB	P07858	cathepsin B	0.0149	10	41.6	82	65
AFP	P02771	alpha-fetoprotein	0.0148	0	41.1	83	66
CPN2	P22792	carboxypeptidase N subunit 2	0.0146	80	40.7	84	95
COMP	P49747	cartilage oligomeric matrix protein	0.0146	7	40.6	85	71
PLEK2	Q9NYT0	pleckstrin	0.0143	0	39.8	86	73
AGT	P01019	angiotensinogen	0.0142	200	39.4	87	62
HGFAC	Q04756	hepatocyte growth factor activator preproprotein	0.0138	20	38.5	88	84
MASP1	P48740	mannan-binding lectin serine protease 1	0.0137	20	38.3	89	60
LCAT	P04180	phosphatidylcholine-sterol acyltransferase	0.0136	20	38.0	90	88
TUBB	P07437	tubulin beta-1 chain	0.0133	4	37.2	91	83
SERPINB6	P35237	serpin B6	0.0132	8	36.9	92	106

LTBP1	Q14766	latent-transforming growth factor beta-binding protein 4-like	0.0129	8	36.0	93	87
KRT75	O95678	keratin type II cytoskeletal 75	0.0129	3	35.9	94	123
K2C7	P08729	keratin type II cytoskeletal 7	0.0129	0	35.9	95	138
C1R	P00736	complement component 1 r subcomponent	0.0127	150	35.4	96	75
APOE	P02649	apolipoprotein E	0.0127	300	35.3	97	85
GGH	Q92820	gamma-glutamyl hydrolase	0.0126	10	35.1	98	125
CL43/COLEC10	P42916	collectin-43	0.0125	0	34.7	99	90
SERPINA3_7	A2I7N3	serpin A3-7	0.0120	0	33.4	100	104
PROS1	P07225	vitamin K-dependent protein S	0.0119	100	33.0	101	63
F5	P12259	coagulation factor V	0.0113	15	31.5	102	101
C9	P02748	complement component C9	0.0109	200	30.5	103	82
APOD	P05090	apolipoprotein D	0.0106	200	29.5	104	80
KRT6B	P04259	keratin type II cytoskeletal 6B	0.0105	8	29.3	105	130
C4A	P0C0L4	complement C4-A	0.0103	200	28.8	106	91
GSN	P06396	gelsolin isoform a	0.0102	200	28.6	107	96
C5	P01031	complement C5a anaphylatoxin	0.0101	100	28.3	108	110
IGFALS	P35858	insulin-like growth factor-binding protein complex acid labile subunit	0.0098	80	27.4	109	119
RAB6B	Q14964	ras-related protein Rab-6B	0.0096	0	26.8	110	69
HBEGF	Q99075	proheparin-binding EGF-like growth factor	0.0096	0	26.8	111	92
FGG	P02679	fibrinogen gamma-B chain	0.0087	600	24.3	112	135
APOH	P02749	beta-2-glycoprotein 1	0.0087	800	24.2	113	112
CCDC76	Q9NUP7	tRNA guanosine-2'-O-methyltransferase TRM13 homolog	0.0083	0	23.2	114	121
ASPN	Q9BXN1	asporin	0.0081	0	22.6	115	105
ACTN1	P12814	alpha-actinin-1	0.0078	1	21.9	116	114
OIT3	Q8WWZ8	oncoprotein-induced transcript 3 protein	0.0073	3	20.4	117	117
COLEC10	Q9Y6Z7	collectin-10	0.0072	8	20.1	118	103
ACTN4	O43707	alpha-actinin-4	0.0066	6	18.4	119	133
FLNA	P21333	Filamin-A	0.0064	3	17.9	120	118
NUCB1	Q02818	nucleobindin-1	0.0063	10	17.6	121	140
AKR1C3	P42330	dihydrodiol dehydrogenase 3	0.0062	8	17.3	122	128
F9	P00740	coagulation factor IX	0.0062	40	17.2	123	77
COL6A3	P12111	collagen alpha-1(VI) chain	0.0058	1	16.3	124	132
YIPF3	Q9GZM5	protein YIPF3	0.0058	1	16.1	125	107

PKM2	P14618	pyruvate kinase isozymes M1/M2	0.0056	10	15.7	126	109
LAMB1	P07942	laminin subunit beta-1	0.0056	4	15.6	127	145
BGN	P21810	biglycan	0.0054	0	15.1	128	115
NSFL1C	Q9UNZ2	NSFL1 cofactor p47	0.0054	1	15.1	129	100
PRDX2	P32119	peroxiredoxin-2	0.0050	15	14.0	130	24
COL1A1	P02452	collagen alpha-1(XII) chain	0.0046	1	12.7	131	148
PDGFRB	P09619	beta-type platelet-derived growth factor receptor	0.0045	1	12.6	132	141
EFHC2	Q5JST6	EF-hand domain-containing family member C2	0.0044	0.5	12.4	133	126
ZBTB48	P10074	zinc finger and BTB domain-containing protein 48	0.0044	0	12.2	134	144
ELTD1	Q9HBW9	EGF latrophilin and seven transmembrane domain-containing protein 1	0.0044	1	12.1	135	161
ADAMTS13	Q76LX8	A disintegrin and metalloproteinase with thrombospondin motifs 13	0.0042	5	11.7	136	137
CEP290	O15078	centrosomal protein of 290 kDa	0.0041	0.01	11.5	137	162
GNL2	Q13823	nucleolar GTP-binding protein	0.0041	0	11.4	138	129
DARS	P14868	aspartyl-tRNA synthetase cytoplasmic	0.0040	0	11.1	139	120
SLC2A4	P14672	solute carrier family 2 facilitated glucose transporter member 4	0.0039	0	11.0	140	116
LRRN4	A4D1F6	leucine-rich repeat transmembrane neuronal protein 4	0.0039	0	10.7	141	127
CDH6	P55285	cadherin-6	0.0038	0.8	10.6	142	150
TLR6	Q9Y2C9	toll-like receptor 6	0.0038	0	10.5	143	146
PLG	P00747	plasminogen	0.0037	400	10.3	144	139
SRC	P12931	v-src sarcoma (Schmidt-Ruppin A-2) viral oncogene homolog	0.0037	0	10.3	145	122
HSPD1	P10809	60 kDa heat shock protein mitochondrial	0.0035	1	9.7	146	111
CCDC147	Q5T655	coiled-coil domain-containing protein 147	0.0034	0	9.5	147	131
TMTC3	Q6ZXV5	transmembrane and TPR repeat-containing protein 3	0.0033	0	9.1	148	136
CYLC1	P35663	cylicin-1	0.0030	0	8.4	149	153
APP	P05067	amyloid beta A4 protein	0.0029	4	8.0	150	143
PIGG	Q5H8A4	GPI ethanolamine phosphate transferase 2	0.0029	0	8.0	151	157
LTF	P02788	lactotransferrin	0.0028	2	7.9	152	155
MMRN1	Q13201	multimerin-1	0.0028	7	7.7	153	163

HSPG2	P98160	basement membrane-specific heparan sulfate proteoglycan core protein	0.0027	2	7.6	154	156
VCAM1	P19320	vascular cell adhesion molecule 1	0.0027	9	7.5	155	154
VCL	P18206	vinculin	0.0026	3	7.4	156	158
XP_874095_4	LOC616876	uncharacterized protein LOC616876 (~C1QC)	0.0025	100	7.1	157	134
AFG3L2	Q9Y4W6	AFG3-like protein 2	0.0025	0	6.9	158	152
NCAM1	P13591	neural cell adhesion molecule 1	0.0023	4	6.5	159	142
DNM2	P50570	dynamin-2	0.0023	0	6.4	160	147
ETAA1	Q9NY74	ewing's tumor-associated antigen 1 homolog	0.0022	0.3	6.2	161	149
NEBL	O76041	nebulette	0.0020	0	5.5	162	160
CSPG4	Q6UVK1	chondroitin sulfate proteoglycan 4	0.0017	0.2	4.8	163	166
ACAN	P16112	aggrecan core	0.0017	3	4.8	164	174
SMC1A	Q14683	structural maintenance of chromosomes protein1	0.0016	0	4.6	165	167
NRD1	O43847	nardilysin	0.0016	0	4.5	166	151
TLN2	Q9Y4G6	talin-2	0.0016	0.9	4.4	167	176
WDR17	Q8IZU2	WD repeat-containing protein 17	0.0016	0	4.3	168	159
TTLL5	Q6EMB2	tubulin polyglutamylase TTLL5 isoform 1	0.0016	0	4.3	169	168
CIT	O14578	citron Rho-interacting kinase	0.0014	0	4.0	170	165
NOTCH3	Q9UM47	neurogenic locus notch homolog protein 3-like	0.0013	0.5	3.6	171	173
NRXN2	P58401	neurexin-2-beta	0.0012	0	3.3	172	171
ARID2	Q68CP9	AT-rich interactive domain-containing protein 2	0.0011	0	3.0	173	175
CEP350	Q5VT06	centrosome-associated protein 350 isoform 1	0.0010	0.1	2.7	174	169
MYH9	P35579	myosin-IXb	0.0009	1	2.6	175	170
FLNC	Q14315	filamin-C	0.0007	0.7	2.1	176	172
DNAH8	Q96JB1	dynein heavy chain 2 axonemal	0.0005	0.07	1.3	177	177
TTN	Q8WZ42	titin	0.0004	0.07	1.0	178	178

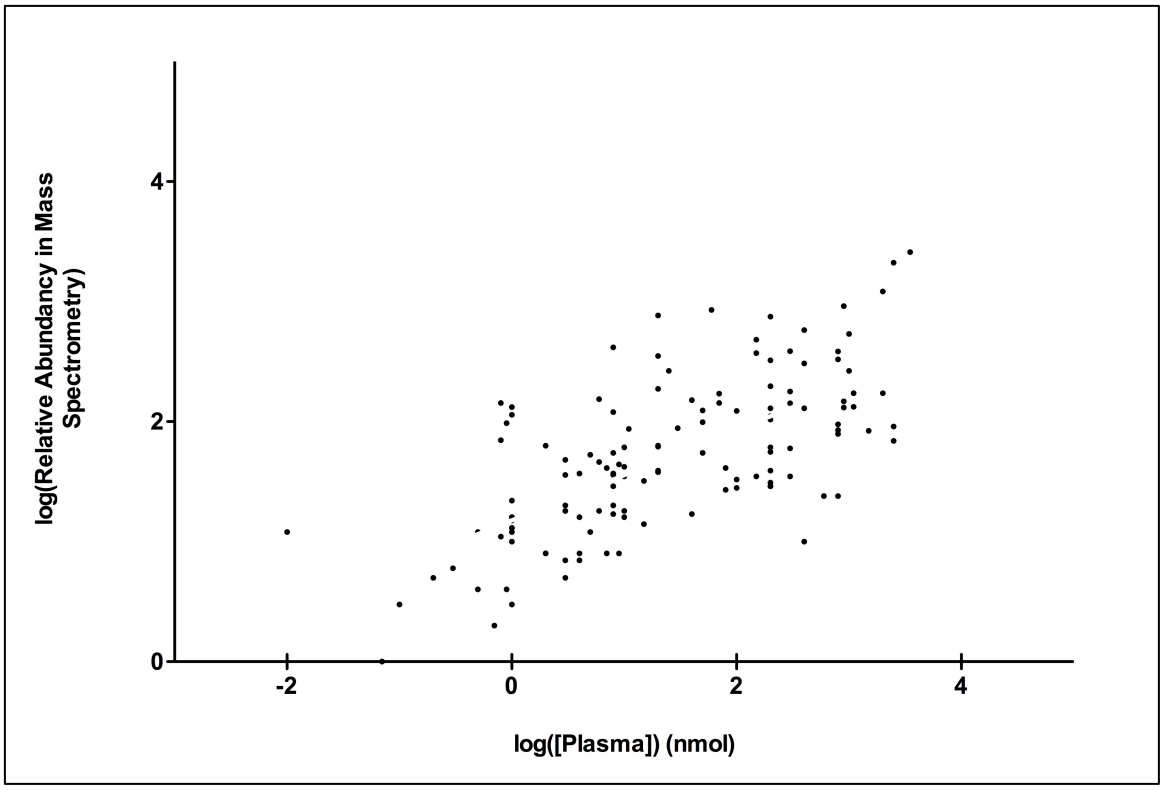

Supplementary Figure 3. Linear regression analysis between the logarithm of plasma concentration (nmol) and the logarithm of relative abundance as obtained by mass spectrometry data. Regression analysis at a 95% confidence level showed a linear correlation between protein abundance in mass spectrometry and the concentration in plasma ($r=0.66$, $p < 0.0001$).

Supplementary Table 2. **Relative abundance at the domain level**. A list of selected frequently appearing InterPro domains (IP number & IP name), their function as accepted and annotated by Gene Ontology, the number of different proteins sharing them, and their mean of relative abundance.

IP_Number	IP_Name	Protein function (Gene Ontology)	Number	Mean of domain RA
"IPR000215"	Protease_inhib_I4_serpin	serine-type endopeptidase inhibitor activity (GO)	13	51
"IPR002035"	VWF_A	protein binding (GO)	6	53
"IPR001599"	Macroglobln_a2	endopeptidase inhibitor activity (GO)	5	59
"IPR018039"	Intermediate_filament_CS	cytoskeleton structure	7	71
"IPR016060"	Complement_control_module	protein binding	9	75
"IPR013806"	Kringle-like	regulation of proteolytic activity	5	77
"IPR009003"	Pept_cys/ser_Trypsin-like	(protease) catalytic activity (GO)	7	78
"IPR003591"	Leu-rich_rpt_typical-subtyp	LRR proteins	6	78
"IPR000372"	LRR-contain_N	N-terminal LRR	7	82
"IPR001254"	Peptidase_S1_S6	serine-type endopeptidase activity (GO)	9	84
"IPR000859"	CUB	MEROPS peptidase	5	91
"IPR001881"	EGF-like_Ca-bd	calcium ion binding (GO)	14	92
"IPR001611"	Leu-rich_rpt	LRR proteins	9	95
"IPR011992"	EF-hand-like_dom	calcium ion binding (GO)	6	97
"IPR013032"	EGF-like_reg_C	-	17	98
"IPR006210"	EGF-like	protein binding (GO)	18	107
"IPR008985"	ConA-like_lec_gl	adhesion	8	108
"IPR013320"	ConA-like_subgrp	lectin	8	119
"IPR008160"	Collagen	adhesion	5	125
"IPR006209"	EGF	protein binding (GO)	9	126
"IPR013783"	Ig-like_fold	-	12	127
"IPR011993"	PH_type	signalling	5	127
"IPR007110"	Ig-like	protein binding (GO)	8	130
"IPR003961"	Fibronectin_type3	protein binding(GO)	5	141
"IPR013098"	Ig_I-set	adhesion	5	155

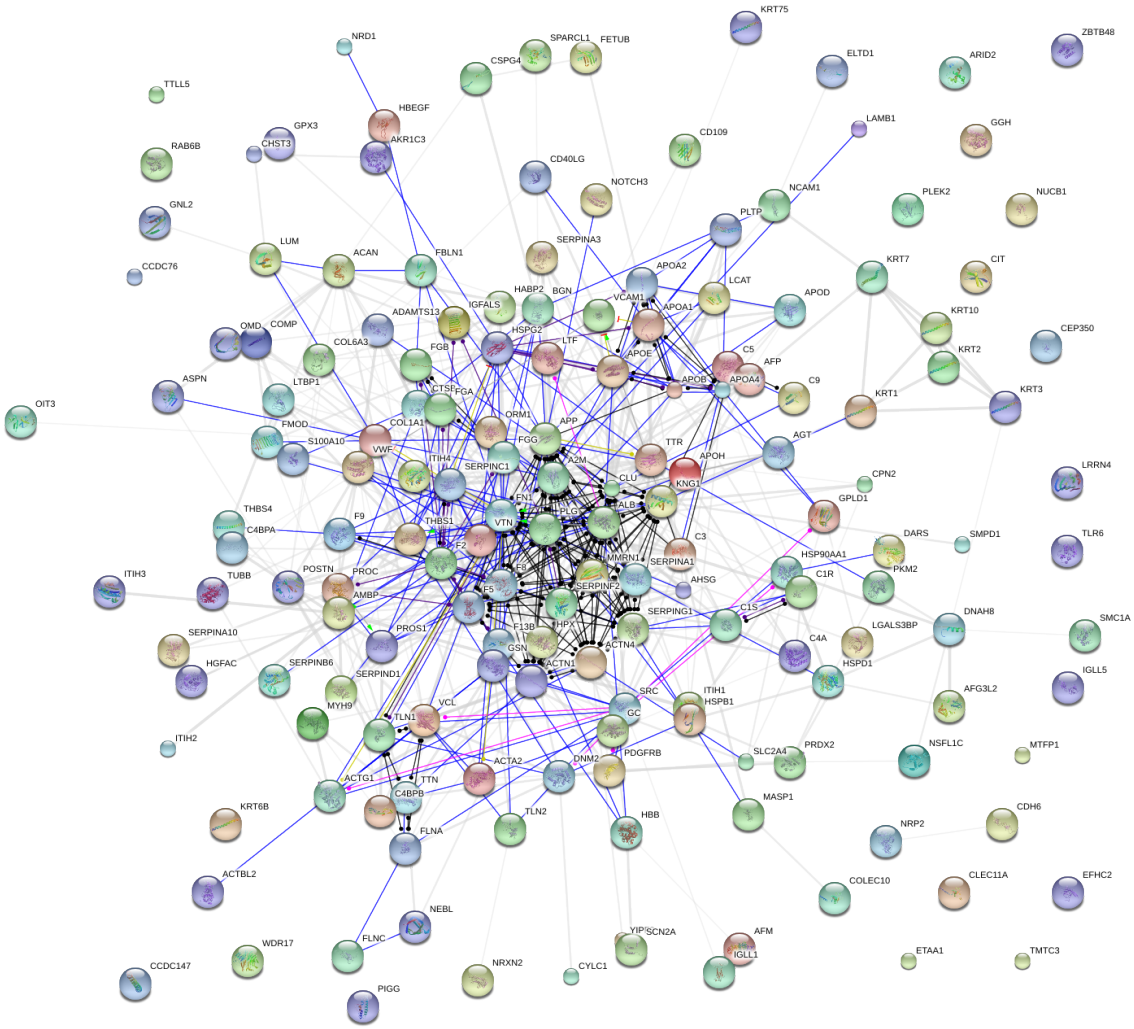

Supplementary Figure 4. Interactions of purified gene products at the action level as retrieved from String. A total of 178 identified genes were submitted to the STRING database (http://string-db.org/). Of these, 169 genes were recognized by the STRING database and more than 80% showed interactions, either at the evidence, confidence, or action level.

Supplementary Table 3[2]. List of significantly upregulated genes in HMEC 184 cells (90% confluence) following 24h exposure to ENPs (25 µg/mL) identified with DAVID Genecard DB. Gene, description, breast expression, fold change as compared to control (FC), and p-value.

Gene or Biological process	**Description of gene or Gene Ontology**	**Breast Expres-sion***	**FC**	***p value***
	Inflammatory response (GO:0006954)			
PLA2G4D	phospholipase A2_group IVD	1	5.44	7.22E-05
ELF3	E74-like factor 3 (ets domain transcription factor_epithelial-specific)	43	4.07	1.06E-04
PLBD1	phospholipase B domain containing 1	33	3.07	1.42E-04
IL36RN	interleukin 36 receptor antagonist	0	2.96	1.06E-04
HPGD	hydroxyprostaglandin dehydrogenase 15-(NAD)	11	2.90	2.72E-06
IL1RN	interleukin 1 receptor antagonist	38	2.66	4.61E-05
SAA3P	serum amyloid A3 pseudogene	11	2.61	4.78E-03
IL36G	interleukin 36_gamma	0	2.60	3.32E-04
HMOX1	heme oxygenase (decycling) 1	38	2.57	5.51E-04
S100A12	S100 calcium binding protein A12	4	2.44	6.45E-05
IL8	interleukin 8	16	2.20	3.64E-04
TLR1	toll-like receptor 1	14	2.15	1.43E-03
PLA2G7	phospholipase A2_group VII (platelet-activating factor acetylhydrolase_plasma)	19	2.15	6.46E-04
ANXA1	annexin A1	285	2.12	5.10E-05
TLR2	toll-like receptor 2	13	2.05	5.03E-04
	Cell junction (GO:0005911)			
CLDN4	claudin 4	49	6.07	6.21E-06
CLDN3	claudin 3	23	3.61	8.05E-05
CGN	cingulin	14	2.95	2.85E-04
CLDN7	claudin 7	20	2.62	1.49E-04
DSG4	desmoglein 4	2	2.22	2.09E-05
CDSN	corneodesmosin	0	2.18	6.43E-04
	Cell-Cell adhesion (GO:0016337)			
PCDH1	protocadherin 1	28	2.83	1.28E-05
CEACAM6	carcinoembryonic antigen-related cell adhesion molecule 6	4	2.78	1.16E-04
CEACAM1	carcinoembryonic antigen-related cell adhesion molecule 1 (biliary glycoprotein)	20	2.13	3.25E-04
ADAM8	ADAM metallopeptidase domain 8	7	2.09	6.57E-04
Cellular process: Biosynth-esis				
	Glycosphingolipid biosynthesis (hsa00601#)			
FUT2	fucosyltransferase 2 (secretor status included)	4	3.02	4.40E-04
B3GNT3	UDP-GlcNAc:betaGal beta-1.3-N-acetylglucosaminyltransferase 3	13	2.71	3.42E-05

[2] *: in Illumina Body Map (100xFPKM$^{1/2}$, Fragments Per Kilobase of exon per Million fragments mapped were calculated using the Cufflinks program and thereupon rescaled by multiplying FPKM by 100 and then calculating the root); #: has a gene ID retrieved from www.genome.jp/kegg/

FUT3	fucosyltransferase 3 (galactoside 3(4)-L-fucosyltransferase_Lewis blood group)	3	2.57	4.37E-05
	Glycoprotein biosynthetic process (GO:0009101)			
B3GALT4	UDP-Gal:betaGlcNAc beta 1.3-galactosyltransferase_polypeptide 4	20	3.06	8.81E-05
	Glycerolipid biosynthetic process (GO:0045017)			
CWH43	hypothetical protein FLJ21511	0	3.08	1.06E-04
DGAT2	diacylglycerol O-acyltransferase homolog 2 (mouse)	215	2.75	8.90E-04
AGPAT9	1-acylglycerol-3-phosphate O-acyltransferase 9	16	2.47	2.50E-04
	Lipid biosynthetic process (GO:0008610)			
FA2H	fatty acid 2-hydroxylase	6	2.97	8.49E-05
ELOVL4	elongation of very long chain fatty acids (FEN1/Elo2_SUR4/Elo3_yeast)-like 4	7	2.09	3.75E-04
	purine nucleotide biosynthetic process (GO:0006164)			
ATP12A	ATPase_H^+/K^+ transporting_nongastric_alpha polypeptide	0	5.85	5.71E-06
GUCY1A3	guanylate cyclase 1_soluble_alpha 3	29	2.66	1.62E-05
	ATP binding (GO:0005524)			
PRR15L	ATPase family_AAA domain containing 4	12	5.14	2.94E-05
OASL	2'-5'-oligoadenylate synthetase-like	10	2.88	2.36E-04
ERBB3	v-erb-b2 erythroblastic leukemia viral oncogene homolog 3 (avian)	31	2.71	9.35E-05
NLRP10	NLR family_pyrin domain containing 10	0	2.49	5.86E-05
PIM1	pim-1 oncogene	44	2.06	1.51E-04
KIF13B	kinesin family member 13B	20	2.00	3.44E-06
	Ribosome biogenesis			
ISG20	interferon stimulated exonuclease gene 20kDa	22	2.70	3.49E-07
	Angiogenesis (GO:0001525)			
S100A7	S100 calcium binding protein A7	4	3.12	9.75E-04
CEACAM1	carcinoembryonic antigen-related cell adhesion molecule 1 (biliary glycoprotein)	20	2.13	3.25E-04
Cellular process: Proliferation				
	Regulation of cell proliferation (GO:0042127)			
CAPN14	calpain 14	2	22.87	9.73E-09
S100P	S100 calcium binding protein P	11	7.74	4.01E-06
VTCN1	V-set domain containing T cell activation inhibitor 1	25	5.29	3.93E-05
LIPH	lipase_member H	8	4.99	2.27E-06
CDKN1C	cyclin-dependent kinase inhibitor 1C (p57_Kip2)	63	4.48	5.36E-05
RASSF3	Ras association (RalGDS/AF-6) domain family member 3	61	3.99	2.88E-04
RTKN2	rhotekin 2	4	2.65	5.06E-05
MARCKSL1	MARCKS-like 1	49	2.48	2.70E-04
RARRES1	retinoic acid receptor responder (tazarotene induced) 1	24	2.38	1.19E-04
CAPN5	calpain 5	13	2.21	2.24E-05
IGFL2	IGF-like family member 2	0	2.09	2.34E-05
KLK6	kallikrein-related peptidase 6	11	2.06	1.83E-04
	Proliferation: Wnt signaling pathway			
NDRG2	NDRG family member 2	118	2.16	5.48E-04
APCDD1	adenomatosis polyposis coli down-regulated 1	46	2.09	6.51E-04
	Cell cycle phase (GO:0022403)			
MAP2	microtubule-associated protein 2	16	2.77	8.53E-05
MAPRE2	microtubule-associated protein_RP/EB family_member 2	33	2.45	1.34E-04

OVOL1	ovo-like 1(Drosophila)	4	2.31	9.03E-05
Transcript-ion				
	Regulation of transcription_DNA-dependent (GO:0006355)			
HOPX	HOP homeobox	13	3.25	4.73E-04
	Regulation of transcription (GO:0006355)			
MACC1	metastasis associated in colon cancer 1	8	3.00	5.63E-04
Cell structure				
	cytoskeletal part (GO:0044430)			
KRT23	keratin 23 (histone deacetylase inducible)	29	8.59	2.04E-04
KRT80	keratin 80	11	6.64	6.43E-07
KRT34	keratin 34	0	2.96	4.23E-04
KRT24	keratin 24	1	2.55	1.51E-04
FLG	filaggrin	2	2.27	3.49E-04
	Golgi membrane (GO:0000139)			
CHST6	carbohydrate (N-acetylglucosamine 6-O) sulfotransferase 6	1	2.96	9.72E-04
MALL	mal_T-cell differentiation protein-like	33	2.68	7.61E-05
	Organelle membrane (GO:0031090)			
RAB11FIP1	RAB11 family interacting protein 1 (class I)	23	4.60	7.30E-05
CYP4B1	cytochrome P450_family 4_subfamily B_polypeptide 1	26	3.34	4.60E-05
SPINK5	serine peptidase inhibitor_Kazal type 5	5	2.58	7.79E-04
Cellular process: cell death and apoptosis				
	Negative regulation of apoptosis (GO:0043066)			
SERPINB2	serpin peptidase inhibitor_clade B (ovalbumin)_member 2	9	3.48	3.63E-04
	Regulation of apoptosis (GO:0042981)			
MMP10	matrix metallopeptidase 10	2	3.54	7.88E-05
MMP1	matrix metallopeptidase 1	0	3.18	4.66E-04
MMP9	matrix metallopeptidase 9 (gelatinase B_92kDa gelatinase_92kDa type IV collagenase)	39	2.06	7.62E-04
	Cell death			
BNIPL	BCL2/adenovirus E1B 19kD interacting protein like	12	3.19	5.63E-06
LCN2	lipocalin 2	18	2.30	6.47E-06
Endocyto-sis and trafficking				
RAB11FIP1	RAB11 family interacting protein 1 (class I)	23	4.60	7.30E-05
MARCKSL1	MARCKS-like 1	49	2.48	2.70E-04
MARCO	macrophage receptor with collagenous structure	46	2.11	3.03E-04
SPON2	spondin 2_extracellular matrix protein	46	2.06	7.42E-04
MYO5B	myosin VB	13	2.05	3.03E-05
MAL2	mal_T-cell differentiation protein 2 (gene/pseudogene)	68	2.01	2.90E-04
Oxydant stress				
NCF2	neutrophil cytosolic factor 2	30	3.61	8.57E-05
GGT6	gamma-glutamyltransferase 6	11	2.00	1.34E-04
Miscellan-eous				
MUC16	mucin 16_cell surface associated	9	2.70	1.09E-04

Supplementary Table 4[3]. Functional annotation analysis of microarry data sets using ADVID. GO terms were significantly enriched in genes at least twofold upregulated in HMEC 184 cells (90% confluence) in response to 24h exposure to 25 µg/mL ENPs.

Cluster *	Category	Term	Count	P value#	FE
Cluster 1	GOTERM_CC_FAT	cornified envelope	9	1.78E-11	41.83
	SP_PIR_KEYWORDS	keratinization	7	6.27E-07	22.29
	GOTERM_BP_FAT	keratinocyte differentiation	12	8.22E-12	21.02
	GOTERM_BP_FAT	epidermal cell differentiation	13	8.83E-13	20.88
	GOTERM_BP_FAT	keratinization	7	1.64E-06	18.82
	GOTERM_BP_FAT	peptide cross-linking	4	1.38E-03	17.79
	GOTERM_BP_FAT	epithelial cell differentiation	16	6.41E-13	13.50
	GOTERM_BP_FAT	epidermis development	18	2.81E-13	11.31
	GOTERM_BP_FAT	ectoderm development	18	1.02E-12	10.46
	GOTERM_BP_FAT	epithelium development	16	9.11E-10	8.15
Cluster 2	SP_PIR_KEYWORDS	inflammatory response	5	3.09E-03	8.27
	GOTERM_BP_FAT	inflammatory response	10	1.91E-03	3.56
	GOTERM_BP_FAT	response to wounding	15	1.74E-04	3.27
	GOTERM_BP_FAT	defense response	12	1.64E-02	2.26
Cluster 3	INTERPRO	keratin_type I	3	2.80E-02	11.39
	INTERPRO	filament	4	1.95E-02	6.96
	INTERPRO	Intermediate filament protein_conserved site	4	1.95E-02	6.96
	GOTERM_MF_FAT	structural molecule activity	14	1.24E-03	2.81
Cluster 4	GOTERM_CC_FAT	desmosome	3	1.58E-02	15.34
	SP_PIR_KEYWORDS	tight junction	3	8.21E-02	6.26
	GOTERM_CC_FAT	apical junction complex	6	2.74E-03	6.20
	GOTERM_CC_FAT	apicolateral plasma membrane	6	3.12E-03	6.02
	GOTERM_CC_FAT	cell-cell junction	8	2.50E-03	4.31
Cluster 5	SP_PIR_KEYWORDS	inflammatory response	5	3.09E-03	8.27
Cluster 6	KEGG_PATHWAY	glycosphingolipid biosynthesis	3	1.12E-02	17.95
	SP_PIR_KEYWORDS	signal-anchor	10	5.85E-03	3.03
Cluster 7	GOTERM_BP_FAT	glycerolipid biosynthetic process	4	3.13E-02	5.78
Cluster 8	GOTERM_BP_FAT	wound healing	6	2.43E-02	3.63

[3] *: Biological process (BP), cellular component (CC), and molecular function (MF) in Gene Ontology (GO), single protein of protein information ressource (SP_PIR), protein domains or sites (INTERPRO) and pathway extracted from Kyoto Encyclopedia of Genes and Genomes (KEGG); #: or EASE score, modified Fisher's exact test according to DAVID software cut-off.

REFERENCES

1. Agarwal R, and Gupta MN. Sequential precipitation with reversibly soluble insoluble polymers as a bioseparation strategy: purification of beta-glucosidase from Trichoderma longibrachiatum. *Protein Expr Purif* 7: 294-298, 1996.
2. Benjamini Y, Drai D, Elmer G, Kafkafi N, and Golani I. Controlling the false discovery rate in behavior genetics research. *Behav Brain Res* 125: 279-284, 2001.
3. Bhardwaj P, Chaurasia H, Chaurasia D, Prajapati SK, and Singh S. Formulation and in-vitro evaluation of floating microballoons of indomethacin. *Acta Pol Pharm* 67: 291-298, 2010.
4. Boag AH, and Sefton MV. Microencapsulation of human fibroblasts in a water-insoluble polyacrylate. *Biotechnol Bioeng* 30: 954-962, 1987.
5. Broughton RL, and Sefton MV. Effect of capsule permeability on growth of CHO cells in Eudragit RL microcapsules: use of FITC-dextran as a marker of capsule quality. *Biomaterials* 10: 462-465, 1989.
6. Cui W, Li J, Zhang Y, Rong H, Lu W, and Jiang L. Effects of aggregation and the surface properties of gold nanoparticles on cytotoxicity and cell growth. *Nanomedicine* 8: 46-53, 2012.
7. Dekeyser CM, Zuyderhoff E, Giuliano RE, Federoff HJ, Dupont-Gillain Ch C, and Rouxhet PG. A rough morphology of the adsorbed fibronectin layer favors adhesion of neuronal cells. *J Biomed Mater Res A* 87: 116-128, 2008.
8. Eidi H, Joubert O, Attik G, Duval RE, Bottin MC, Hamouia A, Maincent P, and Rihn BH. Cytotoxicity assessment of heparin nanoparticles in NR8383 macrophages. *Int J Pharm* 396: 156-165, 2010.
9. Eidi H, Joubert O, Nemos C, Grandemange S, Mograbi B, Foliguet B, Tournebize J, Maincent P, Le Faou A, Aboukhamis I, and Rihn BH. Drug delivery by polymeric nanoparticles induces autophagy in macrophages. *Int J Pharm* 422: 495-503, 2012.
10. Gao J, Gu H, and Xu B. Multifunctional magnetic nanoparticles: design, synthesis, and biomedical applications. *Acc Chem Res* 42: 1097-1107, 2009.
11. Hamamoto R, Yamada K, Kamihira M, and Iijima S. Differentiation and proliferation of primary rat hepatocytes cultured as spheroids. *J Biochem* 124: 972-979, 1998.
12. Huang da W, Sherman BT, and Lempicki RA. Systematic and integrative analysis of large gene lists using DAVID bioinformatics resources. *Nat Protoc* 4: 44-57, 2009.
13. Huang Z, and Leong SS. Molecular-assisted refolding: study of two different ionic forms of recombinant human fibroblast growth factors. *J Biotechnol* 142: 157-163, 2009.
14. Huang Z, Ni C, Zhou X, Liu Y, Tan Y, Xiao J, Feng W, Li X, and Yang S. Mechanism of pH-sensitive polymer-assisted protein refolding and its application in TGF-beta1 and KGF-2. *Biotechnol Prog* 25: 1387-1395, 2009.
15. Hussien R, and Brooks GA. Mitochondrial and plasma membrane lactate transporter and lactate dehydrogenase isoform expression in breast cancer cell lines. *Physiol Genomics* 43: 255-264, 2011.
16. Kamihira M, Kaul R, and Mattiasson B. Purification of recombinant protein A by aqueous two-phase extraction integrated with affinity precipitation. *Biotechnol Bioeng* 40: 1381-1387, 1992.

17. Lorentzen A, Lewinsky RH, Bornholdt J, Vogel LK, and Mitchelmore C. Expression profile of the N-myc Downstream Regulated Gene 2 (NDRG2) in human cancers with focus on breast cancer. *BMC Cancer* 11: 14, 2011.
18. Mosmann T. Rapid colorimetric assay for cellular growth and survival: application to proliferation and cytotoxicity assays. *J Immunol Methods* 65: 55-63, 1983.
19. Oberdorster E. Manufactured nanomaterials (fullerenes, C60) induce oxidative stress in the brain of juvenile largemouth bass. *Environ Health Perspect* 112: 1058-1062, 2004.
20. Oberdorster G. Pulmonary effects of inhaled ultrafine particles. *Int Arch Occup Environ Health* 74: 1-8, 2001.
21. Oberdorster G, Maynard A, Donaldson K, Castranova V, Fitzpatrick J, Ausman K, Carter J, Karn B, Kreyling W, Lai D, Olin S, Monteiro-Riviere N, Warheit D, and Yang H. Principles for characterizing the potential human health effects from exposure to nanomaterials: elements of a screening strategy. *Part Fibre Toxicol* 2: 8, 2005.
22. Pignatello R, Bucolo C, Ferrara P, Maltese A, Puleo A, and Puglisi G. Eudragit RS100 nanosuspensions for the ophthalmic controlled delivery of ibuprofen. *Eur J Pharm Sci* 16: 53-61, 2002.
23. Rivera_Gil P, Clift MJD, Rutishauser BR, and Parak WJ. Methods for understanding the interaction between nanoparticles and cells. In: *Nanotoxicity: methods and protocols*, edited by Reineke J. New York: Humana Press, 2012, p. 33-56.
24. Safarik I, and Safarikova M. Magnetic techniques for the isolation and purification of proteins and peptides. *Biomagn Res Technol* 2: 7, 2004.
25. Santamaria A. *Nanotoxicity: Methods and Protocols, Methods in Molecular Biology*. New York: Humana Press, 2012, p. 426 pages.
26. Sharma A, and Gupta MN. Macroaffinity ligand-facilitated three-phase partitioning (MLFTPP) for purification of xylanase. *Biotechnol Bioeng* 80: 228-232, 2002.
27. Shimomura Y, Agalliu D, Vonica A, Luria V, Wajid M, Baumer A, Belli S, Petukhova L, Schinzel A, Brivanlou AH, Barres BA, and Christiano AM. APCDD1 is a novel Wnt inhibitor mutated in hereditary hypotrichosis simplex. *Nature* 464: 1043-1047, 2010.
28. Song Y, Li X, and Du X. Exposure to nanoparticles is related to pleural effusion, pulmonary fibrosis and granuloma. *Eur Respir J* 34: 559-567, 2009.
29. Taipa MA, Kaul RH, Mattiasson B, and Cabral JM. Recovery of a monoclonal antibody from hybridoma culture supernatant by affinity precipitation with Eudragit S-100. *Bioseparation* 9: 291-298, 2000.
30. Toulza E, Mattiuzzo NR, Galliano MF, Jonca N, Dossat C, Jacob D, de Daruvar A, Wincker P, Serre G, and Guerrin M. Large-scale identification of human genes implicated in epidermal barrier function. *Genome Biol* 8: R107, 2007.
31. Vazquez SM, Mladovan AG, Perez C, Bruzzone A, Baldi A, and Luthy IA. Human breast cell lines exhibit functional alpha2-adrenoceptors. *Cancer Chemother Pharmacol* 58: 50-61, 2006.
32. Waite CL, and Roth CM. Nanoscale drug delivery systems for enhanced drug penetration into solid tumors: current progress and opportunities. *Crit Rev Biomed Eng* 40: 21-41, 2012.

33. Wang R, Kim JH, Kim BS, Park CS, and Yoo SH. Preparation and characterization of non-covalently immobilized amylosucrase using a pH-dependent autoprecipitating carrier. *Bioresour Technol* 102: 6370-6374, 2011.
34. Warheit DB, Laurence BR, Reed KL, Roach DH, Reynolds GA, and Webb TR. Comparative pulmonary toxicity assessment of single-wall carbon nanotubes in rats. *Toxicol Sci* 77: 117-125, 2004.
35. Worle-Knirsch JM, Pulskamp K, and Krug HF. Oops they did it again! Carbon nanotubes hoax scientists in viability assays. *Nano Lett* 6: 1261-1268, 2006.
36. Yang J, McNeish B, Butterfield C, and Moses MA. Lipocalin 2 is a novel regulator of angiogenesis in human breast cancer. *Faseb J* 27: 45-50, 2012.
37. Yoo JW, Giri N, and Lee CH. pH-sensitive Eudragit nanoparticles for mucosal drug delivery. *Int J Pharm* 403: 262-267, 2011.

CHAPTER 5

Conclusions and Future Directions

CONCLUSIONS

My doctoral dissertation consisted of two research projects investigating normal and cancerous mammary epithelial cells, one project that examined the Warburg Effect and one project that examined the effects of nanoparticle exposure.

In my first study I examined the expression and localization of lactate shuttle proteins, monocarboxylate transporters (MCT), and lactate dehydrogenase (LDH) isoforms in the two human breast cancer cell lines MCF-7 and MDA-MB-231, compared to the normal human breast epithelial cells HMEC 184. I also measured lactate production and oxygen consumption in each cell line and analyzed my findings base on their expression of lactate shuttle proteins. I examined available microarray (7) and MassArray data (18) to extend my findings to a larger set of breast cancer cell lines. My hypothesis was that the Warburg Effect produces changes in the localization and expression of MCTs and of LDH isoforms in cancerous breast cells when compared to normal breast cells, and that these changes correspond to the oxidative capacity of these cancerous cells.

M results showed that MCT 1 was not expressed in MDA-MB-231, but was expressed in MCF-7 cells, where its expression was less than in control HMEC 184 cells. When present in HMEC 184 and MCF-7 cells, MCT 1 was localized to the plasma membrane. MCT 2 and MCT 4 were expressed in all the cell lines studied. MCT 4 expression was higher in MDA-MB-231 compared to MCF-7 and HMEC 184 cells, whereas MCT 2 expression was higher in MCF-7 compared to MDA-MB-231 and HMEC 184 cells. Unlike MCT 1, MCT 2 and MCT 4 were localized in mitochondria in addition to the plasma membrane. LDHA and LDHB were expressed in all the cell-lines, but abundances were higher in the two cancer cell-lines than in the control cells. MCF-7 cells expressed mainly LDHB, while MDA-MB-231 and control cells expressed mainly LDHA. LDH isoforms were localized in mitochondria in addition to the cytosol. These localization patterns were the same in cancerous and control cell lines. In summary, I showed that MCT (1, 2, and 4) and LDH isoforms (A and B) are expressed in both normal and cancerous breast cells, occupying both mitochondrial and extra-mitochondrial cell compartments. Thus breast cancer appears to change the expression of lactate shuttle proteins, but not their sub-cellular localizations.

The HMEC 184 cells, which expressed the highest amount of MCT1 and the lowest amount of LDH, had the highest oxygen consumption and lowest lactate production between the three cell lines examined. MDA-MB-231 cells, which expressed a higher level of MCT4 and LDHA than MCF-7, showed lower oxygen consumption than MCF-7 cells. Using glycolysis and LDH inhibitors, I showed that the lactate produced in the two breast cancer cell lines was not only from glycolysis. My data showed that observed changes in the expression of lactate shuttle proteins were associated with decreased oxidative capacity and increased lactate accumulation within breast cancer cells.

By analyzing the microarray data of Charafe-Jauffret et al. (7) and the MassArray data of Novak et al. (18), we showed there is a reduction in MCT1 expression in breast cancer cell lines when compared to normal breast cell lines. The reduction appears to be specific to luminal-like and mesenchymal-like breast cancer cell lines. The change in MCT1 expression is due to *MCT1* promoter hypermethylation, which appeared in an

earlier stage of cancer progression. Thus our data and those of others indicate that MCT1 expression is downregulated in breast cancer in general.

In conclusion, our study supports the existence of the previously reported lactate shuttle in cancer, and adds a new explanation of its function (12). My study provided additional detail for the way that lactate transporters are expressed in breast cancer cells, and established a foundation for further study of the role and contribution of lactate transporters to the Warburg Effect.

My next project examined the effect of Eudragit® RS 100 (ENP), a copolymer nanoparticle increasingly used to coat and deliver drugs such as chemotherapy agents, on the metabolic activity and proliferation of human mammary epithelial cells (HMEC 184, MCF-7, MDA-MB-231). Cells' metabolic activity and proliferation were measured using tetrazolium salt (WST-1) and 5-bromo-2'-deoxyuridine (BrdU) assays, respectively. I also examined the uptake of these particles inside the cells and their effect on mitochondrial morphology using Nile-red conjugated particles, mitotracker dye, and confocal laser microscopy. Lastly, using mass spectrometry and Micrroarry analyses I was able to map the mechanism that caused these particles to act on the cells.

My results showed that cells treated with ENPs displayed dose-dependent increases in metabolic activity and growth, which was found using tetrazolium salt (WST-1) and total protein content (BCA) assay. The increases in metabolic activity were also seen when ENPs were mixed with culture media, both 24h before seeding the cells and at the same time as cell seeding. At the same time a dose-dependent decrease in cell proliferation, measured with a 5-bromo-2'-deoxyuridine (BrdU) ELISA assay, was observed in the cells after 24h incubation with ENPs. The decrease in proliferation was further confirmed with a proliferation assay that quantified proliferating cells labeled with 5-ethynyl-2´-deoxyuridine (EdU) using a fluorescent azide reaction.

Labeling of ENPs with Nile red fluorescent congregated dye and examination of the cells with confocal microscopy showed that ENPs entered the cells. However, the majority of ENPs aggregated into clumps with proteins from media, forming a clearly visible network closely attached to cells. Mitochondrial networks labeled with mitotracker remained intact with no sign of fragmentation. Using proteomic mass spectrometry I showed that the aggregated ENP-serum protein network contains proteins sharing common InterPro domains and exhibiting protease, antiprotease, epidermal growth factor, adhesion, and binding properties. Collecting RNA from cells treated with ENPs and subjecting them to Micrroarry analyses, I showed that ENP treatment caused an activation of proliferation, growth, differentiation, and transformation pathways in the treated cells. In summary, my data show that empty unloaded ENPs can have direct effect on human mammary epithelial cells by itself. The effect I observed following nanoparticle exposure, namely the increase in metabolic activity and growth in cancer and normal human epithelial breast cells, had not been reported previously, and my research therefore highlighted the need for further investigation into the potentially counter-productive effects of nanoparticles in cancer chemotherapy (13).

FUTURE DIRECTIONS

In my future directions I will focus on the Warburg effect, and have drafted a detailed research plan containing my aims and methods. I have no plans at the moment to continue studying nanoparticles, but have included below several ideas that students may use to continue work in this area.

FUTURE DIRECTIONS: TO STUDY THE WARBURG EFFECT

Based on my results studying lactate shuttle proteins and their relationship to the Warburg Effect in human mammary epithelial cells (HMECs) (12), and the results of the Bissell laboratory, who used the three-dimensional (3D) model of HMECs to show that increased glycolysis in normal cells by itself can be an oncogenic event (19), I have proposed a research plan to map the mechanism by which lactate transport, a process necessary for maintaining increased glycolysis, facilitates breast cancer onset. I propose two main aims in my future research, using the 3D model of MECs: first, to determine whether increased lactate disposal is a required condition for the Warburg Effect to become an oncogenic event, and second, to determine whether lactate acts as a paracrine-signaling molecule in breast cancer.

Objective 1*: To determine whether increased lactate disposal is a required condition for the Warburg Effect (increased glycolysis) to activate oncogenic pathways, increase cell growth, and disturb polarity in mammary epithelial cells.*

Background and Preliminary Data for Objective 1: The 3D model of Human Mammary Epithelial Cells (HMECs) was developed by the Bissell laboratory to support their theory of "dynamic reciprocity," (3), which has expanded the role of ECM beyond just providing a structural scaffold for tissues. Dynamic reciprocity suggests communication between cells and their microenvironment, particularly with respect to a conversation between cells and the ECM. The Bissell laboratory has pioneered the use of 3D cell culture using gels made of laminin rich ECM (lrECM) to investigate the role of the ECM in defining tissue form and function and what goes wrong during cancer progression. Using this 3D assay, non-malignant and malignant breast cells can be distinguished by morphology (20). Furthermore, they developed a unique isogenic breast cancer progression series the (HMT-3522 cell series) without the use of exogenous oncogenes. When grown in lrECM 3D gels, the non-malignant S1 cells form growth arrested, polarized acinar-like structures that resemble acini found in the human breast. On the other hand, the malignant T4-2 cells form disorganized, non-polarized colonies that do not growth arrest. However, T4-2 cells can be phenotypically reverted to resemble the polarized growth arrested S1 colonies by treatment with a number of agents that interfere with aberrant signaling from the microenvironment (1, 23-25). Most importantly, the phenotypic reversion occurs without changes in the genetic make-up of the T4-2 cells. The cells retain the same mutations, but by restoring appropriate signaling the cells behave in a non-malignant manner, speaking to the importance of correct signaling from the microenvironment.

A new study from the Bissell laboratory (19) shows that increased glucose uptake, by overexpression of glucose transporter 3 (GLUT3) in normal S-1 cells, disrupted their

polarized structure, and activated known oncogenic signaling pathways (such as epidermal growth factor receptor (EGFR), β1 integrin, mitogen-activated protein kinase kinase (MEK), and protein kinase B (Akt) pathways). On the other hand, reduction of glucose uptake by the suppression of GLUT3 expression in the T4-2 malignant cells led to suppression of the oncogenic pathways and the subsequent formation of organized, growth-arrested, polarized structures (19). Surprisingly, the mammalian target of rapamycin (mTOR) and hypoxia-inducible factor 1-alpha (HIF-1α) pathways were not involved in the changes seen in S1 and T4-2 cells, but cyclic adenosine monophosphate (cAMP), spindle assembly checkpoint protein (sAC), exchange proteins activated by cAMP (EPAC), Ras-related protein 1 (Rap1), and hexosamine biosynthetic pathway (HBP) seem to play a role in the activation of oncogenic pathways following increased glycolysis (**Figure. 1**). By analyzing the microarray data of Kenny et al. (14), who examined gene profiles of many breast cells including S1 and T4-2 cells, we found significantly increased MCT1 expression alongside a significant reduction in MCT4, with no change in MCT2 in T4-2 malignant cells when compared to S1 nonmalignant cells. Increased MCT1 expression in basal-like breast cancer tissues was previously reported by Pinheiro et al. (21). Thus, the specific activation of MCT1 is specific to T4-2 cells, which are basal-like breast cancer cells. In light of these prior results, it is plausible that MCTs may also contribute to breast cancer progression by playing a role in supporting the Warburg Effect.

Methods and Interpretations for Objective 1:

The non-malignant S1 and the malignant T4-2 cells will be grown in 3D (lrECM) gel. Lactate production, glucose uptake, lactate dehydrogenase (LDH), GLUT3, and MCT (1, 2, and 4) expression will be measured as described previously (10, 12). I expect the non-malignant S1 cells to exhibit lower lactate production, glucose uptake, and expression of LDH, GLUT3, and MCT1, but higher MCT4, with similar MCT2 expression when compared to the malignant T4-2 cells. Next I will examine if MCT1 and MCT4 expression levels affect the above parameters, and whether they affect cell polarity, growth status, and oncogenic pathway activity (See Table. 1). I will do this by amplifying GLUT3, MCT1, and MCT4 cDNAs from the total cDNA of T4-2 cells, then constructing them into a viral vector with commercially available kits. S1 cells will be transfected with GLUT3-vector, and different combinations of MCT1-vector and MCT4-vector (or empty vector as control). Commercially available siRNA for MCT1 and MCT4 will be used to delete the expression of these proteins. The combinations of overexpressed or deleted MCT1 and MCT4 to be used in S1 and T4 cells, is illustrated in the **Table 1** in conditions 1 to 11.

Expected Results and Alternative Approaches for Objective 1: In conditions 1, 2, and 3 I expect GLUT3 overexpression to activate glycolysis, and thereby to activate the oncogenic pathways (EGFR, β1 integrin, MEK and Akt). I also expect increased glycolysis to cause loss of tissue polarity and increased cell growth (as was seen in condition (C) by Onodera et al. (19). Overexpression of either MCT1, MCT4, or both MCT1 and MCT4 should not prevent any of the above changes. In conditions 4, 5, and 6 I expect my deletion of MCT1 and/or MCT4 expression to prevent oncogenic pathway

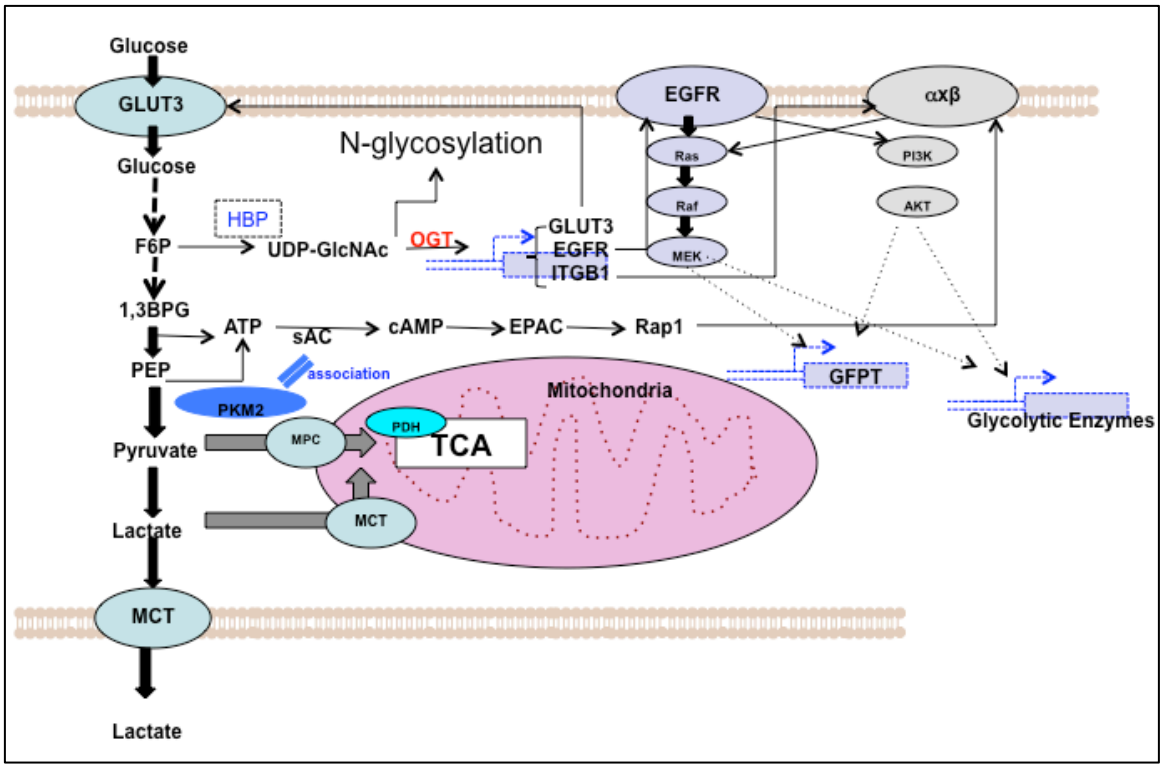

Figure 1: Adapted from Onodera et al. (19) with "MCT & MPC" additions indicating elements of my proposed research. Figure shows how increased glucose uptake activates oncogenic signaling pathways. Increased glucose uptake in 3D model of Human Mammary Epithelial Cells (HMECs) activates oncogenic signaling pathways, including epidermal growth factor receptor (EGFR), β1 integrin (αxβ), mitogen-activated protein kinase kinase (MEK), and protein kinase B (Akt) pathways. There are reciprocal interactions between glucose metabolism and the oncogenic signaling pathways. The sAC-EPAC-Rap1 pathway regulates β1 integrin positively via a direct link between ATP production in the glycolytic pathway and cAMP generation by sAC. The hexosamine biosynthetic pathway (HBP) is also upregulated through activation of oncogenic signaling. The downstream O-GlcNAcylation of target proteins regulates the expression of β1 integrin, EGFR, and GLUT3. Lactate removal is completed through MCTs on plasma and mitochondrial membranes. Note that the entire upstream pathways will be repressed if cells fail to remove lactate.
(ATP: Adenosine triphosphate, 1,3BPG: 1,3-Bisphosphoglycerate, cAMP: Cyclic adenosine monophosphate, EPAC: Exchange proteins activated by cAMP, F6P: Fructose-6-phosphate, GLUT3: Glucose transporter type 3, ITGB1: Gene encoding b 1 integrin protein, MCT: Monocarboxylate Transporters, MPC; Pyruvate transporters, OGT: O-linked N-acetylglucosamine transferase, PDH: Pyruvate dehydrogenase, PEP: Phosphoenolpyruvate, PKM2: Pyruvate kinase enzyme type M2, Rap1: Ras-related protein 1, sAC; Spindle assembly checkpoint protein, TCA: Tricarboxylic acid cycle, UDP-GLcNAc: Uridine diphosphate-N-acetylglucosamine)

activation, polarity loss, and increased cell growth following GLUT3 overexpression. In conditions 7 and 8 I expect MCT1 or MCT4 overexpression to compensate for the loss of other MCT expression, and to allow for activation of oncogenic pathways, for loss of tissue polarity, and for increased cell growth following GLUT3 overexpression.

Similarly, I expect deletion or overexpression of MCT1 and/or MCT4 in conditions 9, 10, and 11 to cause repression of the Warburg Effect (lactate production & glucose uptake) and thereby to inhibit cell growth and activation of oncogenic pathways in T4 malignant cells, and to reorganize them in a polarized structure.

Stress conditions, such as hypoxia (1% O_2), starvation (low glucose), and increased lactate concentration in the medium, can be introduced to exaggerate the Warburg Effect and clarify results. The specific focus of this aim is on MCT1 in S1 and T4-2 cells because they are basal-like breast cells, respectively, but examining other normal and cancer cells from other linages will confirm our findings and the confirm the importance of each transporter. The glycolysis inhibitor iodoacetate (IA), and the LDH enzyme activity inhibitor Oxamate (Ox), could be used to determine if increased lactate production is due to exaggerated glycolysis, or to other metabolic pathways such as enhanced glutamine metabolism.

Condition	**GLUT3**	**MCT1**	**MCT4**	**MCT2**	**Polarity**	**Growth**	**Oncogenic pathways**
(A): S1 cells (Kenny et al. (14))	+	+	+	+	YES	NO	NO
(B): T4 cells (Kenny et al. (14))	↑X	↑X	↓X	*NC*	NO	YES	YES
(C): S1 cells (Onodera et al. (19))	*OVX*	[?]	[?]	[?]	NO	YES	YES
(1): S1 cells	*OVX*	*OVX*	[?]	[?]	[?]	[?]	[?]
(2): S1 cells	*OVX*	[?]	*OVX*	[?]	[?]	[?]	[?]
(9): S1 cells	*OVX*	*OVX*	*OVX*	[?]	[?]	[?]	[?]
(4): S1 cells	*OVX*	*DEL*	[?]	[?]	[?]	[?]	[?]
(5): S1 cells	*OVX*	[?]	*DEL*	[?]	[?]	[?]	[?]
(6): S1 cells	*OVX*	*DEL*	*DEL*	[?]	[?]	[?]	[?]
(7): S1 cells	*OVX*	*OVX*	*DEL*	[?]	[?]	[?]	[?]
(8): S1 cells	*OVX*	*DEL*	*OVX*	[?]	[?]	[?]	[?]
(9): T4 cells	[?]	*DEL*	[?]	[?]	[?]	[?]	[?]
(10): T4 cells	[?]	[?]	*DEL*	[?]	[?]	[?]	[?]
(11): T4 cells	[?]	*DEL*	*DEL*	[?]	[?]	[?]	[?]

Table. 1. The combinations of overexpressed or deleted MCT1 and MCT4 to be used in S1-non-malignant cells and T4-malignant cells. (+) normal level of RNA expressed in the S1 cells, (↑X) increase of RNA expression compared to S1 cells, (↓X) reduction of RNA expression compared to S1 cells, (NC) no change in RNA expression compared to S1 cells, [?] the parameter that will be tested, (OVX) overexpression of the gene, (DEL) deletion of the gene.

Objective 2: *To determine whether lactate, acts as a paracrine-signaling molecule in normal and cancer cells and their microenvironment using the 3D model of human mammary epithelial cells.*

Background and Preliminary Data for Objective 2: While lactate is correlated with poor clinical outcomes, its exact role in cancer and their microenvironment is still uncertain. Studies of lactate metabolism in healthy cells have shown that lactate is an important energy fuel, gluconeogenic precursor, as well as a paracrine signal molecule (2,

4-6), that can stimulates mitochondrial biogenesis (10) and angiogenesis (15). Recent data suggest that lactate may play roles in cancer similar to those it plays in normal cells through the reverse (39), or direct Warburg effect (40). Le Floch et al. (16) showed that fibroblast cells, surrounding epithelial breast cancer cells, release lactate to the nearby cancer cells, which oxidize it due to its higher mitochondrial activity. Vegran et al. (22) showed that lactate released from cancer cells stimulates angiogenesis in human umbilical vein endothelial cells. Surprisingly, acidosis' effect (low pH) in the cancer microenvironment is different than that of hypoxia or lactosis (high lactate). These conditions may coexist in the cancer microenvironment, but Chen et al. have shown that lactosis produce gene-expression profiles that differ from the profile produced by normal breast cells exposed to acidosis. Furthermore, breast cancers marked by high lactate acidosis signatures showed better patient outcomes than those marked by high hypoxia signature. Chen et al. conclude that acidosis redirects breast cancer cell metabolism back to oxidative phosphorylation from glycolysis, and inhibits the oncogenic AKT pathway (41). I hypothesize that acidosis inhibits glycolysis by blocking the release of lactate by MCTs, since MCTs co-transport a proton with the lactate molecule (19).

In light of these prior studies, I hypothesis that lactate, but not acidosis disposed by cancer cells into the microenvironment acts as a paracrine signaling molecule that facilitates cancer progression and leads to disturbed cell polarity and activation of oncogenic pathways in normal epithelial and stromal cells. I expect increased lactate concentration in the cancer microenvironment to change the redox status in surrounding cells, as the LDH enzyme converts lactate to pyruvate using nicotinamide adenine dinucleotide ($NAD^{+)}$ and reduced nicotinamide adenine dinucleotide (NADH). NAD^+ and NADH are involved in many signaling pathways and serve as a substrate for protein modifications. NADH binds directly to the transcription corepressor, carboxyl-terminal binding protein (CtBP), and prevents its degradation. CtBP is linked to tumorigenesis and tumor progression (8, 11). NAD^+ on the other hand serves as a substrate for protein deacetylation (e.g. for Sirtuin, SIRT1), protein mono- and poly-ADP-ribosylation (e.g. for poly ADP-Ribose polymerase 1, PARP1), and as a precursor of intracellular calcium-mobilizing molecules (e.g. for Cyclic ADP Ribose (cADPR), and for nicotinic acid adenine dinucleotide phosphate (NAADP) (17)).

Methods and Interpretations for Objective 2: S1 and T4-2 breast cells, and human microvascular endothelial cells, adult dermis (HMVEC, ad) will be cultured in 3D (lrECM) gel and incubated with their regular media (pH7.5) or media with 25 mM of sodium L-lactate (pH7.5) or 25 mM sodium L-lactate (pH6.5), or regular media with (pH6.5) for one to two days. Cell polarity, growth status, and oncogenic pathway activity (EGFR, β1 integrin, MEK and Akt) will be examined in S1 and T4 cells. Additionally, genes that depend on NAD^+ or NADH and are linked to cancer progression will be examined in S1, T4, and HMVECad cells. The proposed mechanism for lactate's signaling action through altering the NAD^+/NADH ratio is illustrated in Figure 2.

The elements that will be tested in Figure 2 are: The NAD^+/NADH ratio [#3 in Fig. 2], the CTBP protein level in nucleus fraction [#4 in Fig. 2], the binding of CTPB protein to the promoter region of E-Cadherin and SIRT1 [#9 & # 10 in Fig. 2], the p53 protein level and p21 and Bax RNA level [#12 and #13 in Fig. 2], and the vascular endothelial growth factor (VEGF) level and PAR modification of VEGF protein in the medium and cell homogenate [#14in Fig. 2]. The CADPR and NAADP signaling

pathways [#7 &15 in Fig. 2] will not be examined, because the signaling of Ca^{++} works when Ca^{++} is released, not when Ca^{++} release is blocked. A microarray analysis of the S1 and T4-2 cells incubated with lactate or lactate acid will be a necessary step after our initial findings, in order to determine the additional signaling pathway that lactate targets in the 3D culture.

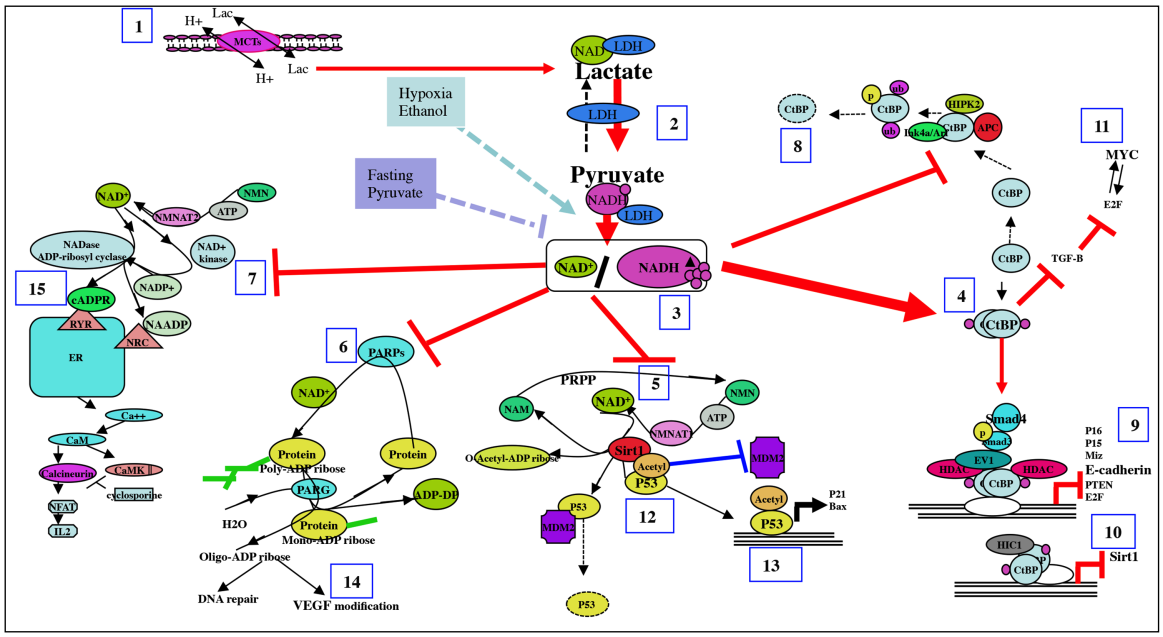

Figure 2: The proposed mechanism for lactate action as signaling molecule on stromal cells. Lactate will enter cells through the plasma membrane MCTs and increase NADH/NAD ratio. The increase in NADH will positively affect the NADH sensitive transcription factors, such as CtBP [#4 in Fig. 2], and will negatively affect the NAD^+-dependent proteins, such as SIRT1 [#5 in Fig. 2], PARP1 [#6 in Fig. 2], cADPR, and NAADP [#7 in Fig.2]

Expected Results and Alternative Approaches for Objective 2: I expect that because cancer cell lines contain mutations that interfere with the lactate signaling pathway, lactate incubation will have a stronger effect on normal cells than cancer cells. I expect S1 cells exposed to lactate at pH7.5 to show disruption in cell polarity and increased oncogenic pathway activity. I expect to see no changes in cells exposed to lactate at pH6.5 or to regular media at pH6.5. I expect T4 cells exposed to lactate at pH6.5 and those exposed to regular media at pH6.5 to show reduction in glucose uptake, and subsequent reduction in oncogenic pathway activity and reorganization of cells in a polarize structure. I do not expect to see a reduction in glucose uptake in T4 cells exposed to lactate at pH7.5. Similarly, I expect to see activation of oncogenic pathways and modification of VEGF protein in HMVECad cells exposed to lactate but not to lactate acid. These results will indicate that lactosis is acting as paracrine signaling molecule, and that acidosis is not necessary for its signaling action. It is possible that S1 and HMVECad cells respond to acidosis, but not to lactosis, which will indicate that acidity and not lactate is the reason for the changes observed. It is also possible that only lactate

with pH6.5 shows an effect on S1 and HMVECad cells, which means that lactate and acidity both are needed for lactate acid to act as a signaling molecule. It is also possible I will not see any changes in the cell lines examined which will tell us that neither lactosis or acidosis acts as signaling molecule. It is possible that a longer lactate incubation time will be needed to observe changes in the proposed pathways. To test whether our results apply to all breast cell lineages, I will examine additional normal and cancer breast cell lines from different lineages, and other stromal cell types such as fibroblast, adipocyte, mesenchymal stem cells, and macrophages. Additionally, the additive effect of hypoxia will also be examined with lactate and lactate acid to determine whether hypoxia is needed for lactate's signaling role.

FUTURE DIRECTIONS: THE STUDY OF NANOPARTICLE EFFECTS

Below I suggest several possibilities for expanding my previous study of the effect of the copolymer nanoparticles Eudragit® RS on the metabolic activity, growth, and proliferation of normal and cancer mammary epithelial cells (3). These suggestions are: 1) to determine if the result obtained is specific to epithelial cells or can be applied to many cells types; 2) to determine whether these particles have negative effects on breast cancer in animal models; and 3) to examine whether these particles can be used to extract and isolate a select group of proteins for medical diagnostic purposes.

To expand our findings to a large set of cells, I would incubate ENP particles with many different cell lines that can be obtained directly from ATCC cell culture collections. The cell lines obtained could be endothelial, lymphocyte, lymphoblast, fibroblast, neuron, glial, etc. The tetrazolium salt (WST-1) and 5-bromo-2'-deoxyuridine (BrdU) assays can be used to determine the response of each cell line to ENPs.

To expand our findings to an animal model of breast cancer, I would use MMTV-Neu or MMTV-PyMT mouse models of breast carcinogenesis. The palpable tumors are detected in these models at about 6 months of age. Animals would be divided into two groups and treated with a control or fluorescent tagged Eudragit® RS for 4 weeks. Animal weight and tumor size would be examined weekly. Animals would be euthanized and tissues saved and examined. The use of fluorescent tagged Eudragit® RS would allow us to examine the accumulation of nanoparticles in breast tissues and other tissues such as brain and liver.

Human fluid samples (serum or cerebrospinal fluid) gathered from healthy humans and from humans with specific diseases (such as Alzheimer's, rheumatoid arthritis, multiple sclerosis) will be use in this aim . The human fluid samples will be incubated with Eudragit RS nanoparticles. The isolated nanoparticle-protein pellet will be examined with MS. My goal is to examine if the isolated nanoparticle-protein pellets are enriched with protein markers that cannot be identified in normal samples due to their low concentration. For example, the presence of Fetuin A in the cerebrospinal fluid samples may be useful as a biomarker for multiple sclerosis. Fetuin A was found to bind to Eudragit nanoparticles in FBS in our study of these particles.

In summary, the results described in this dissertation illustrate only a small fraction of mammary epithelial cells' characteristics and behavior. There is still much more to explore and learn about these fascinating cells.

References

1. Beliveau A, Mott JD, Lo A, Chen EI, Koller AA, Yaswen P, Muschler J, and Bissell MJ. Raf-induced MMP9 disrupts tissue architecture of human breast cells in three-dimensional culture and is necessary for tumor growth in vivo. *Genes Dev* 24: 2800-2811, 2010.
2. Bergman BC, Horning MA, Casazza GA, Wolfel EE, Butterfield GE, and Brooks GA. Endurance training increases gluconeogenesis during rest and exercise in men. *Am J Physiol Endocrinol Metab* 278: E244-251, 2000.
3. Bissell MJ, Hall HG, and Parry G. How does the extracellular matrix direct gene expression? *J Theor Biol* 99: 31-68, 1982.
4. Brooks GA. Cell-cell and intracellular lactate shuttles. *J Physiol* 587: 5591-5600, 2009.
5. Brooks GA. Intra- and extra-cellular lactate shuttles. *Med Sci Sports Exerc* 32: 790-799, 2000.
6. Brooks GA. Lactate shuttles in nature. *Biochem Soc Trans* 30: 258-264, 2002.
7. Charafe-Jauffret E, Ginestier C, Monville F, Finetti P, Adelaide J, Cervera N, Fekairi S, Xerri L, Jacquemier J, Birnbaum D, and Bertucci F. Gene expression profiling of breast cell lines identifies potential new basal markers. *Oncogene* 25: 2273-2284, 2006.
8. Chinnadurai G. The transcriptional corepressor CtBP: a foe of multiple tumor suppressors. *Cancer Res* 69: 731-734, 2009.
9. Dockery DW, Pope CA, 3rd, Xu X, Spengler JD, Ware JH, Fay ME, Ferris BG, Jr., and Speizer FE. An association between air pollution and mortality in six U.S. cities. *N Engl J Med* 329: 1753-1759, 1993.
10. Hashimoto T, Hussien R, Oommen S, Gohil K, and Brooks GA. Lactate sensitive transcription factor network in L6 cells: activation of MCT1 and mitochondrial biogenesis. *Faseb J* 21: 2602-2612, 2007.
11. Hirai H, Izutsu K, Kurokawa M, and Mitani K. Oncogenic mechanisms of Evi-1 protein. *Cancer Chemother Pharmacol* 48 Suppl 1: S35-40, 2001.
12. Hussien R, and Brooks GA. Mitochondrial and plasma membrane lactate transporter and lactate dehydrogenase isoform expression in breast cancer cell lines. *Physiol Genomics* 43: 255-264, 2011.
13. Hussien R, Rihn BH, Eidi H, Ronzani C, Joubert O, Ferrari L, Vazquez O, Kaufer D, and Brooks GA. Unique growth pattern of human mammary epithelial cells induced by polymeric nanoparticles. *Physiol Rep* 1: e00027, 2013.
14. Kenny PA, Lee GY, Myers CA, Neve RM, Semeiks JR, Spellman PT, Lorenz K, Lee EH, Barcellos-Hoff MH, Petersen OW, Gray JW, and Bissell MJ. The morphologies of breast cancer cell lines in three-dimensional assays correlate with their profiles of gene expression. *Mol Oncol* 1: 84-96, 2007.
15. Kumar VB, Viji RI, Kiran MS, and Sudhakaran PR. Endothelial cell response to lactate: implication of PAR modification of VEGF. *J Cell Physiol* 211: 477-485, 2007.
16. Le Floch R, Chiche J, Marchiq I, Naiken T, Ilk K, Murray CM, Critchlow SE, Roux D, Simon MP, and Pouyssegur J. CD147 subunit of lactate/H+ symporters MCT1 and hypoxia-inducible MCT4 is critical for energetics and growth of glycolytic tumors. *Proc Natl Acad Sci U S A* 108: 16663-16668, 2011.

17. Masgrau R, Churchill GC, Morgan AJ, Ashcroft SJ, and Galione A. NAADP: a new second messenger for glucose-induced Ca2+ responses in clonal pancreatic beta cells. *Curr Biol* 13: 247-251, 2003.
18. Novak P, Jensen TJ, Garbe JC, Stampfer MR, and Futscher BW. Stepwise DNA methylation changes are linked to escape from defined proliferation barriers and mammary epithelial cell immortalization. *Cancer Res* 69: 5251-5258, 2009.
19. Onodera Y, Nam JM, and Bissell MJ. Increased sugar uptake promotes oncogenesis via EPAC/RAP1 and O-GlcNAc pathways. *J Clin Invest* 2013.
20. Petersen OW, Ronnov-Jessen L, Howlett AR, and Bissell MJ. Interaction with basement membrane serves to rapidly distinguish growth and differentiation pattern of normal and malignant human breast epithelial cells. *Proc Natl Acad Sci U S A* 89: 9064-9068, 1992.
21. Pinheiro C, Albergaria A, Paredes J, Sousa B, Dufloth R, Vieira D, Schmitt F, and Baltazar F. Monocarboxylate transporter 1 is up-regulated in basal-like breast carcinoma. *Histopathology* 56: 860-867, 2010.
22. Vegran F, Boidot R, Michiels C, Sonveaux P, and Feron O. Lactate influx through the endothelial cell monocarboxylate transporter MCT1 supports an NF-kappaB/IL-8 pathway that drives tumor angiogenesis. *Cancer Res* 71: 2550-2560, 2011.
23. Wang F, Weaver VM, Petersen OW, Larabell CA, Dedhar S, Briand P, Lupu R, and Bissell MJ. Reciprocal interactions between beta1-integrin and epidermal growth factor receptor in three-dimensional basement membrane breast cultures: a different perspective in epithelial biology. *Proc Natl Acad Sci U S A* 95: 14821-14826, 1998.
24. Weaver VM, Lelievre S, Lakins JN, Chrenek MA, Jones JC, Giancotti F, Werb Z, and Bissell MJ. beta4 integrin-dependent formation of polarized three-dimensional architecture confers resistance to apoptosis in normal and malignant mammary epithelium. *Cancer Cell* 2: 205-216, 2002.
25. Weaver VM, Petersen OW, Wang F, Larabell CA, Briand P, Damsky C, and Bissell MJ. Reversion of the malignant phenotype of human breast cells in three-dimensional culture and in vivo by integrin blocking antibodies. *J Cell Biol* 137: 231-245, 1997.